UNIVERSITAT POLITÈCNICA DE CATALUNYA
BARCELONATECH

Escola Tècnica Superior d'Enginyeria
de Telecomunicació de Barcelona

ANALYSIS, SIZING AND CONTROL OF A MICRO-GRID WITH PHOTOVOLTAIC GENERATION AND BATTERIES, FOR RESIDENTIAL APPLICATIONS IN THE CITY OF CÚCUTA, NORTE DE SANTANDER (COLOMBIA)

A Master's Thesis

Submitted to the Faculty of the

Escola Tècnica d'Enginyeria de Telecomunicació de Barcelona

Universitat Politècnica de Catalunya

by

Elmer Alejandro Parada Prieto

In partial fulfilment

of the requirements for the degree of

MASTER IN ELECTRONIC ENGINEERING

Advisor: Francisco Juan Guinjoan Gispert

Barcelona, February 2019

Abstract

Currently, the Colombian electricity sector presents great opportunities for the implementation of electric power generation systems from unconventional energy sources such as photovoltaic solar energy, these opportunities arise from the need to strengthen the national energy matrix to be able to supply the increasing demand for electrical energy of the country, at the same time as the generation system, mainly dominated by generation of hydroelectric energy, is strengthened in front of environmental crises such as those experienced in the past. With this as a reference, the present work carries out a study for the implementation of micro-grid with photovoltaic generation systems and batteries for residential use, within the context of the actual Colombian electricity market, focused on the city of Cúcuta, Norte de Santander. Developing for this purpose a model of the microgrid in Simulink from MathWorks, and evaluating its performance for two particular case studies.

Table of Contents

List of figures

List of tables

Chapter 1. Introduction

The generation of electrical energy from renewable sources is an mechanism that is becoming increasingly important internationally due to the advantages it presents compared to traditional generation mechanisms; advantages such as the great availability of natural resources, such as wind and solar radiation, and the reduced generation of pollution which contributes to tackling problems such as global warming that is already causing irreparable changes in the ecosystems of the entire planet [1]. Within the renewable energies implemented in the generation of electric power is the solar photovoltaic energy, which today represents the second most advanced source of renewable energy with the highest penetration in the world, after wind energy, with an installed capacity of 403,3 GW at the end of 2017 [2].

In Colombia the electricity sector is divided into two big regions: first, the national interconnected system (SIN), made up of all the regions of the country that receive electric power from the national generation plants that supply the electricity demand of the country, and traditionally it has been based on a centralized generation scheme distributed in big hydric centrals and thermal centrals (gas, coal and diesel principally) [3], which provides service to the 95% of the population, covering the 48% of the national territory. The other 52%, on which almost 5% of the population lives, is known as Non-Interconnected Zones (NIZ), represented by the regions of the country that are not connected to the national electric generation system. The NIZ are energetically isolated of the national territory because of their geographical and natural characteristics, and as consequence, the electricity must be generated in each zone. NIZ include 90 towns, 5 of them being department capitals, and 20 special territories (indigenous and afro communities) [4]. The SIN sector is mainly dominated by the hydroelectric generation. Thanks to the particularities of Colombia´s geography, such as the great availability of water and a very rugged relief, the country's energy production is cleaner and more sustainable than others whose main alternatives are gas and oil [1]. Despite the great ecological advantage that this represents, the production of this type of energy is sensitive to climate changes. In 2015, the contribution of hydroelectric generation to the SIN came to represent 72.2% of the energy generated in the month of April [5], however, in the month of December of the same year this production was considerably reduced, representing only 51.0% of the national energy generation [6]. This sensitivity was evidenced in the first semester of 2016

when, due to “El Niño” phenomenon in March, the daily useful volume of the reservoirs was reduced to 24.76% of its total capacity; this event, combined with the putting out of service of some plants due to failures in its generation system, led to the contribution of the hydroelectric sector to the SIN out of only 44.0% of total generation [7] for that month, leading the country to an energy crisis. In these periods of low generation by hydroelectric plants, the void in supply must be covered by thermoelectric plants and in critical cases, such as the one faced at the beginning of 2016, the import of energy from neighboring countries. These actions bring economic and environmental consequences, such as the increase in the emission of greenhouse gases by thermoelectric plants by burning fossil fuels to generate electricity [1], thus receding on the path towards the generation of energy friendly to the environment that has great strength in the country. To avoid a situation like this, it is necessary to work on the solution of the problem from two fronts: the optimization of the electric power consumption by the different sectors of the country and the strengthening of the electric power generation system with the use of alternative energies.

The demand for electricity in Colombia is made up of different sectors characterized by its final use: industrial, commercial and residential [8]. To optimize their consumption, it is necessary to raise awareness among end users and create a culture of savings supported by the implementation of electronic control and management systems, which leads to reducing the demand for electricity. At this point plays an important role the technological development evidenced in the last decades in the field of Home Energy Management Systems (HEMS), implementing control strategies that optimize the consumption of energy by preventing and reducing its waste, as well as modifying the usual consumption patterns to generate benefits, on one side, to the grid operator by helping to stabilize the system and preventing power grid collapses due to over-demand spikes, as well as benefits to the inhabitants of the home by optimizing their energy consumption and reducing costs on the electricity bill.

In the field of electric power generation, Colombia has already made progress in the implementation of power plants driven by alternative energies taking advantage of other available natural resources such as solar energy, which have demonstrated the feasibility of implementing this type of energy in the country [8]. However to consolidate the development of this technology, it is necessary to expand the studies carried out by projecting them into a bigger scale implementation, such as the installation of domestic energy generation systems in the residential sector, taking advantage of the solar potential of the department Norte de Santander reflected in the solar, ultraviolet and ozone radiation atlas of Colombia carried out by the Institute of Hydrology, Meteorology and Environmental

Studies of Colombia IDEAM, which reports an average global horizontal radiation of 3.5 to 5.0 kWh/m^2 per day for this department [9], figures that are above the national average, and the average of countries world leaders in the development of these technologies such as Germany [10].

On the other hand, related to legal issues, On May 13th, 2014, the Law for "Regulating the integration of non-conventional renewable energy to the National Energy System" [10] was signed, which, for the first time in the history of the country, directly opens the door to distributed generation in the national electric system, mainly from Non-Conventional Energy Sources (NCES), which can be installed by any type of user. One purpose of the Law is "... to establish the legal framework and instruments for the promotion of the use of non-conventional energy sources, especially those from renewable sources, as well as for the promotion of investment, research and development of clean technologies for energy production ... ". Following this line, on February 26th, 2018, the Energy and Gas Regulation Commission CREG, issues the 30th resolution of that year, "by which the small-scale self-generation and distributed generation activities in the SIN are regulated" [10]. This resolution establishes the regulations for the connection to the grid of power generation systems from non-conventional sources, such as photovoltaic solar energy, including the benefits of grid injection tariffs for users who implement self-generation, generation of energy for self-consumption, as an incentive for the implementation of these systems nationwide.

Taking into account the scenario described above, the main goal of this work arises from the need that exists to evaluate the implementation of electricity generation from small-scale photovoltaic solar systems in the Colombian residential sector, taking into account the impact of its connection to the stability of the local electrical grid, proposing a control strategy to reduce it, while maximizing the economic benefits by the optimization of its functioning according to the current context of the electricity sector in Colombia. This, in order to guarantee a safe and economically viable expansion of this technology in the residential sector that takes advantage of the current conditions that favor its implementation, foresee and optimize its performance in the face of future market variations, thus enabling the long-term strengthening of the national electrical system.

With this in mind, the general approach of the present work is to develop an analysis, sizing and control of a micro-grid with small-scale photovoltaic generation system and storage in batteries, to optimize the consumption of electricity and system costs in residential applications delimited to a single-family house composed of four inhabitants, located in the city of Cúcuta, Norte de Santander in Colombia, and the specific objectives are detailed as follows:

- Analyze the actual Colombian context regarding the legal and regulatory aspects, and the conventional electricity tariffs to define the cases studies to be evaluated.
- Evaluate the technology currently available in the Colombian market to define the architecture and the equipment that make up the micro-grid.
- Develop a model of the different components of the system that allows the evaluation of the performance of the micro-grid through simulation tools.
- Model the load profile for the proposed study cases and to define the irradiance profile in the city under study, in order to perform a correct sizing of the micro-grid.
- Optimize the operation of the micro-grid to guarantee its correct functioning when connected to the local electricity grid, while maximizing the economic benefits for the home.
- Analyze the impact of variations in the electricity tariffs for injection of electricity into the grid and variations in the size of the micro-grid that allow finding the optimal sizing which offers the best relationship between its performance connected to the grid and the economic benefits generated.

In reference to the fulfillment of these objectives, this document is structured as follows: Chapter 2 presents a brief summary of the state of the art and the programming tool used for the development of the optimization of the micro-grid operation. Chapter 3 summarizes the methodology implemented to carry out the analysis of the Colombian context, the design of the case studies, the modeling of the different components of the system for its simulation and the micro-grid sizing, as well as an explanation of the procedure carried out for the optimization of its operation. Chapter 4 presents the results and the analysis of the impact of the proposed variations for the tariffs of electric energy injections to the main grid and the sizing of the system. finally, the conclusions of the work are presented in chapter 5.

Chapter 2. State of the art

2.1. Micro-grid

As mentioned by D. E. Olivares *et al.* in [1], the concept of micro-grid was first introduced in technical literature as a solution for the reliable integration of Distributed Energy Resources (DERs), including Energy Storage Systems (ESSs) and controllable loads. Such micro-grid would be perceived by the main grid as a single element responding to appropriate control signals. In this way, a micro-grid can be described as a cluster of loads, Distributed Generation (DG) units and ESSs operated in coordination to reliably supply electricity, connected to the host power system at the distribution level at a single point of connection, the Point of Common Coupling (PCC). Table 2.1 and Table 2.2 presents some examples of the different technologies are implemented that actually for the DG and ESS which compound this hybrid energy systems, including their advantages and disadvantages. In general, these technologies present different tradeoffs and the micro-grid`s design will depend on project-specific requirements, economic and environmental considerations.

Table 2.1 Technologies for the Distributed Generation [2].

Options	Advantages	Disadvantages
Diesel and spark ignition reciprocating internal combustion engines.	• Dispatchable. • Quick startup. • Load-following. • Can be used for combined heat and power (CHP).	• Nitrogen oxide and particulate emissions • Greenhouse Gas Emissions • Noise generation
Microturbines	• Dispatchable • Multiple fuel options • Low emissions • Mechanical simplicity • CHP-capable	• Greenhouse Gas Emissions
Fuel cells (including solid oxide, molten-carbonate, phosphoric acid, alkaline, and low-temperature Proton Exchange Membrane or PEM)	• Dispatchable • Zero on-site pollution • CHP-capable • Higher efficiency available versus microturbines	• Relatively expensive • Limited lifetime

Renewable Generation (solar photovoltaic cells, small wind turbines, and mini-hydro)	• Zero fuel cost • Zero emissions	• Not dispatchable without storage • Variable and not controllable

Table 2.2 Technologies for the Energy Storage Systems [2].

Options	Advantages	Disadvantages
Batteries (including lead acid, sodium-Sulphur, lithium ion, and nickel-cadmium)	• Long history of research and development.	• Limited number of charge-discharge cycles. • Waste disposal
"Flow batteries", also known as "regenerative fuel cells" (including zinc-bromine, polysulphide bromide, vanadium redox)	• Decouple power and energy storage • Able to support continuous operation at maximum load and complete discharge without risk of damage	• Relatively early stage of deployment.
Hydrogen from hydrolysis	• Clean	• Relatively low end-to-end efficiency. • Challenge to store hydrogen
Kinetic energy storage (flywheels)	• Fast response • High charge-discharge cycles • High efficiency	• Limited discharge time • High standing losses

Another important aspect to take into consideration when designing the micro-grid is the type of connection that will be implemented to combine the different elements that make up the Hybrid Energy System (HES), this can be of three types: Series HES, Switched HES and Parallel HES [3], [4]. As explained in [4], in the conventional Series HES shown in Figure 2.1, all power generators feed DC power into a battery. Each component has therefore to be equipped with an individual charge controller and in the case of a diesel generator with a rectifier. This results in a typical system operation where a large fraction of the generated energy is passed through the battery bank, therefore resulting in increased cycling of the battery bank and reduced system efficiency. AC power delivered to the load is converted from DC to regulated AC by an inverter or a motor generator unit. The power generated by the diesel generator is first rectified and subsequently converted back to AC

before being supplied to the load, which incurs significant conversion losses. Table 2.3 summarizes the main advantages and disadvantages for this configuration.

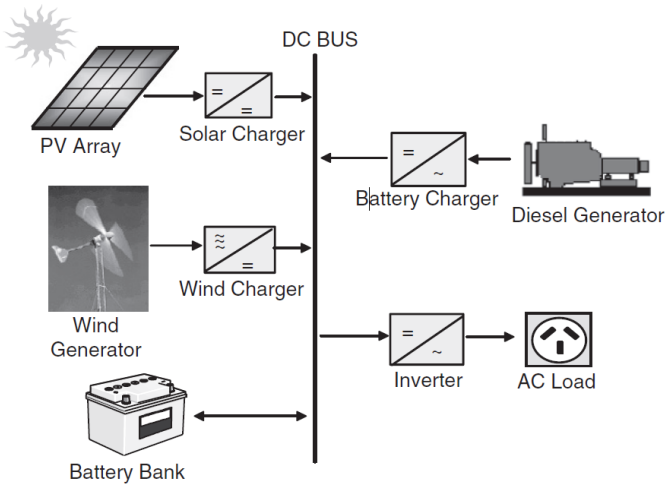

Figure 2.1 Series Hybrid Energy System from [4].

Table 2.3 Advantages and Disadvantages of Series HES [4].

Advantages	Disadvantages
• The engine-driven generator can be sized to be optimally loaded while supplying the load and charging the battery bank, until a battery SOC of 70–80% is reached. • No switching of AC power between the different energy sources is required, which simplifies the electrical output interface. • The power supplied to the load is not interrupted when the diesel generator is started. • The inverter can generate a sine-wave, modified square wave, or square-wave depending on the application.	• The inverter cannot operate in parallel with the engine driven generator, therefore the inverter must be sized to supply the peak load of the system. • The battery bank is cycled frequently, which shortens its lifetime. • The cycling profile requires a large battery bank to limit the depth-of-discharge (DOD). • The overall system efficiency is low, since the diesel cannot supply power directly to the load. • Inverter failure results in complete loss of power to the load, unless the load can be supplied directly from the diesel generator for emergency purposes.

The Switched HES allows operation with either the engine-driven generator or the inverter as the AC source, yet no parallel operation of the main generation sources is

possible. The diesel generator and the RES can charge the battery bank, typically, the diesel generator power will exceed the load demand, with excess energy being used to recharge the battery bank. During periods of low electricity demand the diesel generator is switched off and the load is supplied from the PV array together with stored energy. The main advantage compared with the series system is that the load can be supplied directly by the engine-driven generator, which results in a higher overall conversion efficiency [4]. Figure 2.2 shows the Switched HES configuration and Table 2.4 presents its main advantages and disadvantages.

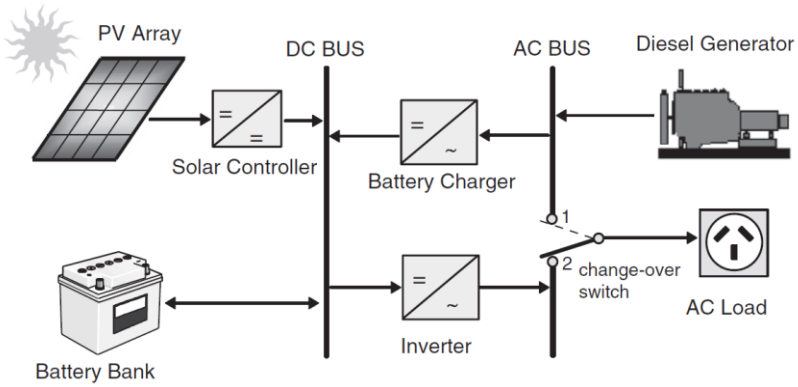

Figure 2.2 Switched Hybrid Energy System from [4].

Table 2.4 Advantages and Disadvantages of Switched HES [4].

Advantages	Disadvantages
• The inverter can generate a sine-wave, modified square-wave, or square-wave, depending on the particular application.	• Power to the load is interrupted momentarily when the AC power sources are transferred.
• The diesel generator can supply the load directly, therefore improving the system efficiency and reducing the fuel consumption.	• The engine-driven alternator and inverter are typically designed to supply the peak load, which reduces their efficiency at part load operation.

Finally, the Parallel HES can be further classified as DC and AC couplings as shown in Figure 2.3. In both schemes, a bi-directional inverter is used to link between the battery and an AC source (typically the output of a diesel generator). The bi-directional inverter can charge the battery bank (rectifier operation) when excess energy is available from the diesel generator or by the renewable sources, as well as act as a DC–AC converter

(inverter operation). In Figure 2.3(a), the renewable energy sources (RES) such as photovoltaic and wind are coupled on the DC side. DC integration of RES results in "custom" system solutions for individual supply cases requiring high costs for engineering, hardware, repair, and maintenance. Furthermore, power system expandability for covering needs of growing energy and power demand is also difficult. A better approach would be to integrate the RES on the AC side rather than on the DC side as shown in Figure 2.3(b). Table 2.5 summarizes the main advantages and disadvantages of this configuration.

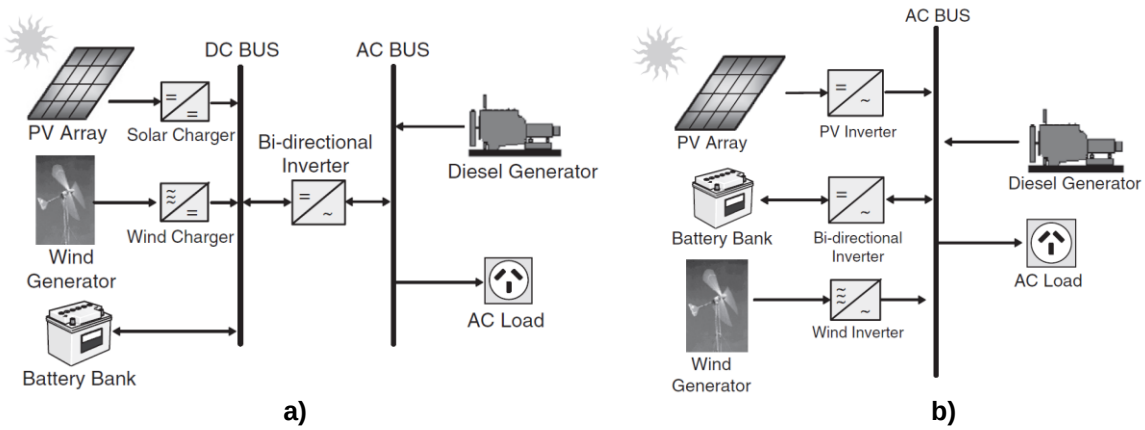

Figure 2.3 Parallel PV-diesel hybrid energy system: a) DC decoupling and b) AC coupling from [4].

Table 2.5 Advantages and Disadvantages of Parallel HES [4].

Advantages	Disadvantages
• The system load can be met in an optimal way. • Diesel generator efficiency can be maximized. • Diesel generator maintenance can be minimized. • A reduction in the rated capacities of the diesel generator, battery bank, inverter, and renewable resources is feasible, while also meeting the peak loads.	• Automatic control is essential for the reliable operation of the system. • The inverter has to be a true sine-wave inverter with the ability to synchronize with a secondary AC source. • System operation is less transparent to the untrained user of the system.

As explained in [2], actually in the literature there is an open question about the optimal aggregation scale of the micro-grid, this is an active area of investigation on: is it better to integrate detached home residential customers into large community micro-grids or to deploy micro-grid technology at the level of individual homes? each one with its

particular advantages. The case of a fully decentralized building integrated micro-grid approach includes advantages as control over energy resources by customers and the fact that individual homes are already connected to the electrical distribution grid, so that any changes performed behind the utility meter to add micro-grid capabilities will likely not introduce significant legal or regulatory complications beyond what is already encountered for interconnection of rooftop solar installations today. At the same time, this fully decentralized approach, especially if it includes islanding capability, forfeits cost-saving economies of scale and the generation and load diversity that comes with networking multiple generators and loads. Additionally, this integration of renewable energies in modern centralized grids presents some significant challenges. First, because of resource geographical scattering, most of the renewable resources, including wind and solar, are inherently intermittent, because of climate features, meteorological phenomenon, geographical location or day-night alternation. This intermittency makes variable renewable energy systems have low capacity factors (variability) and causes temporal mismatch between demand and supply within the grid (uncertainty) [5]. As a result, integration of variable renewable energies requires grid adaptations such as flexible generation, energy storage or geographical aggregation in order to maintain reliable and quality energy supply [6].

2.2. Strategies to influence the electricity usage patterns of customers

2.2.1. Demand Side Management

Demand-side management (DSM) refers to technologies, actions and programs on the demand-side of energy meters that seek to manage or decrease energy consumption, in order to reduce total energy system expenditures or contribute to the achievement of policy objectives such as emissions reduction or balancing supply and demand [7]. The DSM has been traditionally considered as a mode of reducing peak demand so that utilities can delay building the further capacity. In fact, by reducing the overall load of an electricity grid, the DSM has various beneficial effects including mitigating electrical system emergencies, reducing the number of blackouts and increasing system reliability thereby reducing dependency on expensive imports of fuel, energy prices and harmful emissions to the environment [8]. Therefore, DSM plays a major role in deferring high investments in the Generation, Transmission and Distribution networks. Thus, the DSM applied to the

electricity systems provides significant economical, reliability and environmental benefits [9].

DSM is a relatively broader concept, which includes many actions from the replacement of energy-efficient appliances, to the reduction of energy consumption and the shifting of time when electricity is used, to the implementation of complex dynamic pricing mechanisms. Thus, customers' electricity using behaviors can be changed. These changes in the time pattern and magnitude of the grid load lead to the desired changes in their load shapes [10]. The six major types of DSM objectives and tasks are peak clipping, valley filling, load shifting, strategic conservation, strategic load growth, and flexible load shape [11]. The six broad ways of altering the load shapes in DSM are summarized in Table 2.6 and illustrated in Figure 2.4.

Table 2.6 Demand side management (DSM) techniques [11].

Technique	Definition
Peak Clipping	It is generally considered as the reduction of peak load by using direct load control. It can be implemented to reduce peaking capacity or capacity purchases and consider control only during the most probable days of system peak, end also to reduce operating cost and dependence on critical fuels by economic dispatch.
Valley Filling	It encompasses building off-peak loads. This may be particularly desirable for those times of the year where the long-run incremental cost is less than the average price of electricity. Adding properly priced off-peak load under those circumstances decreases the average cost to customers.
Load Shifting	It is the last classic form of load management. This involves shifting load from on-peak to off-peak periods. Popular applications include use of storage water heating, storage space heating, coolness storage, and customer load shifts.
Strategic Conservation	It is the load-shape change that results from utility-stimulated programs directed at end-use consumption. The change reflects a modification of the load shape involving a reduction in sales often as well as a change in the pattern of use.
Strategic Load Growth	It refers to a general increase in sales, stimulated by the utility, beyond the valley filling described previously. Load growth may involve increased market share of loads that are, or can be, served by competing fuels, as well as economic development in the service area.

Flexible Load Shape	This is a concept related to reliability, a planning constraint. Once the anticipated load shape, including demand-side activities, is forecast over the planning horizon, the power supply planner studies the final optimum supply-side options. Among the many criteria he uses is reliability. Load shape can be flexible-if customers are presented with options as to the variations in quality of service that they are willing to allow in exchange for various incentives

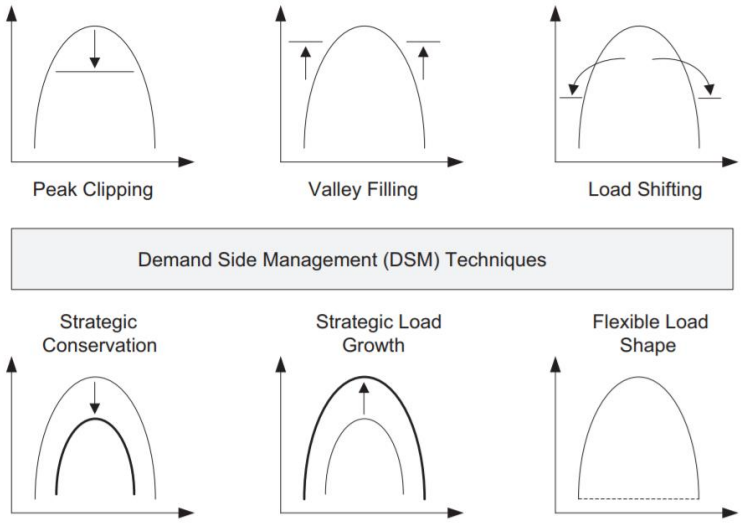

Figure 2.4 Demand side management (DSM) techniques from [10, 11].

2.2.2. Demand Response

Demand Response (DR) can be defined as changes in electric usage by end-use customers from their normal consumption patterns in response to changes in the price of electricity over time, or to incentive payments designed to induce lower electricity use at times of high wholesale market prices or when system reliability is jeopardized [12]. In this way, lower electricity use in peak periods creates benefits by reducing the amount of generation and transmission assets required to provide electric service. Lower demand in response to high prices reduces the costs of electricity production and holds down prices in electricity spot markets. Reduced demand in response to system reliability problems enhances operators' ability to manage the electric grid and reduces the potential for forced outages or full-scale blackouts. Then, DR facilitates the reduction of power consumption and saves energy, while it maximizes capacity utilization of the distribution system's

infrastructure by reducing or eliminating the need to build new lines and expand the system. The two-way communication capability in the smart grid allows for the widespread deployment of DR technologies and programs, thereby allowing load to adjust to supply variations [13].

DR programs can be classified into two broad categories. The first category is referred to as “price-based DR programs”, in these programs the consumers are charged with different rates at different consumption times, therefore, retail electricity tariff is affected by the cost of electricity supply. In the second category of DR programs, referred to as “incentive-based DR programs”, the consumers are awarded incentives for changing their consumption patterns as per the desire of the supply-side [14]. Tables 2.7 and 2.8 summarize the different DR programs that make up these categories.

Table 2.7 Price-based DR Programs [14].

Program	Description
Time of use pricing (TOU)	In this DR program, the electricity price for consumers depends on the time interval that the electricity is used. Typically, a day is divided into three intervals, named as peak interval, mid-peak interval and off-peak interval. The consumers are severely charged for consuming electricity at peak interval. In this way, they are encouraged to reduce their consumption at peak hours and shift their shiftable loads to off-peak hours [15].
Critical peak pricing (CPP)	This program is akin to TOU, except for the time when the reliability of the power system is jeopardized and then the normal peak price is replaced by a very higher price [16, 17] . This program is only employed for a couple of hours per year and improves power system reliability [18].
Real-time pricing (RTP)	In this type of pricing, the electricity tariffs typically change hourly, reflecting the fluctuations in the price of wholesale electricity market. Typically, the consumers are notified on a day ahead or hour-ahead basis [18].
Inclining block rate (IBR)	This program offers a two-level price, based on the total consumption of a consumer. The electricity price goes to a higher level, if the consumption reaches a threshold [18]. This program reduces the need for unnecessary investments in generation, transmission and distribution systems [19].

Table 2.8 Incentive-based DR Programs [14].

Program	Description
Direct load control (DLC) programs	In these programs, some consumers or appliances are registered in the program and allow the utility to shut down or cycle them, when needed (normally during peak demand or events) [20]. The participating consumers are paid incentives.
Load curtailment programs	In these programs, the registered consumers are paid incentives for curtailing their consumption as the wish of the utility. Typically, registered consumers, who fail to respond to incentives, are severely penalised [12].
Demand bidding programs	These programs are typically offered to large-scale consumers (larger than 1 MW). During contingencies or peak demands, the consumers may bid to curtail part of their consumption at a certain bid price [12].
Emergency demand reduction programs	As per this program, in severe contingencies, the consumers are paid a considerable incentive for reducing their usage. These programs may assist a power system to enhance its reliability.

2.3. Dynamic Programming

Dynamic programming (DP) is defined in the literatures as an optimization approach that transforms a complex problem into a sequence of simpler problems; its essential characteristic is the multistage nature of the optimization procedure. DP provides a general framework for analyzing many problem types and, within this, a variety of optimization techniques can be employed to solve particular aspects of a more general formulation [21]. This is a method that in general solves optimization problems that involve making a sequence of decisions by determining, for each decision, subproblems that can be solved in like fashion, such that an optimal solution of the original problem can be found from optimal solutions of subproblems [22]. This method is based on Bellman's Principle of Optimality [23]:

"An optimal policy has the property that whatever the initial state and initial decision are, the remaining decisions must constitute an optimal policy with regard to the state resulting from the first decision".

More succinctly, this principle asserts that "optimal policies have optimal sub-policies." That the principle is valid follows from the observation that, if a policy has a sub-policy that is not optimal, then replacement of the sub-policy by an optimal sub-policy would improve the original policy. The principle of optimality is also known as the "optimal substructure" property in the literature [22].

In [21] the three most important characteristics of dynamic-programming problems are identified:

Stages. The essential feature of the dynamic-programming approach is the structuring of optimization problems into multiple *stages*, which are solved sequentially one stage at a time. Although each one-stage problem is solved as an ordinary optimization problem, its solution helps to define the characteristics of the next one-stage problem in the sequence. Often, the stages represent different time periods in the problem's planning horizon. For example, the problem of determining the level of inventory of a single commodity can be stated as a dynamic program. The decision variable is the amount to order at the beginning of each month; the objective is to minimize the total ordering and inventory-carrying costs; the basic constraint requires that the demand for the product be satisfied. If we can order only at the beginning of each month and we want an optimal ordering policy for the coming year, we could decompose the problem into 12 stages, each representing the ordering decision at the beginning of the corresponding month.

States. Associated with each *stage* of the optimization problem are the *states* of the process. The states reflect the information required to fully assess the consequences that the current decision has upon future actions. The specification of the states of the system is perhaps the most critical design parameter of the dynamic programming model. The essential properties that should motivate the selection of states are: The states should convey enough information to make future decisions without regard to how the process reached the current state; and the number of state variables should be as small as possible, since the computational effort associated with the dynamic programming approach increases as the number of states grow.

Recursive Optimization. The final general characteristic of the dynamic-programming approach is the development of a *recursive optimization* procedure, which builds to a solution of the overall N-stage problem by first solving a one-stage problem and sequentially including one stage at a time and solving one-stage problems until the overall optimum has been found. This procedure can be based on a backward induction process, where the first stage to be analyzed is the final stage of the problem and problems are solved moving back one stage at a time until all stages are included. Alternatively, the recursive procedure can be based on a forward induction process, where the first stage to be solved is the initial stage of the problem and problems are solved moving forward one stage at a time, until all stages are included.

The formal description of these concepts, as well as a great variety of application examples of the dynamic programming can be found in [21] and [22].

Chapter 3. Methodology

3.1. Analysis of the Colombian context

3.1.1. Legal and regulatory aspects

Currently, the Colombian electricity market is starting a transformation related to the inclusion of the energy generated from small scale renewable systems to the main grid, this is driven by the CREG030 decree of 2018 of the Energy and Gas Regulation Commission (CREG for its acronym in Spanish), which establishes the rules of the game for the installation, connection and regulation of these systems within the national electrical system. This decree uses two criteria to classify the systems that generate electricity from unconventional sources of renewable energy (FNCER), such as biomass, hydroelectric, wind, geothermal, solar and seas, which deliver energy to the grid. The first criterion is the purpose of the system, here a difference is established between the Distributed Generators (DG), developed with the purpose of injecting to the grid all the generated electric energy, and the “Self-Generators” that are those systems designed mainly for self-consumption and meet the needs of particular electric power. The second criterion is the size, in this way it differentiates large-scale systems, which have an installed capacity of over 1 MW, and small-scale systems, which have an installed capacity equal to or less than 1 MW, at the same time the small-scale systems are subdivided in two categories: systems with an installed capacity greater to 0.1 MW and systems with equal to or less than 0.1MW of installed capacity.

With the classification of the systems established, the next important aspect that this decree sets are the mechanisms to sell the energy exported to the grid and the price at which it must be invoiced. In this way, it establishes that the operators of the grid to which the generator system is connected will be responsible for marketing and billing the energy delivered by it, and pay it to the generator according to its classification. The present work is focused on the analysis of the implementation of this type of systems at a residential level that fit within the classification of small scale self-generating systems with an installed capacity equal to or less than 0.1 MW, identified as AGPE due to its acronym in Spanish. These systems have a particular consideration in this decree, since, to encourage their installation and the expansion of renewable energies in the country, a special tariff is

established for the energy that is injected into the grid by them. This tariff is established as follows [21]:

> *"a) The surpluses that are less than or equal to their importation will be exchanged for their importation of electric power from the grid in the billing period.*
>
> *Due to these surpluses, the merchant will charge the AGPE for each kWh the marketing cost corresponding to the Cv_m component of Resolution 119 of 2007 or the one that modifies or replaces it.*
>
> *b) The surpluses that surpass their import of electrical energy from the grid in the period of invoicing, will be liquidated to the hourly price of the corresponding energy stock exchange"*

And it can be computed from the following equation:

$$VE_f = \left(Exp1_f - Imp_f\right) * CUv_m - Exp1_f * Cv_m + \sum Exp2_{h,f} * PB_{h,f} \qquad (3.1)$$

Where, VE_f is the monetary valuation of the surplus in the invoiced period. It is an income for the user when this variable is greater than zero. For a better understanding, the monetary values involved in the analysis will be converted from Colombian pesos (COP) to Euros (EUR) according to the conversion rates indicated by the Bank of the Republic of Colombia and that can be consulted in [22]. $Exp1_f$ is the sum of the AGPE energy export during each hour of the billing period, in kWh, this variable can take values between zero (0) and Imp_f, which is the sum of the AGPE energy import during each hour of the billing period, in kWh. CUv_m is the variable component of the unit cost of providing the service in €/kWh, which corresponds to the billing price of the electric energy imported from the grid. Cv_m is the marketing margin in €/kWh, its average value corresponds to 10% of CUv_m. $Exp2_{h,f}$ is the hourly energy export of the AGPE during each hour of the invoiced period, in €/kWh, which exceeds to Imp_f. $PB_{h,f}$ hourly price of electric power in the stock exchange of the hours of the invoiced period, its average value is between 33% to 40% of CUv_m.

3.1.2. Conventional electricity tariff and statement of the case studies.

The operator of the electrical grid in the city of Cúcuta is "Centrales Eléctricas del Norte de Santander" (CENS), it manages a tariff for electric power in the residential sector based on the IBR, which, as explained in section 2.2.2, consists of a monthly fixed tariff whose value depends on whether the consumption in kWh/month for the invoiced period exceeds or not an established threshold. Additionally, this rate varies for the different socioeconomic stratums, including subsidies and benefits for the lower strata (with lower purchasing power), and imposing additional charges on the highest strata (with greater purchasing power). Table 3.1 presents the different tariffs that this model applies in the city.

Table 3.1 Electricity service Tariffs for the residential sector in the city of Cúcuta [23].

Socioeconomic Stratum	Tariff 1 $€/kWh$	Tarif 2 $€/kWh$
1	0,058	0,140
2	0,073	0,140
3	0,119	0,140
4	0,140	0,140
5	0,168	0,168
6	0,168	0,168

In Table 3.1, tariff 1 corresponds to the value of electricity (€/kWh) for consumptions that do not exceed the monthly threshold established in 173 kWh for the city in which the study is carried out, on the other hand, tariff 2 corresponds to the value of energy for consumptions that exceed this threshold. In this way it is possible to observe that the benefit established by the IBR model applies for the stratums 1, 2 and 3, enjoying an economic benefit by keeping its monthly consumption below the threshold. On the other hand, stratum 4 has a flat rate, independent of monthly consumption, which corresponds to the maximum applied to the lower stratums, and strata 5 and 6 have a flat rate that includes a cost overrun of approximately 20% in the value of energy in relation the lower socioeconomic stratums.

Additionally, another aspect to be taken into account, which is similarly related to the purchasing power of the different socioeconomic stratums, and which directly influences

the monthly electricity consumption in the residential sector, is the type and quantity of electrical appliances present in the different homes. Different studies financed by the Mining and Energy Planning Unit (UPME) and carried out by entities such as the National University of Colombia [24, 25], allow observing the tenure of different types of household appliances in the six socioeconomic stratums. As an example, Figure 3.1 shows the results of a study conducted in the city of Barranquilla, which has meteorological conditions similar to those of the city of Cúcuta, regarding the possession of household appliances in the different households surveyed classified by socioeconomic stratum. There it is possible to observe that the appliances from luminaires to the clothes iron have a very similar distribution for the different stratums with holdings between 80% and 100%, this means that of the surveyed households at least 80% of them have these appliances. On the other hand, appliances such as the washing machine, the microwave oven, the air conditioning and the water heater present percentages that vary greatly depending on the stratum, and, as shown in the figure, they have a greater presence in the upper stratum, a fact that is directly related to their purchasing power and as a result, the amount of electrical energy consumed by these appliances increases the average monthly consumption of the households belonging to these stratums.

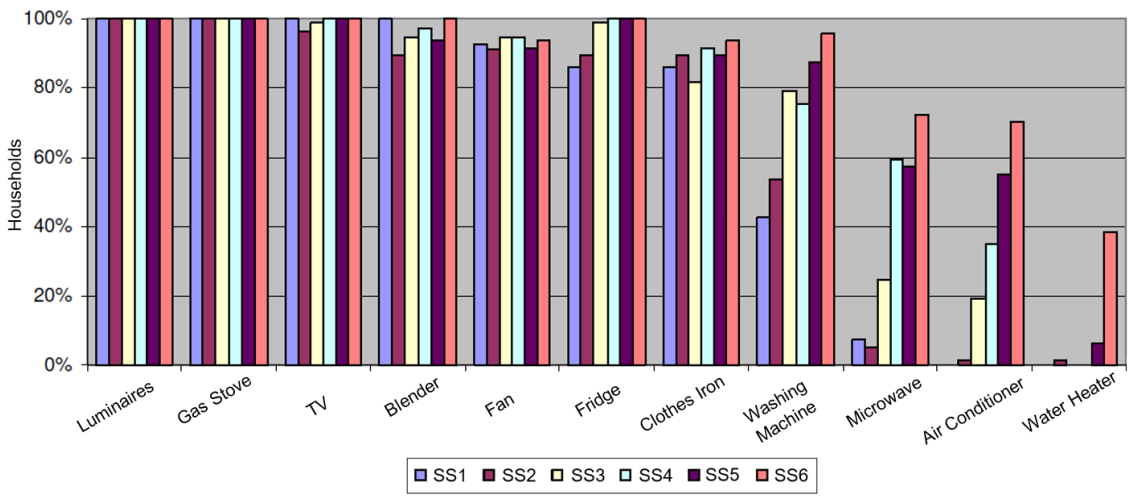

Figure 3.1 Tenure of household appliances by stratum in the city of Barranquilla from [24].

Finally, another aspect considered when establishing the case studies is the number of inhabitants per household, an aspect that has a direct influence on the amount of electricity consumed monthly. According to the last national census of population and housing conducted by the National Administrative Department of Statistics of Colombia

(DANE), the number of people per household for Norte de Santander department is 3.2 to 3.5 [26], for this reason the homes taken as a basis to carry out this study are made up by 4 people.

In this way, taking into account the factors described above, Table 3.2 presents the main case studies established to perform the analysis of the behavior and economic impact of the installation of a photovoltaic generation system with batteries connected to the grid in the city of Cúcuta. The objective of case study 1 is to evaluate the performance of a system installed in a home belonging to a medium-high stratum, with a greater purchasing power that is reflected in the number of appliances and the high average monthly consumption recorded, and that has a flat tariff for the consumption of electrical energy. On the other hand, the case study 2 aims to evaluate the performance of this type of system in a socioeconomic stratum that can benefit from a reduced electricity tariff if it does not exceed the threshold of energy consumption established by the grid operator, conformed by an average family of 4 people with a moderate electrical consumption

Table 3.2 Main case studies established.

Case Study	Description	
Case 1	**Type of housing:**	Single family
	Socioeconomic stratum:	4
	Number of inhabitants:	4
	Number of appliances:	61
	Monthly Average Consumption:	1100 kWh
Case 2	**Type of housing:**	Single family
	Socioeconomic stratum:	2
	Number of inhabitants:	4
	Number of appliances:	28
	Monthly Average Consumption:	212 kWh

3.1.3. Analysis of the Colombian market and selection of system components

To define the architecture of the system and to build up its model, it is necessary to carry out a study of the availability of its components (solar panel, inverter, batteries and charge regulator) in the Colombian market, for this purpose the five main suppliers of photovoltaic solar technology to national level were consulted about the manufacturers, models and prices that currently operate in the market. To start, table 3.3 shows a summary of the commercially available solar panels with the most competitive prices for residential photovoltaic installations. There it is possible to observe that most of the available panels are of polycrystalline technology with nominal powers between 255 Wp and 330 Wp, and with prices that oscillate between the 0,511 €/Wp for polycrystalline panels manufactured by the company Canadian Solar and the 0,619 €/Wp for the monocrystalline panels manufactured by Globalem.

Table 3.3 Solar panels commercially available in the Colombian market

Manufacturer	Model	Technology	Nominal Power Wp	Price €/Wp
Renesola	JC255M-24	Poly-crystalline	255	0,545
Renesola	JC310M-24	Poly-crystalline	310	0,544
Canadian Solar	CS6K-P270	Poly-crystalline	270	0,511
Canadian Solar	CS6U-P330	Poly-crystalline	330	0,511
JA Solar Holdings	JAP72S01	Poly-crystalline	310	0,523
TaleSun	TP672P-330	Poly-crystalline	330	0,602
Globalem	Global 320-72 M	Mono-crystalline	320	0,619

For the selection of the solar panel it is necessary to take into account that PV modules may perform differently under the varying conditions of irradiance, temperature, shading and voltage that are actually experienced in the field. This makes selecting modules a more complex process than it may first appear, and some of the selection criteria that can be taken into account is described in Table 3.4 [27].

Table 3.4 Selection criteria for the photovoltaic module [27].

Criteria	Description
Power tolerance	The nominal power of a module is provided with a tolerance. Most crystalline modules are rated with a positive tolerance (typically 0/+3 percent to 0/±5 percent), while some crystalline, CdTe and CIGS modules may be given with a ±5 percent tolerance. Some manufacturers routinely provide modules at the lower end of the tolerance, while others provide modules that achieve their nominal power or above (positive tolerance).
Temperature coefficient for power	The value of the power change with temperature will be an important consideration for modules installed in hot climates.
Degradation	The degradation properties and long-term stability of modules should be ascertained. PV module manufacturers, independent testing institutes and technical consultants are sources of good information with regards to the potential induced degradation (PID), long-term degradation and, for crystalline modules, light-induced degradation (LID).
Warranty terms	The manufacturers' warranty period is useful for distinguishing between modules, but care should be taken with the power warranty. In terms of the product guarantee, a material and workmanship product guarantee of ten years has become common, some manufacturers guarantee up to 12 years. In addition to the product guarantee, manufacturers grant nominal power guarantees. These vary between manufacturers. A two-step power warranty (e.g., 90 percent until year 10 and 80 percent until year 25) has been the historical industry standard. However, good module manufacturers are now differentiating themselves by providing a power output warranty that is fixed for the first year and then reduces linearly each year by a proportion of the nominal output power. This linear warranty provides additional protection to the plant owner compared to the two-step warranty which would provide no recourse if, for example, the module degrades to 91 percent of its nominal power in the first year.
Maximum system voltage	When sizing strings with modules with a high Open Circuit Voltage (Voc), it should be verified that for extreme ambient temperature conditions (up to 60° and down to -10°), the maximum system voltage (1,000V) will not be exceeded.
Other parameters	Additional important parameters for selection of modules include cost (€/Wp) and the expected operational life. Good quality modules with the appropriate IEC certification have a design life in excess of 25 years. Beyond 30 years, increased levels of degradation may be expected. The lifetime of crystalline modules has been proven in the field.

Table 3.5 presents a comparison of the technical specifications of the two modules that present the best market price, the module CS6U-330 manufactured by Canadian Solar and the module JAP72S01 by JA Solar Holdings. As can be seen in the table, both have very similar characteristics and a very similar performance can be expected from both panels. For the development of this work the panel CS6U-330 was chosen since, considering that the useful life of the system can be estimated in 20-25 years, this module presents a higher maximum power under Standard Test Conditions (STC) (20 W) and an efficiency 1% higher, which can be translated into a greater amount of energy generated during its useful life using the installation area in a better way, besides having the support of a leading company worldwide as Canadian Solar.

Table 3.5 Comparison of PV Module technical specifications [28, 29]

Option	1	2
Manufacturer	Canadian Solar	JA Solar Holdings
Module Model	CS6U- 330	JAP72S01
Type	Poly-crystalline	Poly-crystalline
Nominal Max. Power (Pmax)	330 W	310 W
Power tolerance	0 to +1.5 %	0 to +1.5 %
Opt. Operating Voltage (Vmp)	37,2 V	36,89 V
Opt. Operating Current (Imp)	8.88 A	8.40 A
Open Circuit Voltage (Voc)	45,6 V	45.56 V
Short Circuit Current (Isc)	9.45 A	8.92 A
Maximum System Voltage	1000 V	1000 V
Module efficiency	16.97 %	15.96 %
Operating Temperature	-40ºC to +85ºC	-40ºC to +85ºC
Temperature Coefficient (Pmax)	-0,40 %/ºC	-0,41 %/ºC
Dimensions	1960x992x35 mm	1960x991x40 mm
Module area	1,94 m2	1,94 m2
Weight	22,4 kg	22,5 kg
Product warranty (years)	10	12
Power Output Guarantee	25 years / 0,70% per	25 years / 0,73% per
Cost	0.511 €/Wp	0,523 €/Wp

Table 3.6 presents a summary of the main commercially available solar inverters in the Colombian market for residential applications connected to electric grid. As can be seen in the table, the market is mainly covered by the equipment manufactured by the US headquarters of the Fronius and SMA companies, and the nominal AC power range varies from 2000 W to 10000 W, with the additional possibility of importing other models manufactured by these companies.

Table 3.6 Inverters commercially available in the Colombian market

Manufacturer	Model	Output			Price €/W
		Nominal AC Power (W)	Frequency (Hz)	No. Phases	
SMA Solar Technology AG	3.0-US	3000	60	2/Split Phase	0,682
SMA Solar Technology AG	7.0-US	7000	60	2/Split Phase	0,424
Fronius USA LLC	Galvo 2.0-1	2000	60	2/Split Phase	0,881
Fronius USA LLC	Galvo 2.5-1	2500	60	2/Split Phase	0,753
Fronius USA LLC	Primo 3.1-1	3100	60	2/Split Phase	0,806
Fronius USA LLC	Primo 3.8-1	3800	60	2/Split Phase	0,514
Fronius USA LLC	Primo 5.0-1	5000	60	2/Split Phase	0,446
Fronius USA LLC	Primo 7.6-1	7600	60	2/Split Phase	0,385
Fronius USA LLC	Primo 10.0-1	10000	60	2/Split Phase	0,339

An important aspect to consider for the choice of the inverter is the structure of the residential electrical grid in Colombia, which has a three-wire single-phase structure with solid neutral to ground (also known as Split phase connection) with nominal voltages of 120 V and 240 V and an operating frequency of 60 Hz [30], therefore, solar inverters that intend to be connected to the grid must have this type of connection at their output to be coupled to the installations of the electrical system owned by the homes of the city, operating at the frequency and voltage levels indicated. The models and manufacturers of solar inverters presented in Table 3.6 are those that meet these characteristics, their work at a 60 Hz frequency with an output with two 120 V phases configured in a Split phase connection, as shown in Figure 3.2, which allows an output of 240 V. Additionally, inverters manufactured by the most reputable companies in the global market were given greater importance to evaluate the system with high efficiency and reliability components. Because

the manufacturer Fronius has a larger catalog of solar inverters, with a greater range of nominal power, this option was chosen to model the inverter in the developed system. Table 3.7 presents a summary of the main characteristics of the Galvo and Primo models manufactured by Fronius.

Table 3.7 Fronius inverter technical specifications - Galvo and Primo models [32, 33]

Model	Galvo 1.5-1	Primo 7.6-1
Inputs		
Maximum DC Power (kW)	1.2 to 2.4	6.1 to 11.7
MPP Voltage Range (V)	120 - 335	250 - 480
Maximum Input Voltage (V)	420	600
Maximum Input Current @MPP (A)	13.4	36
Number of MPP Trackers	1	2
Outputs		
Rated AC Power at 25°C (kVA)	1.5	7.6
Maximum AC Output Current (A)	7.2	36.5
Rated AC Voltage (V)	208/240	208/240
Frequency Range (Hz)	45-65	45-66
Nominal Operating Frequency (Hz)	60	60
Total harmonic distortion	<4%	<5%
Power factor Range	0.85 to 1	0.85 to 1
Maximum Efficiency (%)	95.8	96.9
CEC efficiency 208/240 V (%)	94.0/94.5	96.0
General Data		
Dimensions (H x W x D) (mm)	627x429x205	429x627x205
Night time consumption (W)	<1	<1
Ambient operating Temperature Range (ºC)	-40 to 50	-40 to 55
Permitted relative humidity	0 to 100% (non-condensing)	0 to 100% (non-condensing)
Protection		
DC reverse polarity protection	Yes	Yes
Anti-islanding	Internal	Internal
DC disconnect	Included	Included

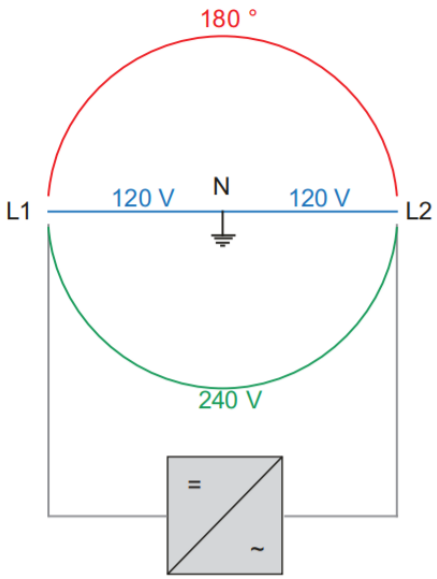

Figure 3.2 120/240 V Split phase Inverter's setup with neutral conductor available from [31].

Regarding the energy storage system, Table 3.8 presents a summary of the electric batteries available in the Colombian market. At this point it is important to pay special attention to the lifespan of the battery generally expressed by the number of cycles (which is understood as the process of charging up to the maximum capacity of the battery and discharge to a certain level), available working up to a certain Depth of Discharge (DOD). Taking into account that one of the functions of this element in the micro-grid is aimed to increasing the self-consumption of the energy generated by the photovoltaic system, the battery is expected to perform a daily cycle of charge and discharge, with a DOD of about 80%, to take full advantage of the capacity of the installed battery without reducing its lifespan. In this way, the table presents batteries of deep cycle AGM technologies, which has a lifespan of about 350 to 1000 cycles for uses with a DOD up to 80%. this record expressed in years, taking into account a daily cycle, is equivalent to a battery lifespan of 0.96 to 2.74 years. On the other hand, the batteries developed from the Lithium Iron Phosphate technology ($LiFePO_4$), have a lifespan of about 2000 to 7000 cycles @ 80% DOD, which would be equivalent to 5.48 to 19.18 years for a use as explained above.

If an analysis of the battery's costs is made against its useful life, taking into account that the lifespan of the micro-grid is at least 20 years, it is possible to observe that although the batteries manufactured by Relion have the highest price in the market (721,73 €/kWh), due to its longer duration it becomes the most viable option when compared with other

solutions. In economic terms, if batteries from the Trojan manufacturer are implemented, the deep-cycle AGMs with longer lifespan, they will need to be replaced at least 7 times to be able to operate the micro-grid throughout their life expectancy, which transforms the investment of 184 €/kWh to 1288 €/kWh. Additionally, the price of lithium-ion batteries has been reduced considerably due to the growth of the electric vehicle (EV) market. When the first mass-market EVs were introduced in 2010, their battery packs cost an estimated € 881,81 per kilowatt-hour (kWh). Today Tesla Inc., one of the EVs manufacturers with the greatest expansion worldwide, offers lithium-ion batteries packs for application in domestic micro-grids at a price of 436,34 €/kWh, while the battery pack for its newest EV, the Model 3, costs 167,54 €/kWh with a prediction of falling below 100 €/kWh for the beginning of the next decade. These facts allow us to infer that there is great potential for the implementation of this technology in the ESS of the micro-grids in the near future.

Table 3.8 Batteries commercially available in the Colombian market

Manufacturer	Technology	No. Of Cycles @80 DOD	Price €/kWh
MAGNA	AGM - Deep Cycle	~350	187,20
Kaise	AGM - Deep Cycle	~350	178,36
Trojan Battery Company	AGM - Deep Cycle	~1000	184,00
INTI	$LiFePO_4$	~2000	428,00
Relion	$LiFePO_4$	~7000	721,73

Regarding the charge controller to manage the battery charge and discharge processes, ensuring optimal its optimal operation, Table 3.9 presents a summary of the main manufacturers and models available in the Colombian market. There only the available MPPT charge controllers are mentioned, these are equipment that perform a control of the maximum power point of the solar panels array at their input, manage the current flow of the battery and regulate the required voltage levels for the appropriate battery care. This equipment plays an important role in the control system of the micro-grid that is intended to be developed in this work, since the exchange of power with the battery is the main control variable that allows regulating the operation of the system. With this in mind, when analyzing the different equipment available in the market, not only Colombian but also global, it is evident that the control of power delivered or extracted from

the battery is quite limited, in this commercial equipment it is only possible to adjust the limits of the charging and discharging current manually, which makes it impossible to implement a central control system that manages this flow. For this reason, for the development of this work, from this analysis of commercial equipment only will be consider as a reference: the efficiency of these teams, for their simulation model, and the €/W cost for economic analyzes.

Table 3.9 Battery Charge Controllers commercially available in the Colombian market

Manufacturer	Type	Model	Price (€/W)
Victron	MPPT	MPPT 150/35	0,20
		MPPT 150/60 TR	0,19
		MPPT 150/100 TR	0,19
Studer		VT-80	0,17
		VS-70	0,28

3.2. System Modelling

In order to test the behavior of the system under the conditions of the Colombian market it is necessary to build up a model which represents the two case studies described in the previous section. The main objective of this model is to emulate the power flow between the different components of the system and, with this information, to compute the economic performance of the photovoltaic installation and the optimization strategy. The proposed system model includes a photovoltaic generator, a DC bus, an Energy Storage System (ESS) represented by a Battery bank, a battery charge controller, a Grid-Tie inverter, the electrical load representing the household's energy consumptions and finally, the electrical power exchange with the grid. Figure 3.3 shows the system architecture and its main components' description and modeling are detailed below. All the model was developed using the tool SIMULINK from Mathworks due to the flexibility that this software offers to make, to program and to manipulate the different components that build up the system.

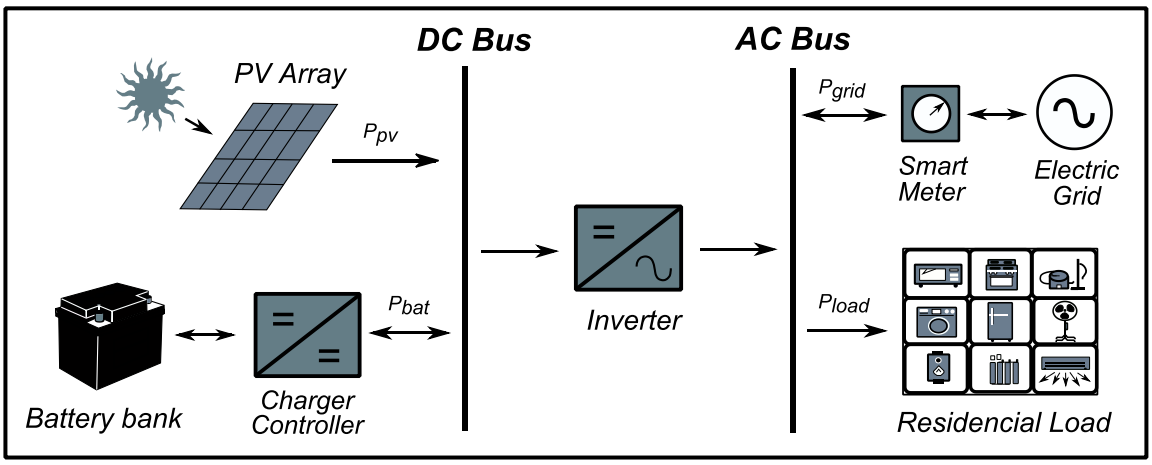

Figure 3.3 Architecture of the micro-grid.

3.2.1. PV Generator Modeling

To estimate the energy produced by the photovoltaic generator under the meteorological conditions of the location under study, a model of the PV array was built based on the modeling of a photovoltaic cell. For simulation of PV cells, there exist different approaches, being the most common ones those that model PV cells as circuits. An appropriate circuit model is the one that accurately emulates the electrical behavior of physical PV cell and is not too complex, in literature, different circuit models include the single diode RS model, single diode RP model and the two-diode model [32]. Therefore, it is necessary to find a suitable trade-off between accuracy and simplicity. In this way, the model chosen to represent the photovoltaic cell was the single diode R_p model represented in Figure 3.4. This model has five parameters: I_{pv} , n , I_o , R_s and R_p and its I–V characteristic is given in Equation (3.2) [32].W

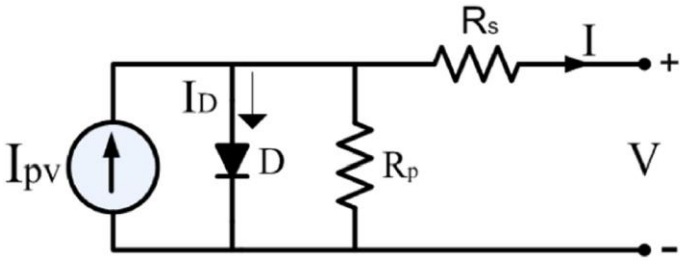

Figure 3.4 Single diode RP model from [32].

$$I = I_{pv} - I_o \left[\exp\left(\frac{(V + R_s I)}{a} \right) - 1 \right] - \frac{V + R_s I}{R_p} \tag{3.2}$$

With,

$$a = \frac{nkT}{q} \tag{3.3}$$

Where n is the diode ideality factor, q is the electron charge ($1.6x10^{-19}$ C), k is the Boltzmann constant ($1.38x10^{-23}$ J/K), and T is the cell temperature.

In Equation (3.2) I_{pv} represents the generated photocurrent due to the photovoltaic effect, which is very sensitive to environmental conditions and can be represented by the following equation

$$I_{pv}(T,G) = (I_{pv,STC} + K_I(T - T_{STC}))\frac{G}{G_{STC}} \tag{3.4}$$

There, $I_{pv,STC}$, T_{STC} and G_{STC} represent the values of photocurrent, temperature and irradiation at standard test conditions (STC). At STC, the temperature is 25° of centigrade, the irradiation is 1000 W/m^2 and air mass is 1.5. Symbols T and G respectively represent temperature and irradiation at which the photocurrent is computed. K_I represents temperature coefficient of photocurrent. Since during short circuit, diode current may be neglected in comparison with generated photovoltaic current, the photovoltaic current and short circuit current may be taken approximately equal. Short circuit current is denoted by I_{sc}. I_o is the saturation current of diode, and it is approximated by the following equation [32],

$$I_o = \frac{I_{sc}}{\exp\left(\frac{V_{oc}}{a}\right) - 1} \tag{3.5}$$

Finally, In this model the contact resistance between silicon and electrodes surfaces, the resistance of electrodes and the current flow resistance are taken into account and modelled as a series resistance denoted by R_s, and, In order to take the leakage current of P–N junction into account, a shunt resistance R_p is added to the PV cell model [32].

To adapt this model of the solar cell to the commercial panels chosen for modeling the system, it is necessary to estimate the value of the parameters R_s, R_p and n based on the characteristics delivered by the panel manufacturer in the product specification sheet. This process was carried out in two stages: initially the value of these parameters were calculated following the methodology of the compound method to extract the five parameters (I_{pv} , a , I_o, R_s and R_p) of PV modules described in [33], then, with this first estimate and with the help of the parameter estimation tool by MATLAB, an adjustment of the calculated values was made to match the behavior of the model with the characteristic curves of I vs V specified by the manufacturer.

As explained in [33], the parameters of the module can be obtained from the manufacturer data values of short circuit current I_{sc}, open circuit voltage V_{oc}, optimum operating voltage (for the maximum power operating point) V_{mp} and optimum operating current I_{mp}, and two differential values at the short circuit and open circuit points, that is $dV/dI\ at\ V = 0$ and $dV/dI\ at\ I = 0$. Hence, the main issue of this method is to obtain the values of dV/dI $(\mathrm{V} = 0 \text{ or } \mathrm{I} = 0)$ at STC conditions. These calculations are made through the equations (3.6) and (3.7).

$$\left.\frac{\mathrm{dV}}{\mathrm{dI}}\right|_{V=0} = -\frac{a_4 \ln\left(\frac{0.5\left(I_{sc} - I_{mp}\right)}{I_{o,4}} + 1\right) - 0.5(I_{sc} + I_{mp})R_{s,4}}{0.5(I_{sc} - I_{mp})} \tag{3.6}$$

$$\left.\frac{\mathrm{dV}}{\mathrm{dI}}\right|_{I=0} = -\frac{a_4 \ln\left(\frac{0.5\left(I_{sc} - I_{mp}\right)}{I_{o,4}} + 1\right) - 0.5 I_{mp} R_{s,4} - V_{oc}}{0.5 I_{mp}} \tag{3.7}$$

Where the new parameters a_4, $I_{o,4}$ and $R_{S,4}$ are computed by the Equations (3.8) to (3.10).

$$a_4 = (2V_{mp} - V_{oc}) / \left(\frac{I_{sc}}{I_{sc} - I_{mp}} + ln\left(1 - \frac{I_{mp}}{I_{sc}}\right)\right) \tag{3.8}$$

$$I_{o,4} = I_{sc} exp(-V_{oc}/a_4) \tag{3.9}$$

$$R_{s,4} = \frac{a_4 ln\left(1 - \frac{I_{mp}}{I_{sc}}\right) - V_{mp} + V_{oc}}{I_{mp}} \tag{3.10}$$

Finally, the parameters of interest are calculated from the following equations

$$R_s = \frac{V_{mp}\left(\left.\frac{\mathrm{dV}}{\mathrm{dI}}\right|_{I=0} - \left.\frac{\mathrm{dV}}{\mathrm{dI}}\right|_{V=0}\right)\left[\left.\frac{\mathrm{dV}}{\mathrm{dI}}\right|_{V=0}\left(I_{sc} - I_{mp}\right) + V_{mp}\right] - \left.\frac{\mathrm{dV}}{\mathrm{dI}}\right|_{I=0}\left(\left.\frac{\mathrm{dV}}{\mathrm{dI}}\right|_{V=0} I_{mp} + V_{mp}\right)\left(\left.\frac{\mathrm{dV}}{\mathrm{dI}}\right|_{V=0} I_{sc} + V_{oc}\right)}{I_{mp}\left(\left.\frac{\mathrm{dV}}{\mathrm{dI}}\right|_{I=0} - \left.\frac{\mathrm{dV}}{\mathrm{dI}}\right|_{V=0}\right)\left[\left.\frac{\mathrm{dV}}{\mathrm{dI}}\right|_{V=0}\left(I_{sc} - I_{mp}\right) + V_{mp}\right] + \left(\left.\frac{\mathrm{dV}}{\mathrm{dI}}\right|_{V=0} I_{mp} + V_{mp}\right)\left(\left.\frac{\mathrm{dV}}{\mathrm{dI}}\right|_{V=0} I_{sc} + V_{oc}\right)} \tag{3.11}$$

$$R_p = -R_s - \left.\frac{\mathrm{dV}}{\mathrm{dI}}\right|_{V=0} \tag{3.12}$$

$$a = \left(\left.\frac{\mathrm{dV}}{\mathrm{dI}}\right|_{I=0} + R_s\right)\left(\left.\frac{\mathrm{dV}}{\mathrm{dI}}\right|_{V=0} I_{sc} + V_{oc}\right) \Big/ \left(\left.\frac{\mathrm{dV}}{\mathrm{dI}}\right|_{I=0} - \left.\frac{\mathrm{dV}}{\mathrm{dI}}\right|_{V=0}\right) \tag{3.13}$$

And solving the Equation (3.2) for the Diode ideality factor

$$\mathrm{n} = \frac{aq}{kT} \tag{3.14}$$

Table 3.10 shows the main electrical characteristics at STC of the PV panel CS6U-330P manufactured by Canadian Solar, information necessary to perform the calculation of the aforementioned parameters from equations (3.6) to (3.14). Table 3.11 summarizes the results of the calculations that were made.

Table 3.10 PV panel CS6U-330P: Electrical characteristics at STC [28].

Parameter	Value
I_{sc}	$9.45\ A$
I_{mp}	$8.88\ A$
V_{oc}	$45.6\ V$
V_{mp}	$37.2\ V$

Table 3.11 Parameters' computed value for the cell model.

Parameter	Value
R_s	$6.5\ m\Omega$
R_p	$124.78\ \Omega$
n	0.57

Once this first estimation of the value of the model parameters has been made, it is necessary to perform an optimization of the calculated values so that the behavior of the model coincides in a better way with the actual behavior of the panel. In this stage, the model was implemented in MATLAB and with the help of its parameter estimation tool, the optimization of the values was performed to reproduce with greater accuracy the curves described by the panel manufacturer. Figure 3.5 shows the current vs voltage relationship, under different irradiance and temperature conditions, for the CS6U-330P panel

manufactured by Canadian Solar. To extract the data from the I vs V graph, the SCANLT software was used, this tool allows, through the identification of the axes of the graph, to extract the coordinates that make up the line layout. With this method it is possible to obtain data pairs that relate the current generated by the PV panel and the voltage through its connection terminals at STC.

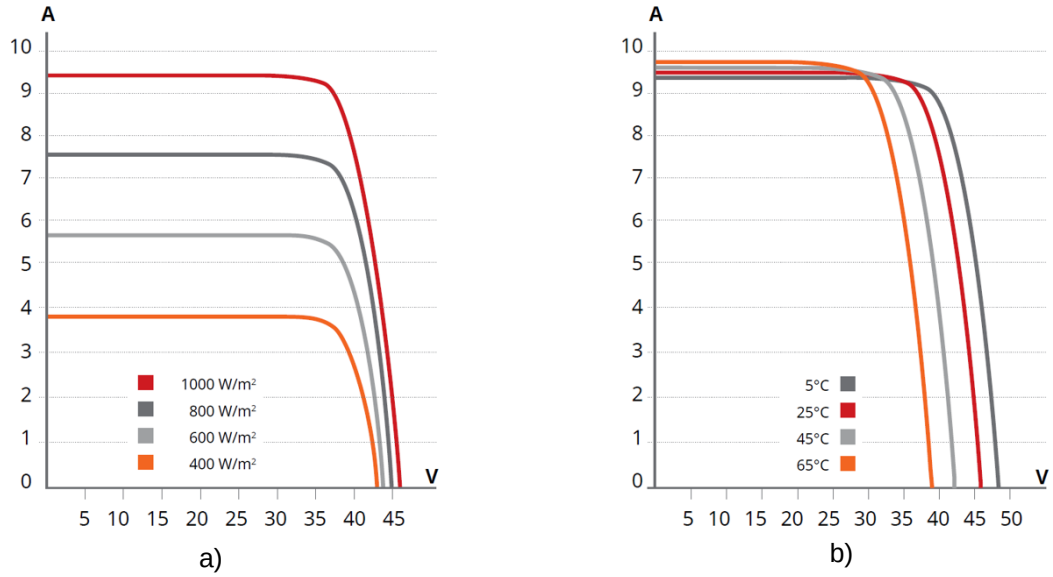

Figure 3.5 PV panel CS6U-330P I vs V curves: a) at different irradiance conditions, b) at different cell temperature conditions [28].

With the data obtained from the curve I vs V it is possible to perform the optimization of the values of the parameters of interest using the MATLAB software. For this, the equations of the model were implemented in the SIMULINK software and through its parameter estimation tool the values of R_s, R_p and n that achieve a better match between the behavior of the model and the characteristics registered by the PV panel manufacturer were found. This process is summarized in the flowchart illustrated in Figure 3.6 and the results of the optimization are presented in the Table 3.12.

Table 3.12 Parameters' estimated value for the cell model.

Parameter	Value
R_s	$3.9\ m\Omega$
R_p	$25.33\ \Omega$
n	1.118

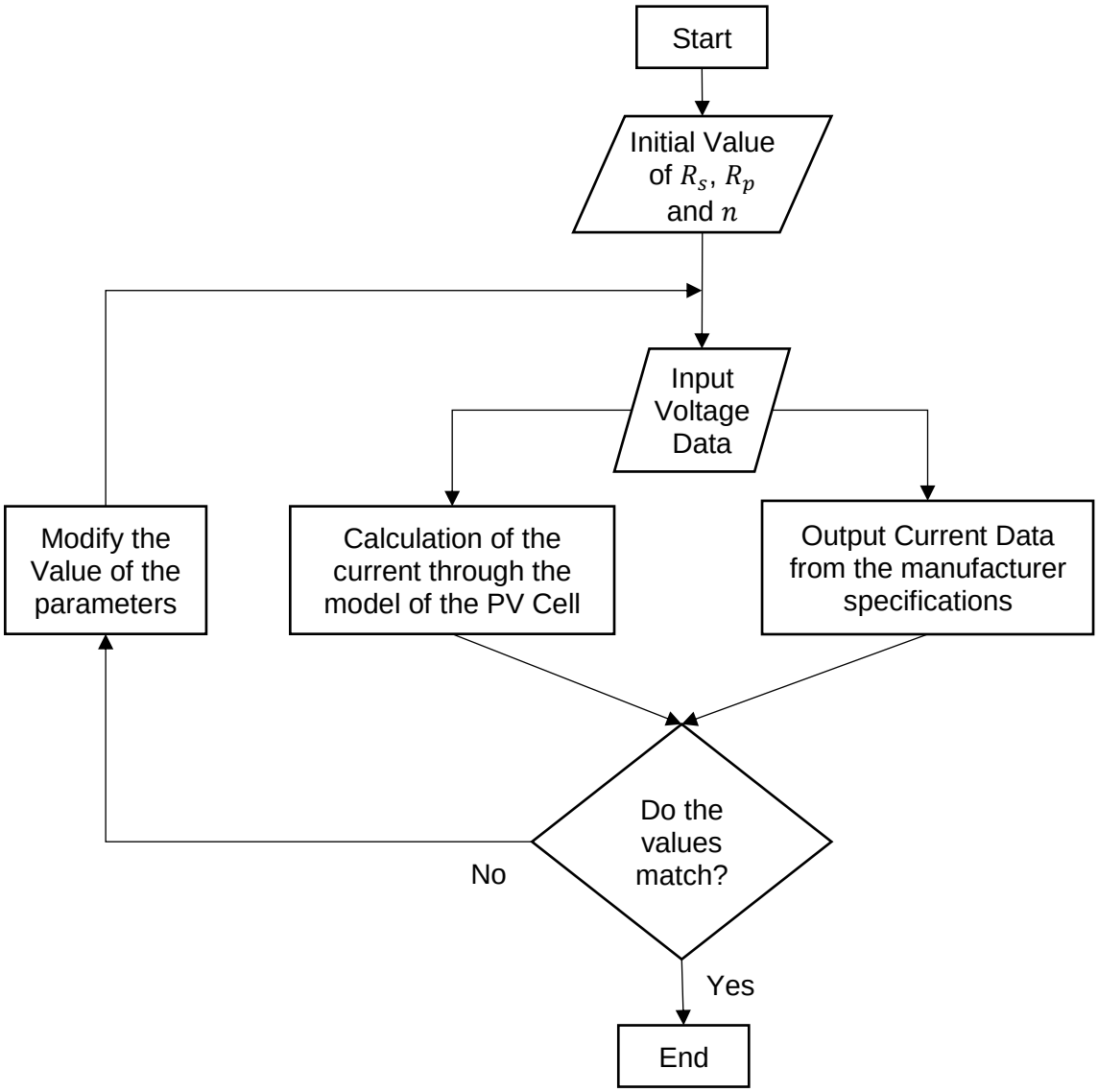

Figure 3.6 Parameter Estimation flowchart

To illustrate the results obtained in the estimation process of the parameters, Figure 3.7 shows the behavior of the simulated model with the values of the parameters calculated in stage 1 and the estimated values in stage 2. Figure 3.7(a) and 3.7(b) shows the curves of I vs V and P vs V for the simulated model of the panel with the parameters' value calculated in stage 1, there, the solid line represents the data shown in the manufacturer's specifications, while the dashed line represents the results of the simulation of the model. it can be seen that the model follows in a good way the behavior described by the manufacturer up to the region near the point of maximum power, but decreases its precision as the voltage approaches V_{oc}.

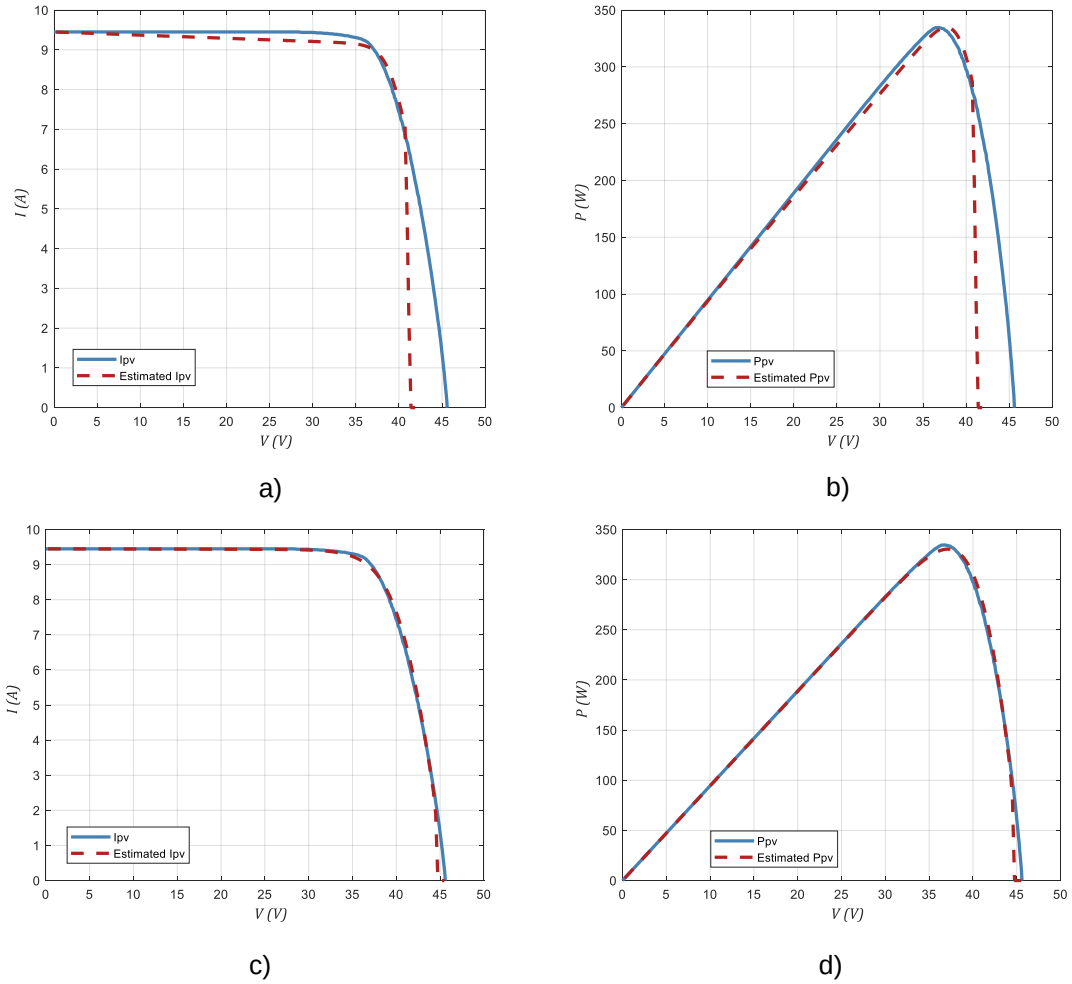

Figure 3.7 Results of the model simulation. (a) I vs V, (b) P vs V with the parameter computed value in stage 1, (c) I vs V, (d) P vs V with the parameter estimated value in stage 2.

On the other hand, Figure 3.7(c) and 3.7(d) shows the results of the simulation of the model with the parameters estimated value in stage 2. Once again, the solid line represents the manufacturer's data and the dashed line represents the results of the simulation. There it can be seen that the output of the model follows in a more precise way the actual behavior of the panel under STC, demonstrating the effectiveness of the parameter estimation that was performed.

Additionally, it is necessary to take into account that the value of these calculated parameters for the model also depends on the temperature and irradiance conditions to which the panel is subjected. To make the adjustment to the parameters value, and to include these considerations in the model, the following equations were implemented [33].

$$I_{o,T}(T) = I_{o,STC}\left(\frac{T}{T_{STC}}\right)^3 exp\left(\frac{E_g}{k}\left(\frac{1}{T_{STC}} - \frac{1}{T}\right)\right) \quad (3.15)$$

$$n_T(T) = n\frac{T}{T_{STC}} \quad (3.16)$$

$$R_{s,T}(T,G) = R_s\frac{T}{T_{STC}}\left(1 - 0.217ln\frac{G}{G_{STC}}\right) \quad (3.17)$$

$$R_{p,T}(G) = R_p\frac{G_{STC}}{G} \quad (3.18)$$

where T_{STC}, G_{STC} and $I_{o,STC}$ correspond to the value of temperature, irradiance and diode saturation current (computed from Equation (3.5)) at STC, respectively. R_s, R_p and n are the parameters' values estimated in the previous section, and $I_{o,T}$, n_T, $R_{s,T}$ and $R_{p,T}$ are the corresponding values at the specific cell temperature T and irradiance G conditions. To evaluate the behavior of the model, simulations at different weather conditions was made, the results are summarized in Figure 3.8(a) which shows the performance of the model under different irradiance levels and Figure 3.8(b) which shows the results of the simulation at different temperatures values.

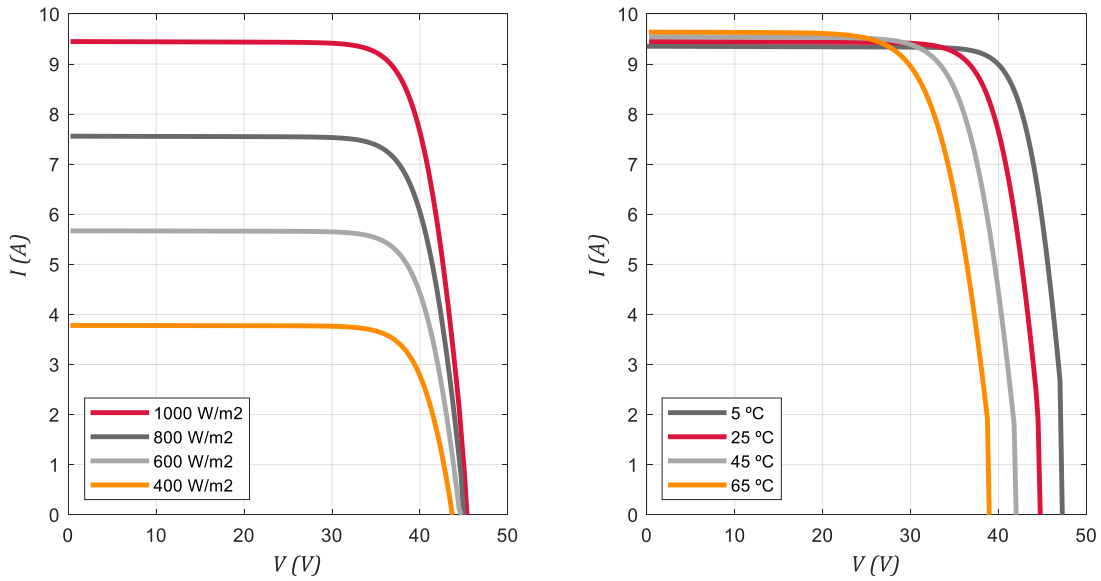

a) b)

Figure 3.8 Results of the model simulation I vs V (a) at different irradiance conditions, (b) at different temperature conditions.

Finally, the performance of the model under the Nominal Module Operating Temperature (NMOT, at irradiance of 800 W/m^2, spectrum AM 1.5 and ambient temperature 20°C) was checked and compared with the data provided by the manufacturer, Table 3.13 presents the results. There it is possible to observe that the error is lower than 2% for the different parameters provided by the manufacturer's datasheet and the model simulation results at the maximum power, open circuit and short circuit points.

Table 3.13 Comparison between the manufacturer data and simulations results at NMOT.

Parameter	Manufacturer	Simulation	Error
Nominal Maximum Power (P_{max})	243 W	238.27 W	1.95 %
Operating Voltage (V_{mp})	34.2 V	33.75 V	1.32 %
Operating Current (I_{mp})	7.1 A	7.06 A	0.56 %
Open Circuit Voltage (V_{oc})	42.5 A	42.01 V	1.15 %
Short Circuit Current (I_{sc})	7.63 A	7.64 A	0.13 %

Through the different tests carried out on the performance of the model it is possible to observe that it emulates the behavior of the photovoltaic module described by the manufacturer in the data sheet, especially in the operation areas near to the maximum power point. With this in mind, and to ensure the extraction of the maximum power of the panels during their operation under different climatic conditions, a Maximum Power Point Tracking algorithm (MPPT) was implemented, due to its simplicity and ease of implementation the chosen method was the known as Perturb and Observe (P & O). This method is based on the trial and error process in finding and tracking the MPP, and is one of the most used methods in practice. At every cycle, the tracking controller measures the PV current and voltage and deduces the actual PV power, then perturbs the operating point by sweeping the operating voltage and monitoring the variation of power. If the power increases, the next perturbation of the operating voltage should be in the same direction. However, if the power decreases, the operating voltage is perturbed in the opposite direction. This scenario is repeated until reaching the MPP. The maximum point is reached when $dP/dV = 0$ [34]. The basic flowchart of the P & O algorithm is shown in Figure 3.9.

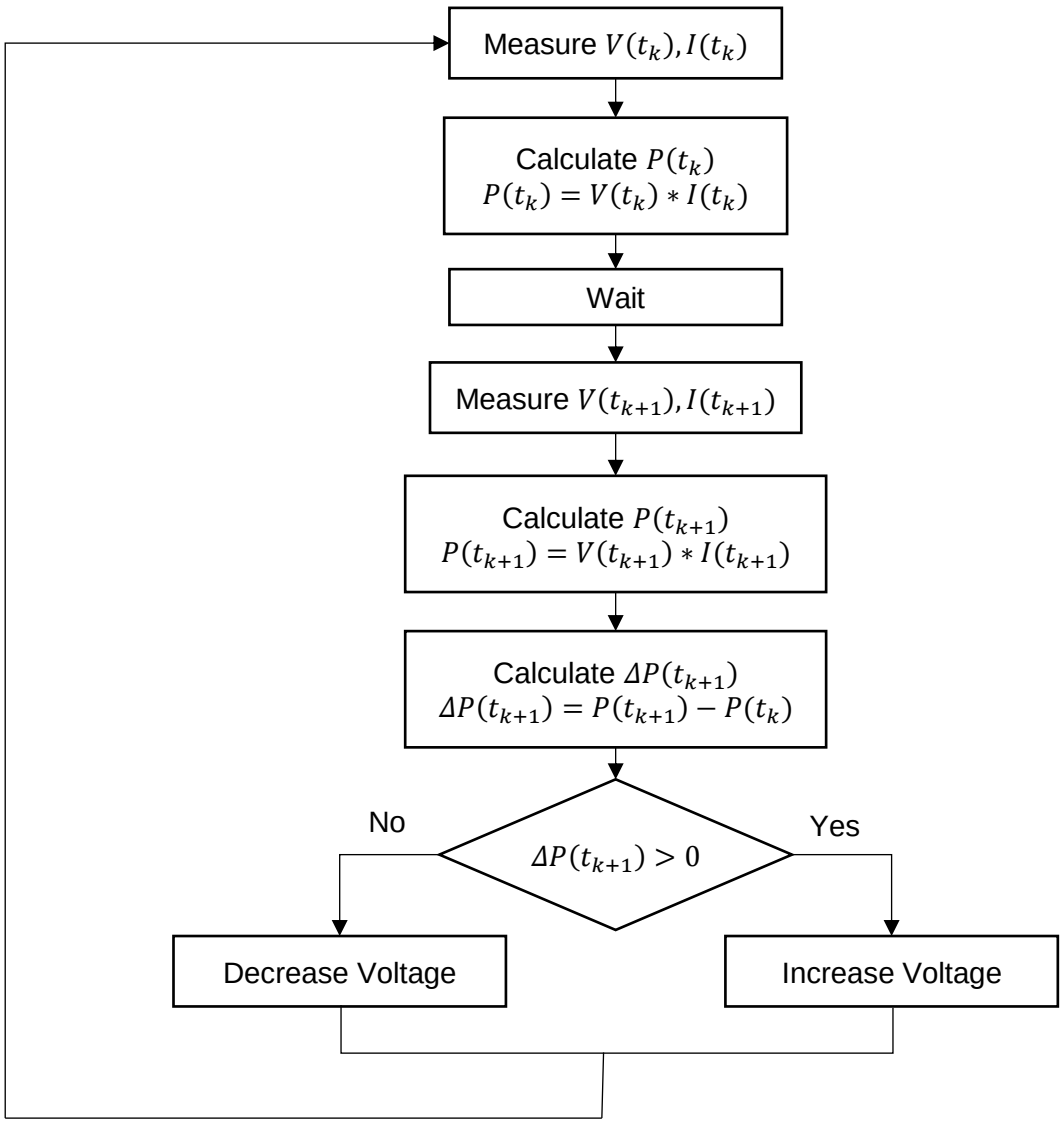

Figure 3.9 P & O algorithm flowchart [34].

3.2.2. Battery Modeling

In order to correctly estimate the flow to and from the energy storage system (ESS), it is necessary to have an accurate representation of the battery. Battery modeling involves two categories: electrochemical modeling and electrical circuit modeling. The electrochemical model of a battery is structurally based on the internal electrochemical actions and reactions of a cell. It is not obtained from an electrical network. Although accurate, this model is complex and needs a precise recognition of the electrochemical processes in the cell. It is not applied in power and dynamic systems studies. Electrical circuit modeling is another useful model presented by many researchers. In the electrical

circuit modeling, the electrical characteristics of the battery are considered and passive linear elements are used [35]. Due to the development of a particular electrical model requires the estimation of the different elements that make up the system (resistances, capacitors, etc.) through the use of experimental data obtained from controlled processes of charging and discharging of the battery to be modelled, for the implementation of the micro-grid it was decided to use the general battery model offered by MATLAB's SIMULINK software adapted to the particular characteristics of a commercial battery. The SIMULINK battery block implements a generic dynamic model parameterized to represent most popular types of rechargeable batteries, Figure 3.10 shows the equivalent circuit that the SIMULINK block models.

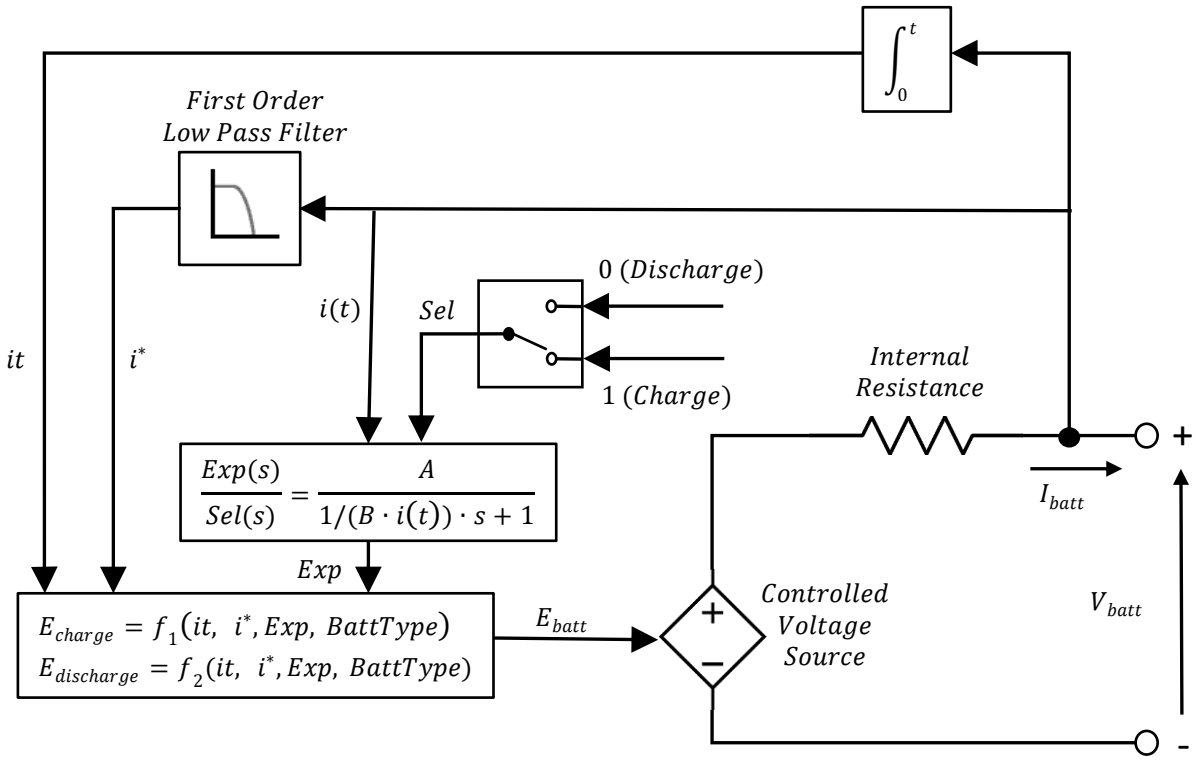

Figure 3.10 Battery equivalent circuit [36].

For the Lithium-ion battery type, the model implements the following equations:

- Discharge Model ($i^* > 0$)

$$f_1(it,\ i^*, i) = E_o - K \cdot \frac{Q}{Q - it} \cdot i^* - K \cdot \frac{Q}{Q - it} \cdot it + A \cdot \exp(-B \cdot it) \tag{3.19}$$

– Charge Model ($i^* < 0$)

$$f_2(it,\ i^*, i) = E_o - K \cdot \frac{Q}{it + 0.1 \cdot Q} \cdot i^* - K \cdot \frac{Q}{Q - it} \cdot it + A \cdot \exp(-B \cdot it) \qquad (3.20)$$

In this model E_{batt} represents the nonlinear voltage (V), E_o is constant voltage (V), $Exp(s)$ is exponential zone dynamics (V), $Sel(s)$ represents the battery mode ($Sel(s) = 0$ during battery discharge, $Sel(s) = 1$ during battery charging), K is polarization constant (Ah^{-1}), i^* is low frequency current dynamics (A), i is battery current (A), it is extracted capacity (Ah), Q is maximum battery capacity (Ah), A is exponential voltage (V), B is exponential capacity (Ah^{-1}). These parameters can be modified to represent a particular battery type, based on its discharge characteristics. A typical discharge curve consists of three sections as can be observed in Figure 3.11. There, the first section represents the exponential voltage drop when the battery is charged. The width of the drop depends on the battery type. The second section represents the charge that can be extracted from the battery until the voltage drops below the battery nominal voltage. Finally, the third section represents the total discharge of the battery, when the voltage drops rapidly [36].

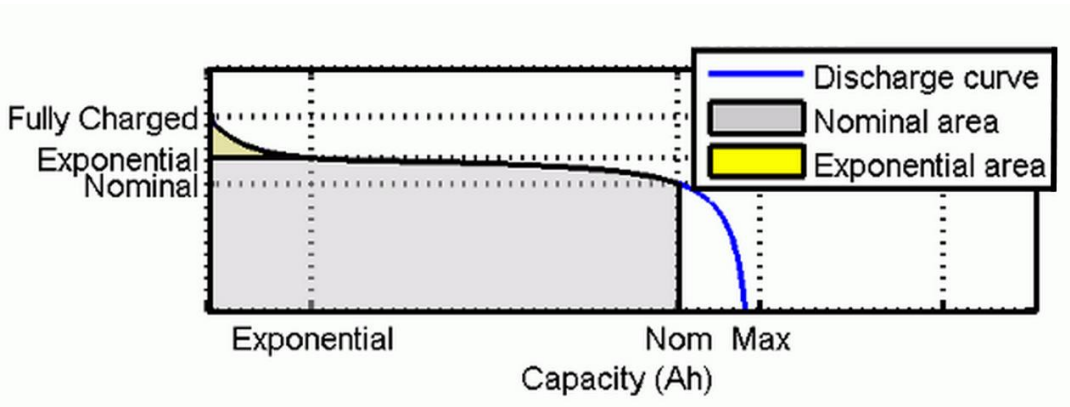

Figure 3.11 Battery typical discharge characteristics [36].

Figure 3.12 shows the parameters that can be used in the SIMLULINK model to represent the chosen commercial battery. Most of these parameters can be extracted from the specifications in the data sheet as well as in the discharge characteristics provided by the manufacturer, this information is presented in Figure 3.13 and summarized in Table 3.14.

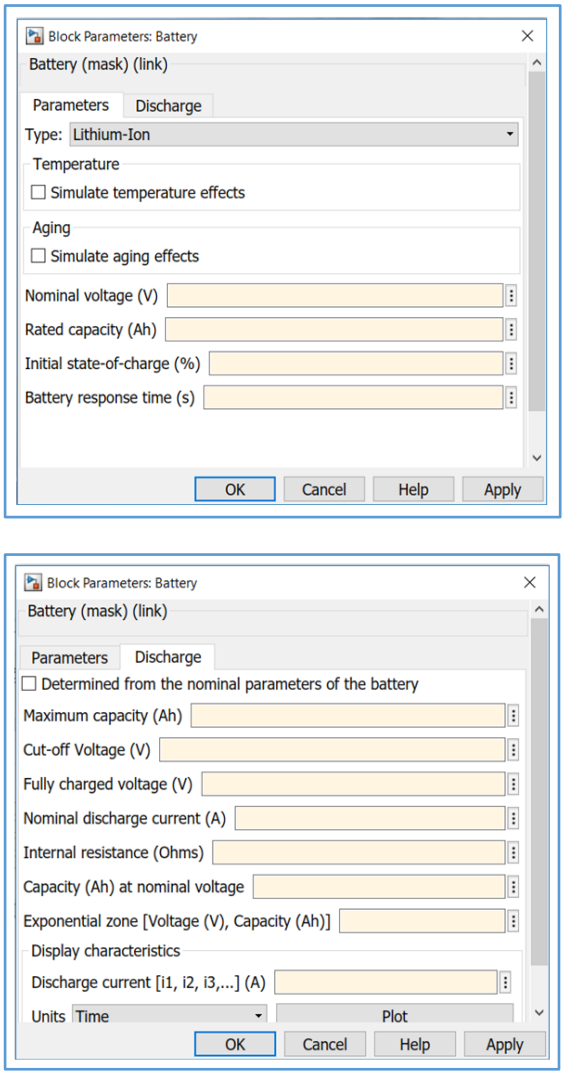

Figure 3.12 Battery Block Parameters. Screenshot from SIMULINK-MATLAB.

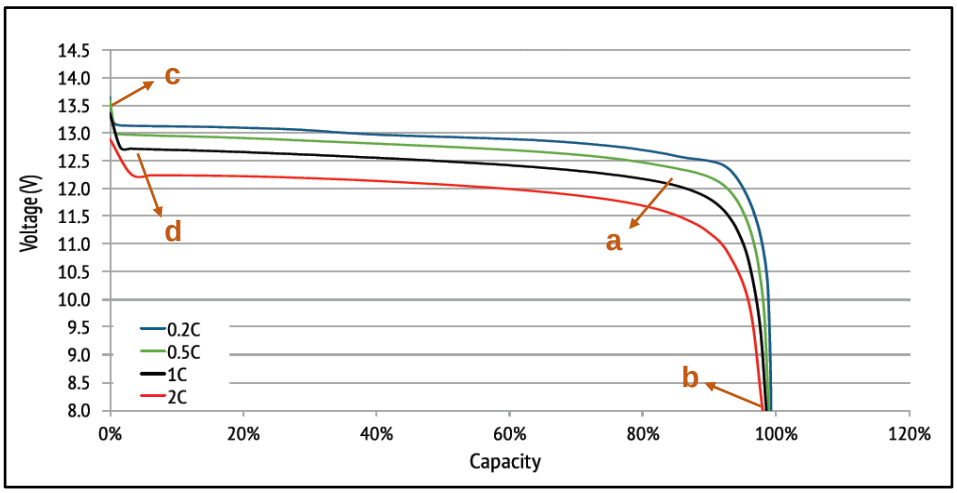

Figure 3.13 Battery discharge voltage characteristics at various rates – 25ºC [37].

In Figure 3.13 the point (a) corresponds to the nominal voltage which represents the end of the linear zone of the discharge characteristics, point (b) correspond to the cut-off voltage representing the end of the discharge characteristics (at this voltage the battery is fully discharged), point (c) corresponds to the fully charged voltage for a given discharge current and point (d) corresponds to the end of the exponential zone represented by a voltage value and a corresponding capacity [36].

Finally, it is necessary to estimate the battery response time to complete the model, this can be done following a procedure similar to that carried out to estimate the value of the parameters of the solar panel model summarized in Figure 3.6, this estimation process was done with the SIMULINK tool in order to calculate the nominal voltage value, the internal resistance and the response time of the battery so that the model can more accurately represent the charge and discharge behavior of the battery. The results of the parameter estimation are presented in Table 3.15.

Table 3.14 Battery's parameters extracted from the manufacturer specifications [37].

Parameter	Value
Rated Capacity	$100\ Ah$
Internal Resistance	$\leq 30\ m\Omega$
Nominal Voltage [(a)]	$12.8\ V$
Cut-off Voltage [(b)]	$8\ V$
Maximum Capacity	$100\ Ah$
Fully Charged Voltage [(c)]	$13.62\ V$
Nominal Discharge Current	$50\ A$
Capacity @ Nominal Voltage [(a)]	$42.83\ Ah$
Exponential Voltage [(d)]	$12.98\ V$
Exponential Capacity [(d)]	$1.037\ Ah$

Table 3.15 Estimated Parameters' value.

Parameter	Value
Nominal Voltage	$12.88\ V$
Battery Response Time	$1167.2\ s$
Internal Resistance	$2.8\ m\Omega$

Once the battery model was completed, some tests were performed to verify its validity with respect to the data delivered by the battery manufacturer. Figure 3.14 shows a comparison of the simulation of the battery model in SIMULINK for a discharge process at nominal current and temperature values. There it is possible to observe that the battery model works as a good approximation to the behavior of the simulated physical battery.

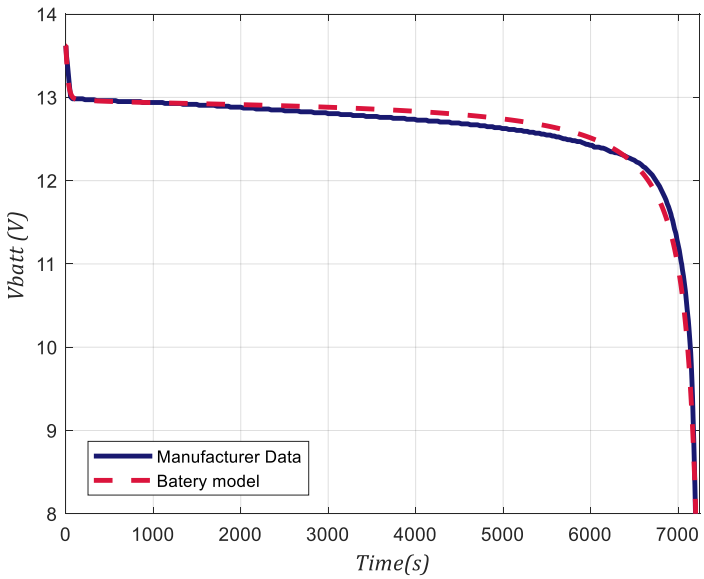

Figure 3.14 Battery discharge characteristics: Comparison between the Manufacturer Data and Simulated Battery Model.

3.2.3. Inverter Modeling

The elaboration of the complete model of the system is oriented to the simulation of its behavior during a period of time of a year, so its temporal scale is in the order of the seconds. For this reason, to model the performance of the commercial inverter it is assumed that its high frequency dynamics related to the switching of its components are regulated by its control circuits and the attention is focused on the impact of the inverter's efficiency on the overall performance of the system. In this way, to represent the behavior of the inverter, its model is based on the efficiency curves provided by the manufacturer in the product data sheet. As can be observed in Figure 3.15, the efficiency curve of the inverter is determined by two factors: the first of these is the relationship between the DC power at the input of the equipment and its nominal power, this relationship depends on the climatic conditions to which the panels are submitted because they establish the maximum power that the PV array can deliver; the second factor is the operating DC voltage supplied by the array, equally dependent on the maximum operating power point

set by the P & O algorithm. SIMULINK allows the implementation of these characteristic curves through a Lookup table, for its elaboration the corresponding data were taken from Figure 3.15 and are presented in Table 3.16.

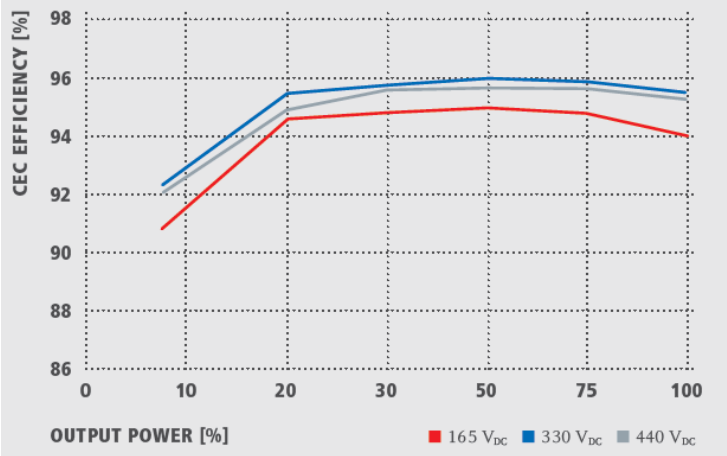

Figure 3.15 Fronius Galvo 3.1-1 Efficiency Curve [38].

Table 3.16 Lookup table for inverter efficiency.

Output Power (%)	DC Voltage (V)		
	165	330	440
5	90.81	92.28	92.02
10	91.51	92.9	92.56
15	93.03	94.16	93.72
20	94.55	95.45	94.88
25	94.68	95.58	95.22
30	94.79	95.74	95.56
35	94.84	95.79	95.58
40	94.87	95.84	95.61
45	94.92	95.92	95.61
50	94.94	95.97	95.64
55	94.92	95.94	95.64
60	94.87	95.92	95.61
65	94.84	95.89	95.61
70	94.79	95.87	95.61
75	94.74	95.84	95.58
80	94.58	95.76	95.53
85	94.43	95.69	95.46
90	94.27	95.61	95.38
95	94.12	95.53	95.3
100	93.97	95.46	95.25

3.2.4. Load Modeling

Due to the lack of a database that contains real measures of electricity consumption for households under analysis, it is necessary to make a model of it. For this labor, the method known as Conditional Demand Analysis (CDA) was taken as a reference. The CDA method performs a regression based on the presence of end-use appliances. By regressing total dwelling energy consumption onto the list of owned appliances it is possible to obtain the consumption pattern of the house. The primary strength of this technique is the ease of obtaining the required input information: a simple appliance survey from the occupant and energy billing data from the energy supplier [39]. Taking this into account, the process for modeling the consumption pattern of the dwelling was divided into the following steps: Initially a survey was applied to the inhabitants of the dwelling to identify the average monthly consumption of electric energy registered in the service bill, the quantity of electrical appliances, their electrical characteristics (average consumption) and their schedules and time of use. With this information, the second stage of the process consisted in the elaboration of a profile of daily electric energy consumption that modeled the use and consumption by each household appliance. Finally, the third stage consisted in the discrimination of consumption patterns by the type of day (working day or weekend) and the inclusion of a randomization algorithm to take into account the variability in the use of household appliances derived from the behavior of the inhabitants and the occupancy of the house, which are factors that have a direct influence on the pattern of electricity consumption in the home as explained in [40], [41] , in this way, the generation of a flat consumption pattern that is repeated every day is avoided.

In the first stage of the process the survey was applied through a predefined the form. There, it asks for the information of each household appliance corresponding to the space in which it is located, the type of household appliance, the manufacturer and the model, the average power that consumes according to the manufacturer specifications, the average time of use for each hour of the day or its average use per week (for household appliances for occasional use such as the washing machine). Table 3.17 summarizes the information collected for the house for the case study 1, this case corresponds to the household made up of a family of 4 people belonging to socioeconomic stratum number 4. There can be evidenced the existence of 61 household appliances with regular use that make up a monthly average electrical energy consumption of approximately 1313.52 kWh according to the data collected by the survey. This estimated value based on the response of the inhabitants of the household to the time of use of each household appliance

corresponds to the maximum consumption that the household can present, and it is related to the maximum consumption values recorded in the electricity bill for the household in a year, with an average monthly consumption of 1100 kWh.

Table 3.17 Case Study 1: Household appliances.

Appliance	Quantity	Average Power Consumption (W)	Average Use Time per day (h)	Average Daily Consumption (Wh)	Average Monthly Consumption (kWh)
Lights					
CFL 15W	11	15	17,75	266,25	7,99
CFL 20W	17	20	27,75	555,00	16,65
TVs					
LCD 32"	2	153	9	1377,00	41,31
LCD 42"	2	206	8	1648,00	49,44
Air Conditioning					
AC 18 BTU	5	1160	26,9	31204,00	936,12
Fans					
Pedestal Fan 60W	1	50	2	100,00	3,00
Floor Fan	2	60	2	120,00	3,60
Pedestal Fan 70W	1	70	0,5	35,00	1,05
Computers					
Laptop	1	70	3	210,00	6,30
Desktop Computer 1	1	220	0,5	110,00	3,30
Desktop Computer 2	1	350	5	1750,00	52,50
Video Game Consoles					
Console 70W	1	70	1	70,00	2,10
Console 137W	1	137	2	274,00	8,22
Others					
Fridge	1	375	8	3000,00	90,00
Washing Machine	1	400	1,14	456,00	13,68
Blender	1	400	0,1	40,00	1,20
Clothes iron	1	1000	0,8	800,00	24,00
Microwave oven	1	1200	0,033	39,60	1,19
Water Pump	1	745,7	1,5	1118,55	33,56
Phone Charger	5	7,75	10	77,50	2,33
Modem Wifi/TV	4	13	41	533,00	15,99
Total	**61**	**-**	**-**	**-**	**1313,52**

In the second stage, once the information on the average use of the appliances and the hours in which they are used are collected, an average consumption pattern is established with 15-minute intervals. For this purpose, a chronogram with 96 intervals that complete the 24 hours of operation of a day is established for each appliance based on the survey information, to later add all the consumptions of the appliances that are active during the same interval. Figure 3.16(a) shows an example of the consumption pattern generated for a day, related to each time interval, while Figure 3.16(b) shows the same consumption

pattern related to the corresponding hour of the day. As can be observed the started hour is chosen to be 6:00 in the morning, this is done in a deliberate manner so that the beginning of the consumption pattern coincides with the approximate time of the sunrise and then the beginning of generation of energy by the photovoltaic system, an aspect that is considered when optimizing the functioning of the system which will be explained later.

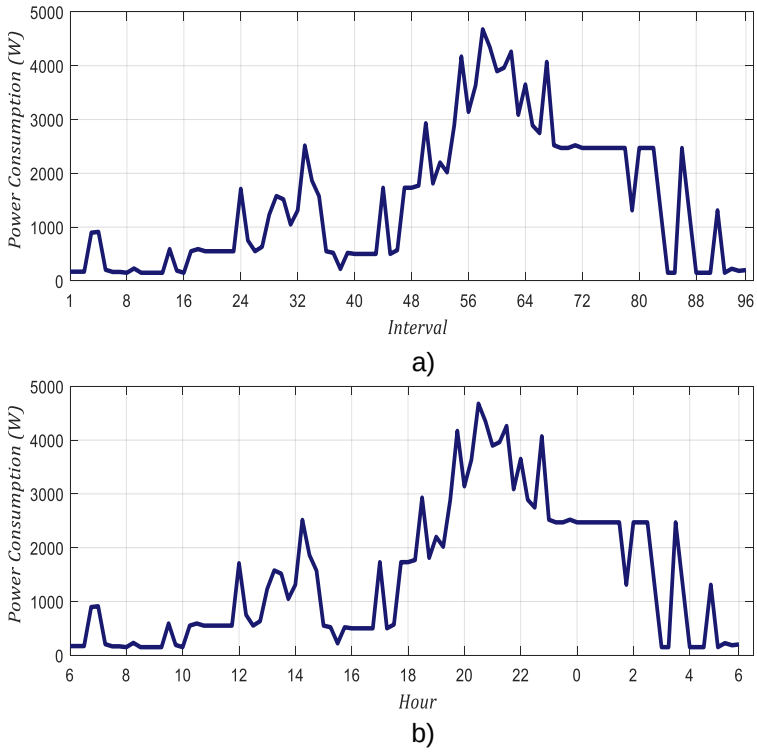

Figure 3.16 Case Study 1: Consumption pattern generated from the collected information related to each: a) time interval, b) hour of the day.

Finally, in the third stage of the process, the necessary considerations were made for the generation of a weekly consumption pattern, which can likewise be extended to a monthly and annual consumption pattern. To achieve this, discrimination of household consumption by the type of day represented was first made, in this way the algorithm can establish whether the generated pattern corresponds to a working day (Monday to Friday) or to the weekend (Saturday and Sunday). This is because, on the one hand, in the information collected it can be observed that there are household appliances such as the washing machine and the clothes iron that are used on specific days of the week, and on the other hand the habitability of the house varies for these types of days, which in turn generates changes in the consumption pattern. Additionally, to include the variability in the operation of the different appliances, product of the slight changes that can occur within the daily routine of the inhabitants of the home, and to avoid the generation of a repetitive weekly consumption pattern, the information of the use of each electric appliance for each one of the 96 intervals in which the day was divided, was transformed into a usage

probability for each hour, in this way, a device that is used for 15 minutes in an hour has a using probability of 25% for that respective time interval, an appliance that is used for 30 minutes has a 50% usage probability, one that is used for 45 minutes has a 75% usage probability and finally a device that is used during the full hour it has a 100% probability of use during this time interval. With this information, the algorithm that generates the consumption pattern performs the inverse process and assigns in a random way to each household appliance, respecting the probability of use, the number of intervals in which it remains active for each hour of the day, Figure 3.17 shows the flowchart of this process.

The flowchart presents the generation process of the daily consumption pattern for each household appliance that registers activity during the day under evaluation. This process begins with the establishment of the initial time (6 o'clock in the morning as mentioned above), for this hour the algorithm reads the corresponding usage probability and assigns random values "ON" or "OFF" for each of the four intervals of 15 minutes that compose the hour, then it is verified that the total number of intervals in "ON" state (or what is the same, the total usage time of the appliance), does not exceed the maximum time of use of the appliance for the corresponding hour as established from the information collected in the survey. At this point, if the time of use of the device is exceeded, the process of assigning values to each interval is repeated until this condition is satisfactorily fulfilled. Once this process is finished, the algorithm identifies the power consumption value for the device (registered in table 3.6) and generates the consumption pattern in watts for the respective hour. This process is repeated for each hour of the day until assigning the values for all the 96 intervals of 15 minutes that comprise it, and for each of the appliances.

It is possible to extend the methodology implemented by the algorithm described above to generate weekly, monthly and annual consumption patterns that can be used in the evaluation of the system's performance. Figure 3.18(a) shows the consumption pattern generated for a week (from Monday to Sunday), there it is possible to observe the variations generated for the different days in the time slot between 6:00 h and 18:00 h corresponding to the factors mentioned above; for example, point A on the graph represents a power consumption higher than 1150 W in the morning hours that is not present in previous days and that is related to the use of the clothes iron on Friday, on the other hand, points B and C represent variations in the consumption pattern attributed to the increase in the number of inhabitants present in the home during Saturday, and the decrease in energy consumption to minimum values due to the absence of occupants on Sunday afternoon respectively. Figure 3.18(b) shows the consumption pattern generated for a month with an average consumption value of 1070 kWh, finally, thanks to the fact that in the city where

this study is proposed there are no significant variations in the climatic conditions throughout the year, this factor does not affect the pattern of energy consumption in the home and the methodology can be expanded to generate the consumption pattern of one year, Figure 3.18(c) shows the results.

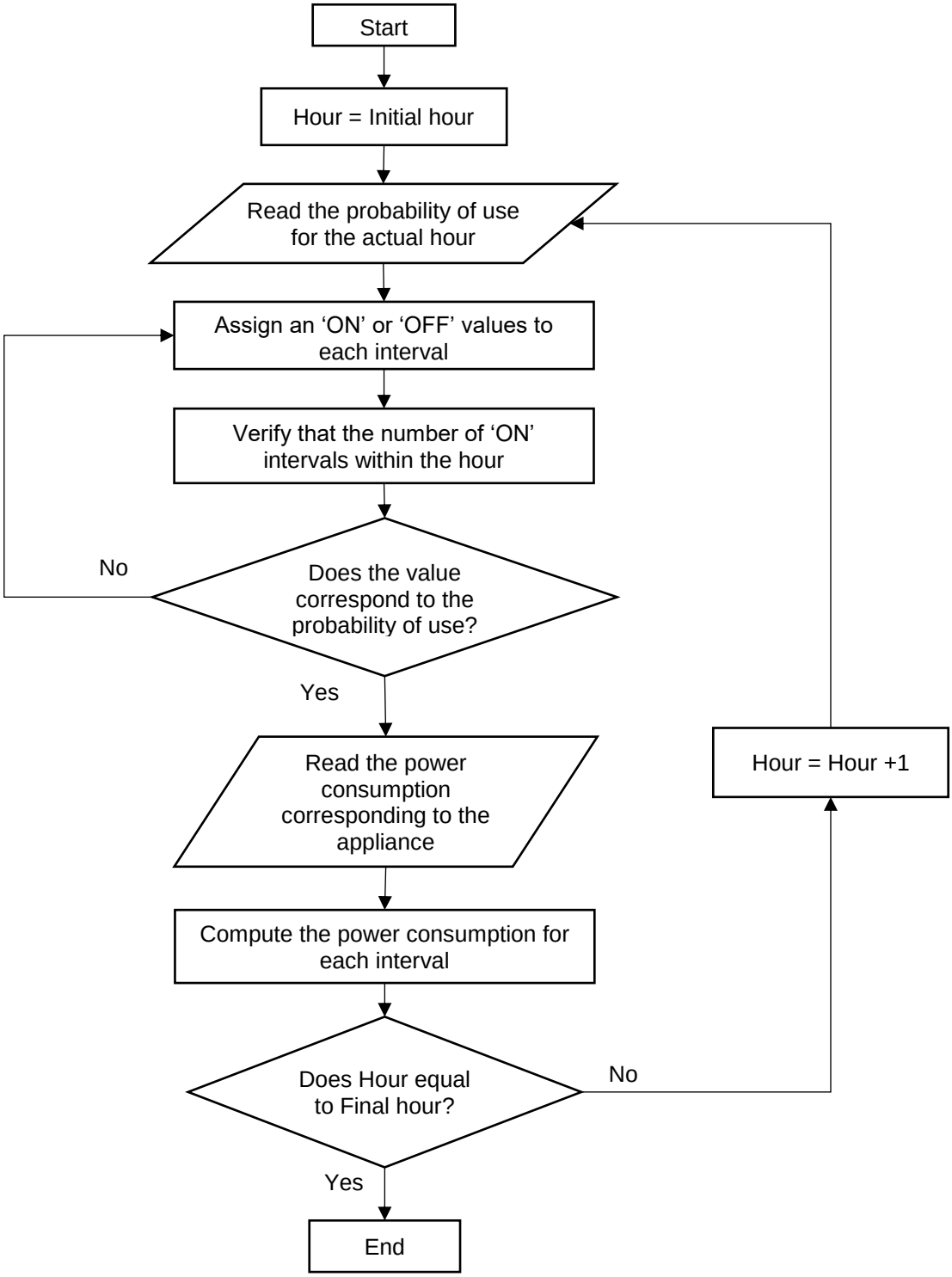

Figure 3.17 Algorithm for generating the consumption pattern for each household appliance - flowchart.

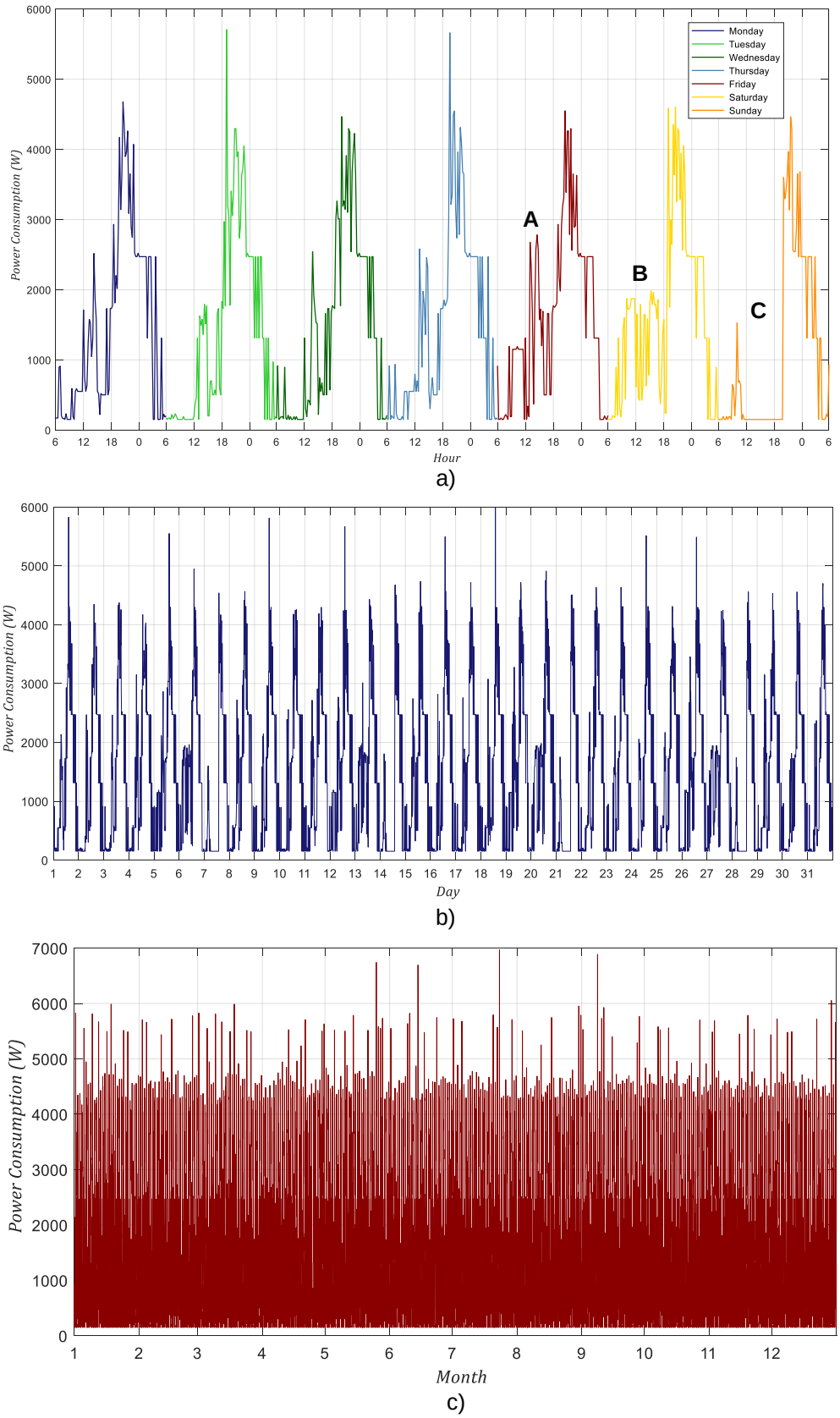

Figure 3.18 Case Study 1: Generated consumption pattern for the household under study, a) Weekly, b) Monthly and c) Yearly.

This methodology was applied in the same way to the household taken as reference for the case of study 2, Table 3.18 and Figures 3.19 and 3.20 summarize the results of the process.

Table 3.18 Case Study 2: Household appliances.

Appliance	Quantity	Average Power Consumption (W)	Average Use Time per day (h)	Average Daily Consumption (Wh)	Average Monthly Consumption (kWh)
Lights					
CFL 15W	12	15	20,02	300,30	9,01
TVs					
TV 21"	1	70	8	560,00	16,80
Fans					
Pedestal Fan 70W	5	70	41	2870,00	86,10
Others					
Fridge	1	290	8	2320,00	69,60
Washing Machine	1	400	0,57	228,00	6,84
Blender	1	400	0,16	66,40	1,99
Clothes iron	1	1000	0,4	400,00	12,00
Phone Charger	4	7,75	8	62,00	1,86
Modem Wifi/TV	2	13	32	416,00	12,48
Total	**28**	**-**	**-**	**-**	**216,68**

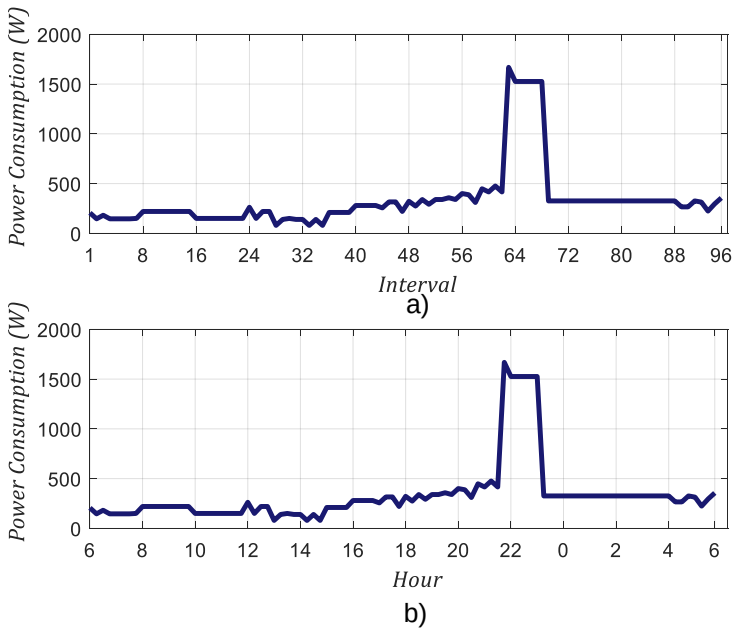

Figure 3.19 Case Study 2: Consumption pattern generated from the collected information related to each: a) time interval, b) hour of the day

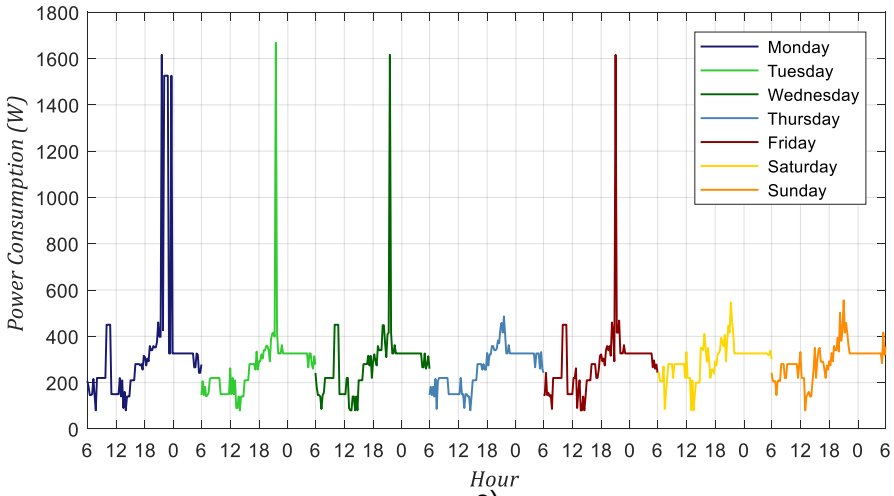

a)

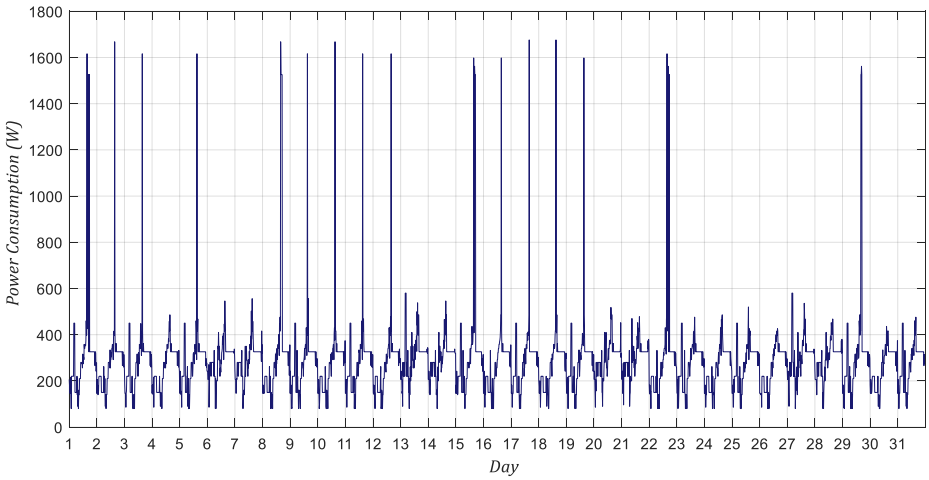

b)

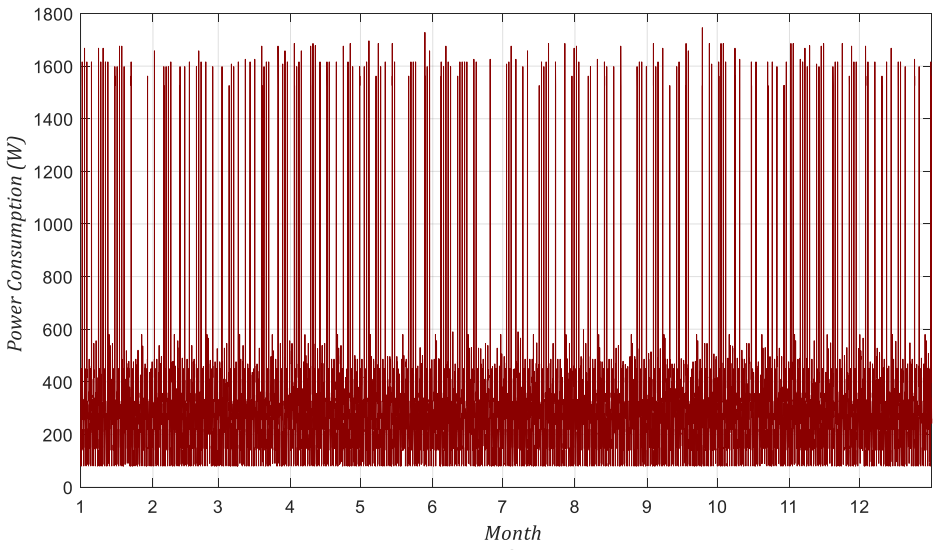

c)

Figure 3.20 Case Study 2: Generated consumption pattern for the household under study, a) Weekly, b) Monthly and c) Yearly.

3.2.5. Meteorological data for the system Simulation

The meteorological data of Global Solar Radiation and temperature necessary for the simulation of the model of the solar panel were taken from the database of the Institute of Hydrology, Meteorology and Environmental Studies of Colombia IDEAM, for which a formal request was made of the data obtained by the automatic satellite station FRANCISCO DE PAULA SANTANDER UNIVERSITY (16015110), located in the city of Cúcuta, during the period of time between 2006 and 2017, with a time interval between samples of one hour. The sample size obtained in the IDEAM response was 73592 data for the variable irradiance and 73882 for the variable temperature.

Once the meteorological data was obtained, this global data set was classified by the date the measurements were taken, thus creating subsets of daily data. The next step was to perform a processing of this subsets to analyze which of them represents a reliable data sample; for this, a similar concept to the one used in [46] was applied, to determine the maximum amount of missing data that can be tolerated in a specific group. There, although the evaluation of the data was monthly, it posed that if close 16.6% of the data of the set were lost, this set of data (days of each month) was deleted. Adapting this criterion to the daily subsets of data, and placing special emphasis on the set of data recorded between 6 a.m. and 6 p.m., which are the usual hours of sunrise and sunset during the year, only 2 of the 12 values evaluated can be lost in the analysis, being this limit the 16.6% of the sample under appraisal. In this way, the algorithm developed to do this evaluation takes the following considerations:

1. Days with more than 2 missing data are deleted of the total group of data
2. Days with 2 missing data or less use interpolation or extrapolation techniques according to the case to fill the missing values and re-build the irradiance profile of the day [46]. Interpolation method implemented in the algorithm was the Piecewise Cubic Hermite Interpolating Polynomials (PCHIP) [46], and for the extrapolation process a Polynomial Regression based on data modeling in Matlab is applied.

Figure 3.21 shows the amount of data per month before and after the processing described. After this process, the number of available samples is 51360 for the variable irradiance and 61104 for the variable temperature. The first process performed with this data set is the calculation of the Peak Sun Hours (PSH), it refers to the solar insolation which a particular location would receive if the sun were shining at its maximum value for

a certain number of hours. Since the peak solar radiation is 1 kW / m2, the number of peak hours is numerically identical to the average daily solar insolation. To calculate this value, an average of the global radiation was made for the different hours of the day, obtaining at the end the average daily solar radiation, Figure 3.22 shows the results of this process for each month of the year. Subsequently, these values were averaged obtaining a peak sun hour, calculated on an annual basis, of $PSH = 5.22\ h/day$. This is an important parameter that will be implemented later for system sizing.

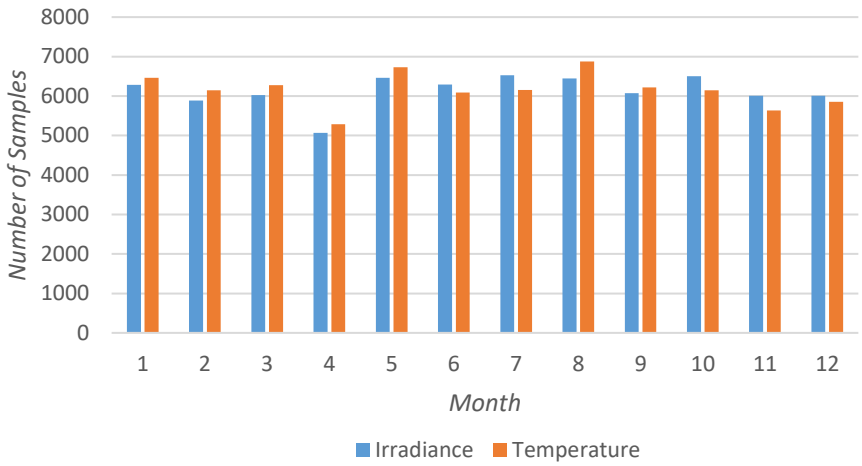

a)

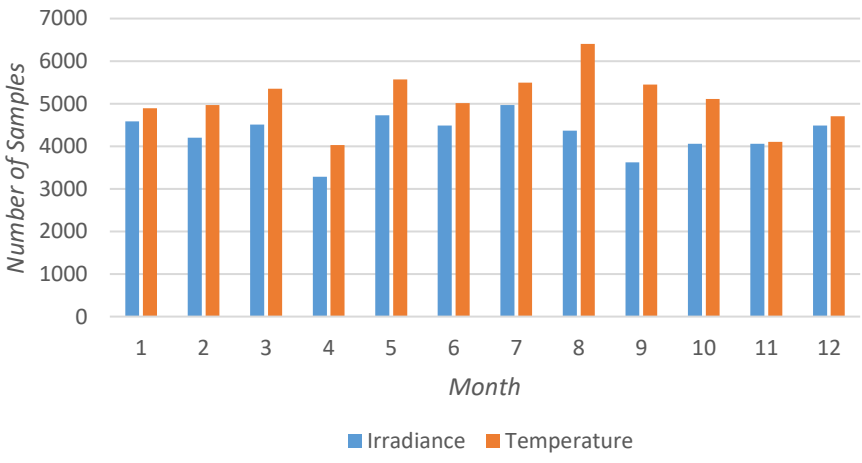

b)

Figure 3.21 Number of samples per month. a) Data supplied by IDEAM, b) Data available after the processing.

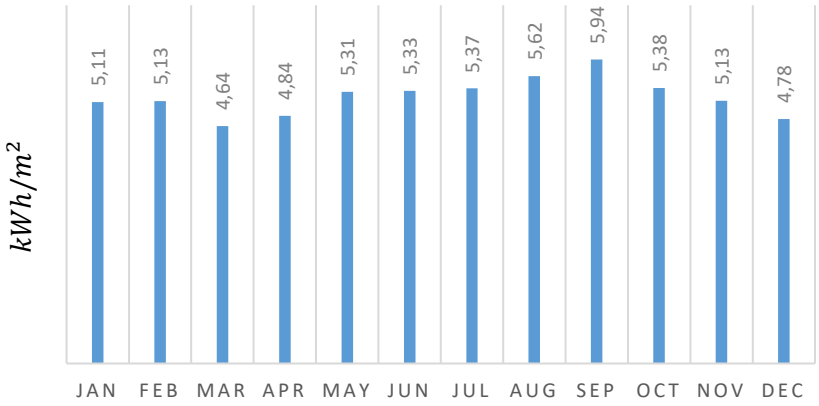

Figure 3.22 Average daily radiation per month.

Finally, with the help of the information provided by the Photovoltaic Geographical Information System (PVGIS), which is a European database where global historical records of the meteorological variables of interest for this work can be consulted; a typical year was defined within the data set provided by the IDEAM to be implemented later in the simulation of the system.

3.2.6. System sizing

Once the load profile was modeled, the different components of the system were defined and the average PSH was calculated for the city of Cúcuta, an initial sizing of the micro-grid was carried out to satisfy the annual electricity consumption needs of each of the homes under study. The design based on the average value of Peak Solar Hours is oriented to fulfill the condition expressed in Equation (3.21):

$$N_s V_{mp} N_p I_{mp} \overline{PSH} \cdot D = E_{DC} \tag{3.21}$$

Where V_{mp} and I_{mp} are the voltage an current coordinates of the MPP of a single PV module under standard conditions, N_s and N_p are the number of modules in series and the number of parallel rows forming the PV generator respectively, E_{DC} is the DC output energy generated by the PV generator along a period of time of D days having an average value of peak solar hours $\overline{PSH}$. The peak power of the PV system, P_{DCpeak}, can be written as:

$$N_s V_{mp} N_p I_{mp} = P_{DCpeak} \quad (3.22)$$

The first step of this process is to calculate the nominal power of the inverter, this is done through the following equation:

$$P_{ACPeak} = \frac{E_{AC}}{D\overline{PSH}} \quad (3.23)$$

Where P_{ACPeak} is the peak AC power and has to be smaller than the nominal inverter power, E_{AC} is the AC energy demanded by the house in one year. Table 3.19 presents a summary of the used values and the results of the calculation of the inverter's peak power when applying Equation 3.23 in the two case studies. From these results, it is established that the nominal powers for the inverters should be higher than 6.94 kW for the scenario proposed in case 1 and higher than 1.28 kW for case 2, in this order of ideas, commercial inverters are selected with powers of 7.6 kW and 1.5 kW respectively for the development of the system. These inverters were introduced in table 3.7 of section 3.1.3 and a summary of their main characteristics is presented in table 3.20.

Table 3.19 Implemented values and results from Equation (3.23)

Parameter	Value	
	Case 1	Case 2
E_{AC} (MWh)	13,2	2,45
D $(days)$	365	365
$\overline{PSH}$ (h/day)	5,21	5,21
$\boldsymbol{P_{ACPeak}}$ $\boldsymbol{(kW)}$	**6,94**	**1,28**

Table 3.20 Main parameters of selected inverters.

Parameter	Inverter	
	Primo 7.6-1	Galvo 1.5-1
Rated AC Power at 25°C (kVA)	7,6	1,5
Maximum DC Power (kW)	6,1 to 11,7	1,2 to 2,4
MPP Voltage Range (V)	250 - 480	120 - 335
Nominal Input Voltage (V)	420	260
Maximum Input Current @MPP (A)	36	13,4
Maximum Efficiency (%)	96,9	95,8
Number of MPP Trackers	2	1

Once the inverter is selected, it is possible to calculate the DC power that the photovoltaic array must deliver through the Equation (3.24), where P_{DCPeak} is the DC power of the array and η_{inv} is the inverter efficiency. When performing the calculations, it is determined that for the system developed for the scenario of case 1 the DC power of the array must be of 7.84 kW and for case 2 it must be of 1.57 kW.

$$P_{DCPeak} = \frac{P_{ACnom}}{\eta_{inv}} \tag{3.24}$$

Once the power of the array has been calculated, the next step is to define the configuration of the array, that is, the number of modules that must be connected in series and in parallel, to achieve the generation of the expected power while protecting the correct operation of the inverter. For this purpose, it is necessary to comply with the conditions expressed in the equations (3.25) and (3.26)

$$N_p \leq \frac{I_{max}}{I_{mp}} \tag{3.25}$$

$$V_{minmp} \leq N_s V_{mp} \leq V_{maxmp} \tag{3.26}$$

The first condition seeks to protect the inverter against current peaks that may cause faults in the inverter, for this reason the combined current of the branches in parallel of the array, computed as $N_p \cdot I_{mp}$, must not exceed the maximum inverter input current, I_{max}. The Fronius Primo 7.6-1 model has two MPP trackers with a total maximum input current of 36 A, taking into account that for the selected solar module $I_{mp} = 8.88\,A$, to take advantage of the two MPP trackers, a $N_p = 2$ was selected for the system of case 1. On the other hand, the Fronius Galvo 1.5-1 inverter has a single MPP tracker with a maximum input current of 13.4 A, taking into account the value of I_{mp}, the number of modules in parallel for the case 2 system has to be equal to $N_p = 1$. Now, taking into account that $V_{mp} = 37.2\text{V}$ for the selected pv module, N_s can be calculated from Equation (3.22), resulting in $N_s = 12$ for the system of case 1, and $N_s = 5$ for the system of case 2. With these values it is possible to check if the condition expressed in Equation (3.26) is fulfilled, this seeks to ensure that the voltage of the PV generator, computed as $N_s \cdot V_{mp}$, is between

the limits of the MPP tracker of the inverter (V_{minmp}, V_{maxmp}). Table 3.21 summarizes the results of the system sizing for each case study and compliance with these conditions can be verified. On the other hand, Figure 3.23 shows the results of the simulation of the PV generation systems for one year, there it is possible to detail the power generation profiles and observe that in neither of the two cases the allowed operating limit for the selected inverters is exceeded.

Regarding the initial battery sizing, to ensure a good level of matching between the generation of energy by the PV array and its consumption, it has been assessed in previous studies that an effective energy storage capacity of 60% of the average daily is needed [43, 44]. Additionally, to protect the battery lifespan and optimize its operation, operating limits were established between 90% and 20% of the nominal battery capacity as will be explained in the following section, leaving a usable effective capacity of 70%. Taking this into account, Table 3.22 presents the selected capacities for the batteries in each of the case studies.

Table 3.21 PV generator sizing results

Parameter	Value	
	Case 1	**Case 2**
Inverter	Fronius Primo 7.6-1	Fronius Galvo 1.5-1
Rated AC Power at 25°C (kVA)	7,6	1,5
Maximum Inverter Efficiency (%)	96,9	95,8
PV array Peak DC power (kW)	7,84	1,57
Number of parallel branches	2	1
PV generator max Current (A)	17,76	8,88
Maximum Inverter Input Current @MPP (A)	36	13,4
Number of modules in series	12	5
PV generator max Voltage (V)	446,4	186
Inverter MPP Voltage Range (V)	250 - 480	120 - 335
PV generator nominal Power (kWp)	7,92	1,65

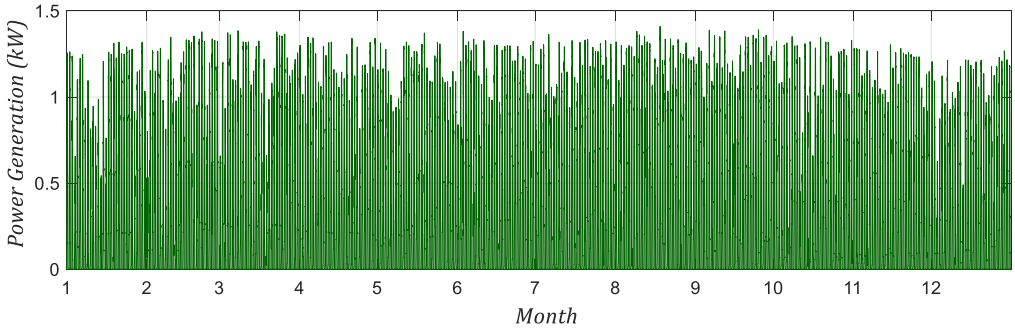

(a)

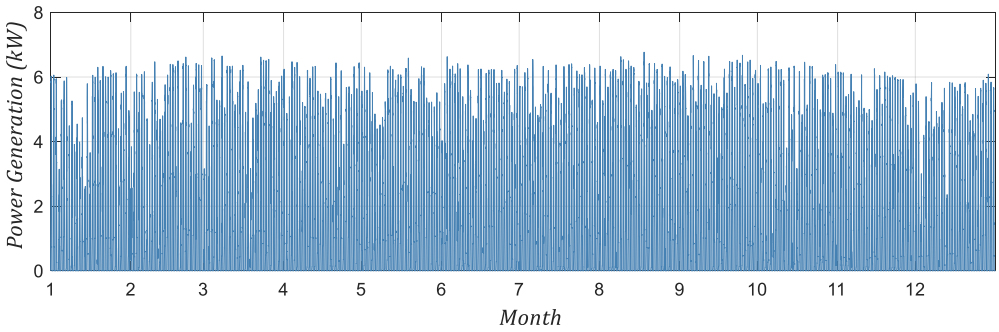

(b)

Figure 3.23 Annual power generation profile: a) Case 2 and b) Case 1

Table 3.22 Battery Sizing results

Parameter	Value	
	Case 1	**Case 2**
Average Annual Consumption of electrical energy (MWh)	13,2	2,45
Average Daily Consumption of electrical energy (kWh)	36,16	6,71
Usable battery capacity needed (kWh)	21,69	4,02
Nominal capacity of the battery (kWh)	31	5,74

3.3. Optimization of system operation

3.3.1. Previous criteria and system analysis

To ensure the optimal management of the ESS and a proper operation of the micro-grid, it is necessary to optimize the battery's charging and discharging to adjust them to the generation of energy by the PV generator and the demand of electricity of the household appliances and its load pattern. Generally, this optimization is carried out to fulfill two main objectives, the reduction of costs in the electricity bill [45] and the reduction of the negative impact that the presence of the micro-grid can generate in the main electricity grid [46], being one of these objectives prioritized in the development of the control system. In the first case, optimization to maximize the economic benefit, the control system that performs battery management is usually designed to take advantage of Time of Use (TOU) or Real-Time (RTP) pricing models in which the cost of the electric energy imported from the grid varies for the different day hours; in this way an economic benefit can be obtained by charging the battery not only from the energy excess generated with the PV system, but also when charging the battery from the electricity grid in hours of low price, to then use this energy in hours where the price per kWh is higher [45]. On the other hand, when the objective of the control system is to reduce the impact that the micro-grid generates due to power exchanges with the grid, the control strategy is aimed to smoothing this energy exchange profile, charging the battery from the excesses generated by the PV system or from the grid, to then use that energy in the hours of peak consumption. Table 3.23 presents a summary of the criteria used to evaluate the power exchange profile with the grid.

Table 3.23 Criteria used to evaluate the power exchange profile with the grid [47, 48, 49].

Criteria	Description
Positive and Negative Grid Power Peaks	The positive and negative grid power peaks, $P_{G,max}$ and $P_{G,min}$, are defined as the maximum value of the power delivered by the grid and the maximum value of the power fed into the grid in one year, respectively, and can be computed from the following equations: $$P_{G,max} = \max(P_{GRID}) \quad (3.27)$$ $$P_{G,min} = \min(P_{GRID}) \quad (3.28)$$
Maximum Power Derivative (MPD)	MPD represents the maximum rate-of-change (i.e., the slope of two consecutive samples, being the sampling period $Ts = 15$ min) of the grid power profile in the year under study. The MPD is defined as the maximum absolute value of the slopes during one year, it is expressed in W/h and can be computed from Equation (3.29) , where $\dot{P_{Grid}}$ is the grid power profile ramp-rate defined in Equation (3.30), n is the sample index. $$MPD = \max(\lvert \dot{P_{GRID}} \rvert) \quad (3.29)$$ $$\dot{P_{Grid}}(n) = [P_{Grid}(n) - P_{Grid}(n-1)]/Ts \quad (3.30)$$
Average Power Derivative (APD)	APD is defined as the absolute value of the annual average value of the slopes of two consecutive samples. It is expressed in W/h and can be computed from Equation (3.31), where N is the number of samples in a year. $$APD = \frac{1}{N}\sum_{n=1}^{N} \lvert \dot{P_{Grid}}(n) \rvert \quad (3.31)$$
Energy Dependence with the Grid (EDG)	This criterion quantifies the need of energy coming from the main grid. Note that if $EDG = 1$ the micro-grid does not depend on the energy supplied by the main grid, and if $EDG = 0$ the micro-grid is totally dependent on the main grid. EDG can be computed from the following equation, $$EDG = \frac{E_{load,a} - E_{\sup grid,a}}{E_{load,a}} \quad (3.32)$$ Where, $E_{load,a}$ is the annual energy consumed by the load and $E_{\sup grid,a}$ is the annual energy supplied by the grid.

Power Profile Variability (PPV)

This is defined as the square root of the sum of the squares of the power harmonics evaluated during one year, relative to the constant component, i.e., the yearly mean power absorbed by the micro-grid. PPV can be computed from Equation (3.32),

$$\boldsymbol{PPV} = \frac{\sqrt{\sum_{f=f_i}^{f_f} {P_{Gridf}}^2}}{P_{DC}} \tag{3.33}$$

Where, P_{Gridf} is grid power harmonic at *f* frequency, f_i and f_f are the initial and final frequencies, respectively, and P_{DC} is the yearly power average value. This indicator only evaluates frequencies above $f_i = 1.65x10^{-6}\ Hz$ (i.e., one week or less variation periods), since the energy management strategy seeks to compensate daily variations. Furthermore, because the sample period is 15 min, the maximum frequency considered to calculate the PPV is half the sampling frequency, i.e., the Nyquist frequency, in this case $f_f = 5.55x10^{-4}\ Hz$, corresponding to 30 min variations.

Taking this into account, to carry out the optimization of battery operation, a methodology similar to that implemented in [45] was followed, there, every day before midnight, the energy management system (EMS) optimizes the scheduling of the battery bank for the next 24 hours using the forecasted load profile, PV generation profile and the day-ahead electricity pricing information, dividing this 24 hours of the day in 96 intervals of 15 minutes each. The EMS calculates the average power transfer to the battery and the energy transfer over the selected time intervals and sends this information to the power management system. Then the power management system calculates instantaneous references (power references, current references and/or voltage references) for the component level controllers. For the system developed in this study, the following additional considerations were taken into account, firstly, due to the electricity tariff system implemented in the city of Cúcuta, which consists of a flat tariff that remains constant throughout the day, and that the tariffs for the injection of surplus energy to the grid are always lower than the price of the energy imported from the grid, as explained in section 3.1.1, the most economically viable option for the operation of the system with batteries is the self-consumption; in this way, optimizing the operation of the system will be done with the objective of maximize the amount of energy that is stored in the battery coming from the PV system, being this the only source of energy to charge the battery, to be used later in hours of low or null generation, thus reducing the amount of energy imported from the grid and therefore, the expenses in the monthly electricity bill. Additionally, the schedule

generated by the optimization process begins at 6 o'clock in the morning, to coincide with the average sunrise time, at which the generation of energy by the PV system can begin.

Before starting the optimization process, it is necessary to identify the power flows through the different components of the micro-grid, in order to define the profile of power exchange with the grid, and the constraints in its operation. In Figure 3.24 it is possible to observe the notations used to represent the power flow averaged over a time interval of $\Delta t = 15\ min$ measured at points A, B, C, and D. The arrows to the right in the figure indicate the direction of positive power flow. According to this sign convention, battery discharging and power injection into the grid are considered as positive. η_{ch} and η_{inv} represents the efficiencies of the battery charger and the inverter respectively.

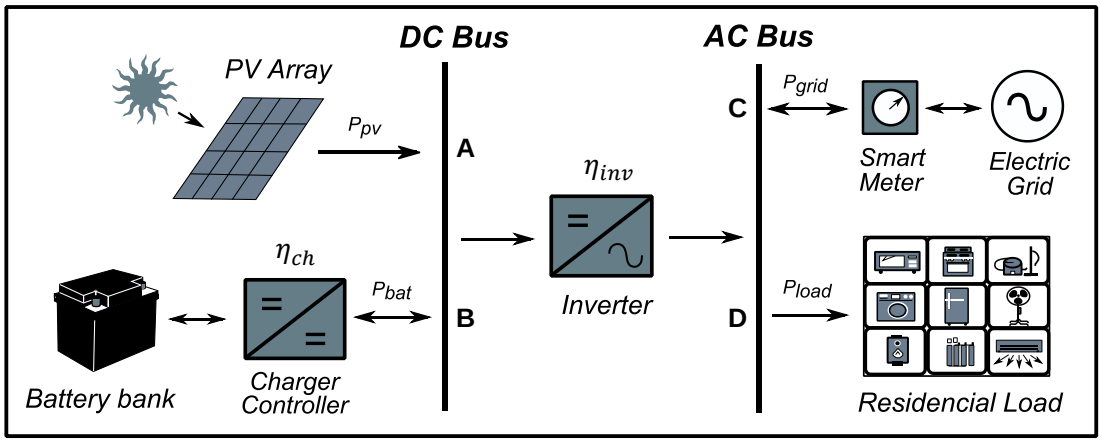

Figure 3.24 Configuration of the micro-grid. Arrows to the right indicate the direction of positive power flow**.**

For the system shown in Figure 3.24, the power balance equation at the k_{th} time interval ($\{k \in \mathbb{Z}^+\}$), can be written as follows:

$$\eta_{inv}\left(P_{pv}(k) + \eta_{\mathrm{ch}} P_{bat}(k)\right) = P_{GRID}(k) + P_{load}(k) \tag{3.34}$$

Where $P_{pv}(k)$ represents the power generated by the PV system in the interval k, $P_{bat}(k)$ is the power injected or extracted from the battery in the interval k, $P_{load}(k)$ is the power demanded by the load in the interval k, and $P_{GRID}(k)$ is the power exported to the grid, when it is positive, or imported from the grid, when it is negative, in the interval k. From Equation (3.34) $P_{GRID}(k)$ can be defined as follows:

$$P_{GRID}(k) = \eta_{inv}\left(P_{pv}(k) + \eta_{ch}P_{bat}(k)\right) - P_{load}(k) \quad (3.35)$$

Once the power balance equation is established, the operation of the system components is limited by a set of physical constraints including rated power, rated capacity, maximum current, and maximum and minimum voltage. In this DC-coupled configuration, the battery discharging and charging rate is determined by the ratings of the battery itself. In addition, the power flow through the grid converter should be below or equal to the grid converter rating. Hence, the following constraints hold:

$$-I_{ch,rated} \leq I_{bat}(k) \leq I_{dis,rated} \quad (3.36)$$

$$P_{pv}(k) + \eta_{ch}P_{bat}(k) \leq P_{inv,rated} \quad (3.37)$$

The purpose of the constraint established in the Equation (3.36) is to protect the battery against currents of charge and discharge that exceed the limits established by the manufacturer, ensuring the correct operation of the battery and the conservation of its useful life. There $I_{ch,rated}$ is the rated charging current and $I_{dis,rated}$ is the rated discharging current of the battery. On the other hand, the Equation (3.37) seeks to protect the inverter from input power higher than the nominal conditions established by the manufacturer, there $P_{inv,rated}$ is the rated capacity of the system inverter**.**

Now, in order to establish a model of the behavior of the energy storage system for the optimization of its functioning Figure 3.25(a) illustrates the steady state equivalent circuit of the battery where E_b is the open circuit voltage and R_{bat} is the internal resistance. In Figure 3.25(b) It´s possible to observe the open circuit voltage vs the SOC characteristic of the lithium-ion battery considered in this study. Unlike other battery types, the voltage profile of a lithium-ion battery is very flat in the SOC range 20-90 %, and the voltage is relatively high close to the fully charged state. High voltages cause the cells to deteriorate, therefore shortens the battery lifetime. Hence, it is not desirable to fully charge lithium-ion batteries [45]. As the open circuit voltage over the acceptable operating range does not vary significantly, it can be assumed to be constant. Then the battery voltage is given by Equation (3.38) where a negative I_{bat} means a battery charging.

$$V_{bat} = E_b - I_{bat}R_{bat} \quad (3.38)$$

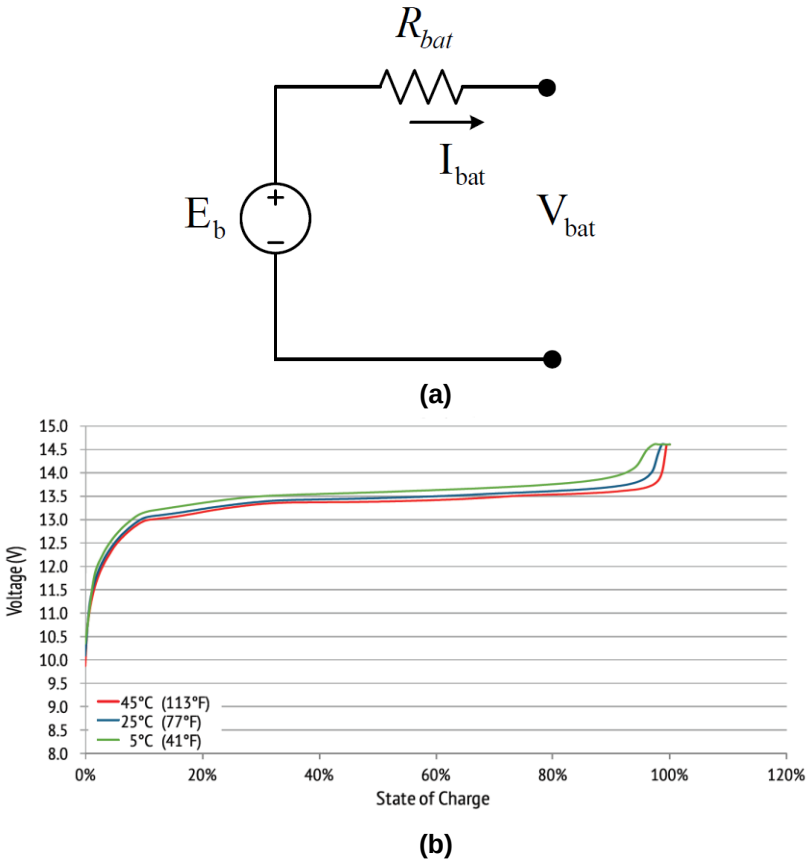

Figure 3.25 a) Equivalent battery model, b) Charge voltage characteristics at various temperatures @0.2C from [39].

The SOC of the battery at the k^{th} time step $k = \{1, 2, 3, \dots, N\}$ can be found from coulomb counting [45], For the charging process, $I_{bat}(k) < 0$:

$$SOC(k) = SOC(k-1) - \frac{\eta_{chrg} I_{bat}(k) \Delta t}{C_{bat}} \tag{3.39}$$

For the discharging process $I_{bat}(k) > 0$:

$$SOC(k) = SOC(k-1) - \frac{I_{bat}(k) \Delta t}{\eta_{dischrg} C_{bat}} \tag{3.40}$$

Where C_{bat} is the nominal capacity of the battery in Ah, whereas η_{chrg} and $\eta_{dischrg}$ are the charging and discharging efficiencies (coulomb efficiency) of the battery, respectively. The battery efficiency depends on the battery current. It is lower at higher currents and vice versa. However, for simplification it is assumed that the battery efficiency

is constant at different operating conditions. Further, that the charging and discharging efficiencies of the battery are the same and equal to the square-root of the battery round-trip efficiency ($\eta_{bat,rt}$).

$$\eta_{chrg} = \eta_{dischrg} = \sqrt{\eta_{bat,rt}} \tag{3.41}$$

For the optimization porpoise, the state of charge (SOC) of the battery should be maintained within certain limits to prolong the battery lifetime. This is expressed in Equation (3.42), where SOC_{min} and SOC_{max} are the minimum and maximum allowable SOC stablished as 20% and 90% of the battery nominal capacity respectively. Additionally, the net energy transfer from the battery during a planning horizon is expected to be zero, in order to maintain the continuity of the battery operation. This constraint is expressed in Equation (3.43). There, N is the total number of discrete intervals per optimization time horizon. $\mathrm{N} = \mathrm{T}/\Delta\mathrm{t}$, where T is the optimization time horizon.

$$SOC_{min} \leq SOC(k) \leq SOC_{max} \tag{3.42}$$

$$\sum_{k=1}^{N} P_{bat}(k)\Delta t = 0 \quad or \quad SOC(0) = SOC(N) \tag{3.43}$$

3.3.2. Optimization Process

This non-linear constrained optimization problem is solved using dynamic programming [45, 46]. As mentioned in section 2, in dynamic programming, the optimization problem is structured into multiple stages, where each stage is comprised of collective states. The optimization is solved using the forward induction process, where the initial stage is analysed first and the problem is solved moving forward one stage at a time until all stages are included. In this particular case, the stages represent different N time intervals of 15 minutes in the 24 hours problem's planning horizon, while discretized SOC with a step size of SOC_{step} corresponds to the states of the system and are given by the following equation,

$$States = \frac{SOC_{max} - SOC_{min}}{SOC_{step}} \tag{3.44}$$

Once the number of states is established, the next step is to establish all the possible trajectories that the SOC of the battery could take when passing from one stage to the next one, to illustrate this, Figure 3.26 shows the possible trajectories for change in SOC from one stage to the other from the initial stage up to three stages. As shown in the figure, the allowable range of variation for the SOC is between SOC_{min} and SOC_{max} to fulfil the constraint given in Equation (3.42). In the figure, ΔSOC_{ij} represents the change in SOC along the trajectory from the i^{th} state in the k^{th} stage to the j^{th} state in the $(k+1)^{th}$ stage. After this is done, corresponding ΔSOC_{ij} values are calculated trough Equation (3.45).

$$\Delta SOC_{ij} = SOC_i(k) - SOC_j(k+1) \tag{3.45}$$

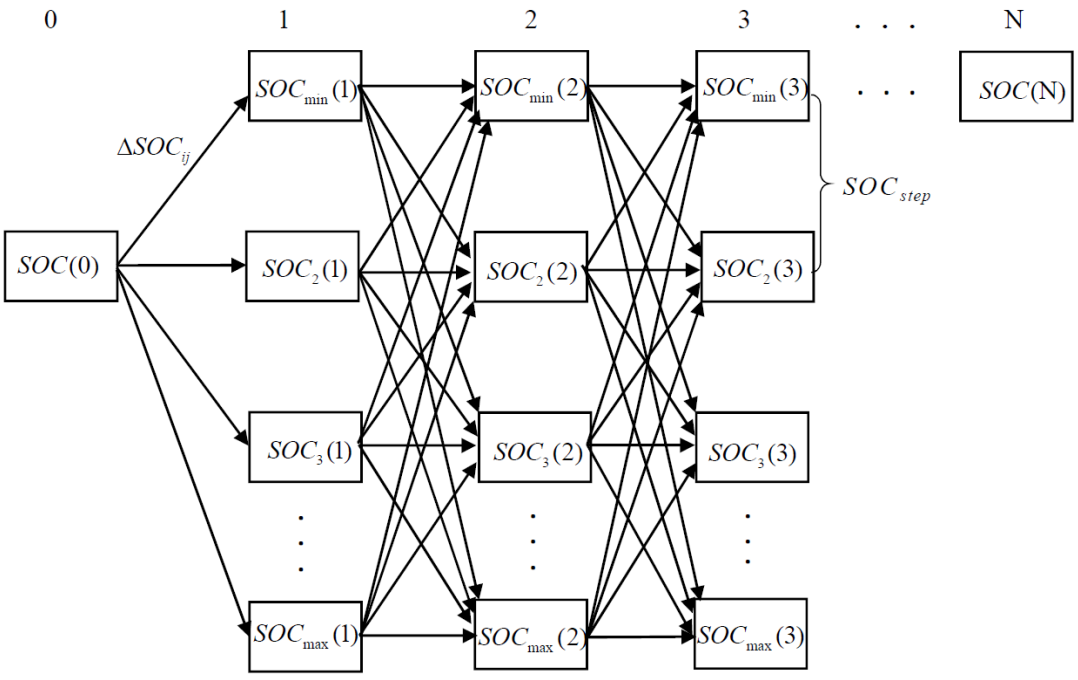

Figure 3.26 Optimization trough Dynamic programming: System stages, states and all possible trajectories between the stages from [45].

Then, the average currents flowing in or out over all trajectories are calculated from the Equation (3.46) for $\Delta SOC_{ij} < 0$, that is, when the battery charging process is performed

and the SOC in the next stage $(k+1)$ is greater than the SOC in the actual stage k, and from the Equation (3.47) for $\Delta SOC_{ij} \geq 0$, that is, when the battery discharging process is performed and the SOC in the next stage $(k+1)$ is lower than the SOC in the actual stage k.

$$I_{bat} = \frac{C_{bat}}{\eta_{chrg}\Delta t}\Delta SOC_{ij} \tag{3.46}$$

$$I_{bat} = \frac{C_{bat}\eta_{dischrg}}{\Delta t}\Delta SOC_{ij} \tag{3.47}$$

While doing this, all the trajectories that violate the constraint given in Equation (3.36) are rejected. Then the average power flowing to/from the battery is calculated from Equation (3.48), where the battery voltage V_{bat} is found using Equation (3.38).

$$P_{bat} = V_{bat}I_{bat} \tag{3.48}$$

At this point, in order to optimize the operation of the battery for self-consumption the following considerations are taken into account:

When $\eta_{inv}P_{pv}(k) > P_{load}(k)$:

- First, the excess of energy has to be used to charge the battery. Then all state changes between stages, or "trajectories", that lead to the discharge of the battery are discarded, allowing only those that charge the battery.

- If the excess energy is higher than the power limits that can be delivered to the battery in that interval of time for its correct operation, the surplus surpluses that cannot be stored will be injected to the grid.

When $\eta_{inv}P_{pv}(k) < P_{load}(k)$:

- The lack of energy will be covered by discharging the energy stored in the battery. Then all the charging trajectories are rejected. The amount of discharging energy

is determined by the amount of the lack of energy, under no circumstance energy from the battery will be injected into the grid.

- If there is not stored energy, the load should be supply by the grid.

At this point, all the trajectories that violate the constraint of the inverter nominal power given in Equation (3.37) are rejected. Next, the average power transfer from/to the grid is calculated from Equation (3.35), from this equation it is possible to observe that the only control variable to modify the amount of power, therefore the energy, which is exported/imported to/from the grid in a certain interval k, is the amount of energy that will be stored in or will be extracted from the battery. in economic terms, because the tariff for electric energy remains constant throughout the day, the representative cost function over all feasible trajectories are calculated from the following equation:

$$Cost(k) = \begin{cases} E_{GRID}(k) \cdot Y_{Feed-in} + E_{bat}(k) \cdot Y_{Bill} & ; P_{GRID}(k) > 0 \\ E_{GRID}(k) \cdot Y_{Bill} & ; P_{GRID}(k) < 0 \end{cases} \quad (3.49)$$

The upper equation considers the exports of energy to the grid ($P_{GRID}(k) > 0$), there it is established that the cost for that given interval k is given by the amount of energy injected into the grid $E_{GRID}(k)$ multiplied by the feed-in tariff $Y_{Feed-in}$ as expressed in the first term of this equation, on the other hand, the second term of the equation gives a representative value to the energy stored in the battery, which consists of the quantity $E_{bat}(k)$ multiplied by the price of the electric power established by the grid operator Y_{Bill}, since this stored energy will be used later to supply the demand of the loads avoiding the necessity for import energy from the grid, and therefore, representing the savings as result of this storage. As mentioned in section 2, $Y_{Feed-in}$ is always lower than Y_{Bill}, for this reason, the cost function is maximized, interpreted as increasing the benefits, as more energy is stored in the battery, the main objective of its use for self-consumption.

The lower equation represents the cost function for importing energy from the grid; for these intervals the amount of energy extracted from the battery is implicit in the calculation of $P_{GRID}(k)$ ($E_{GRID}(k)$ as a result), being these inversely proportional. In this way

the cost function is maximized by extracting the greatest amount of energy from the battery, decreasing as a consequence the amount of energy imported from the grid, and therefore increasing the benefits. At this initial point there are no special considerations regarding the amount of energy injected into the grid, optimization is done to maximize the benefits. Then, the optimum trajectory from stage 0 to stage N, which results in maximum benefits, is found using forward induction.

To evaluate the impact of the optimization Figure 3.27 presents the profile of power exchange with the grid for one year for the study case 1, which represents the micro-grid with the highest installed power, and Table 3.24 summarizes the results of the parameters calculated to evaluate it, this additionally presents the information of the annual cost of the energy bill. As can be expected in this situation, the peaks of maximum and minimum power correspond to the peaks of generation and consumption of the load respectively with values that exceed the | 6 kW |, the value of the MPD is close to 22 kW/h, the APD is in the order of 2.2 kW/h while the PPV has a value of 147.42, to improve the grid profile these values should be decreased. On the other hand, the EDG is 0.22, which means that only 22% of the energy demanded by the loads is covered by the PV generator, in order to improve the performance of the system, the value of this parameter must be increased. Finally, the price of the annual electricity bill is presented as an indication of the economic impact of the system, in this scenario it has a value of -141.14 €, the negative sign indicates that the annual balance delivers a debt for this amount with the operator of the electric grid.

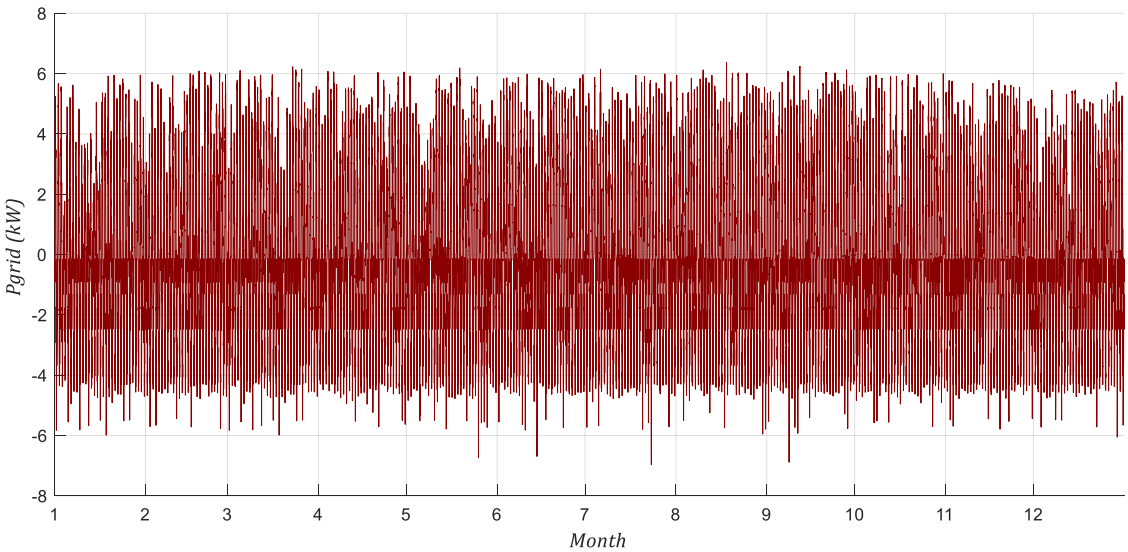

Figure 3.27 Power exchange with the grid without battery.

Table 3.24 Computed evaluation Criteria – System Without Battery

$P_{G,max}$ (kW)	$P_{G,min}$ (kW)	MPD (W/h)	APD (W/h)	EDG	PPV	$Annual\ Bill$ (€)
6,36	-6,97	21874,09	2241,00	0,22	147,42	-141,14

3.3.2.1. Optimization to maximize benefits

Figure 3.28 presents the results for the first optimization, which main objective is to maximize the benefits by storing the maximum amount of energy in the battery and then be used for self-consumption. On the left, Figure 3.28(a) presents the results of the optimization, there it is possible to observe in the upper graph the profiles of power generation "PV Power", and demand by the loads "Pload", for the different 96 stages of optimization, starting from 6 a.m., evidencing the low correlation between them. In the first half of the 24-hour optimization horizon (the first 48 stages), it can be observed that the generation of energy exceeds, most of the time, the demand by the loads, therefore, almost from the beginning of the optimization there is an excess of energy, which is used to start charging the battery as can be seen in the central graph, this presents the profiles of power exchange with the battery "Pbattery", power injection to the grid "Pgrid", in addition to Pload dotted as a guide. The negative values of Pbattery represent a flow of energy towards the battery for its charge. At this point, all the excess energy goes to the battery, so that it is charged quickly and reaches the maximum allowed SOC of 90% on stage 30 as can be seen in the lower graph that shows the evolution of the SOC through the optimization period.

Once the battery has been charged, the excess energy must be injected into the grid, represented by the positive peak power of Pgrid on stage 31, maintaining this positive flow until the generation level falls below of the demand by the loads on stage 44. At this point the battery begins to be discharged to supply the energy demand of the home, Pbattery presents positive values, and as can be seen in the graph, the power quantity extracted from the battery is limited by the level of demand, thus no battery energy is injected into the grid. The discharge of the battery continues until reaching the lower limit of the SOC, set at 20%, after this, the battery goes into stand by and the demand for energy is covered by the grid, represented by the negative values of Pgrid.

On the right, Figure 3.28(b) presents the results of the simulation of the system with the model developed in simulink. For this simulation the same radiation and temperature data used to make the prediction in the optimization process were used, so that the error due to the prediction is neutralized in order to evaluate only the performance of the optimization strategy. The sensitivity of the optimization to the error in the prediction will be evaluated later in this section. In this way, Figure 3.28(b) presents the same profiles explained above, with the addition of the power profile of the inverter "Pinverter" plotted on the upper graph, and for these graphs on the x axis the corresponding time of day is shown. In this way it is possible to observe a good correspondence between the forecasted behavior in the optimization and the behavior of the simulation of the system, observing some variations, product of the differences between the models, like the discharge of the modelled battery slightly faster reaching the limit of 20% before the forecasted, creating as consequence an extra energy consumption form the grid to supply the demand.

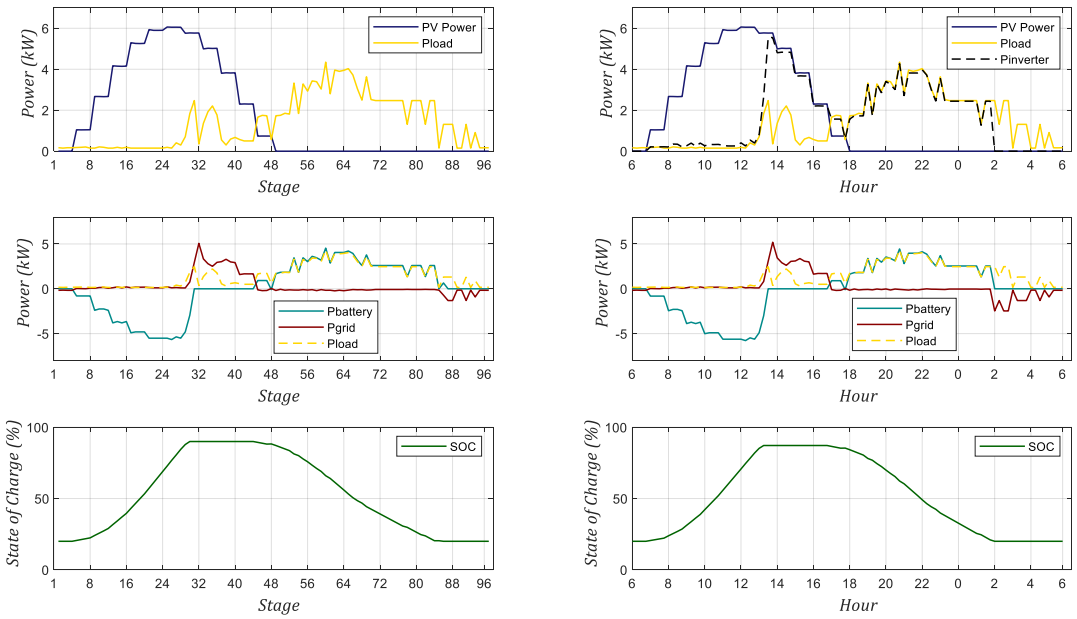

Figure 3.28 Optimization for maximizing the benefits: Power and SOC profiles. a) Optimization process and b) Simulation results.

Figure 3.29(a) presents the profile of the SOC during the simulated year, as evidenced by this, it is kept within the limits of safe operation to guarantee the useful life of the battery thanks to the optimization process. On the other hand, Figure 3.29(b) shows the energy exchange profile with the grid, product of the battery management through the optimization strategy to maximize the benefits. Table 3.25 summarizes the results of the

calculation of the evaluation criteria. As can be seen in the figure, this profile still has high peaks of injection and extraction of energy from the grid, up to 6.23 kW and 5.72 kW respectively, due to the occasional loss of control derived from rapid battery charging and discharging. Consequently, although the APD is reduced by 58.6% to 927 W/h, the MPD increases by 9.4%, to 23.9 kW/h, and the PPV increases by 24.4%, to 183.49, on the other hand the EDG increases to 0.82, which means that now 82% of the demand is supplied with the energy generated and stored in the battery, an increase of 60% in relation to the scenario without a battery. Finally, the debt for the annual energy bill is reduced to 61.78 €, which represents a saving of 56.6%.

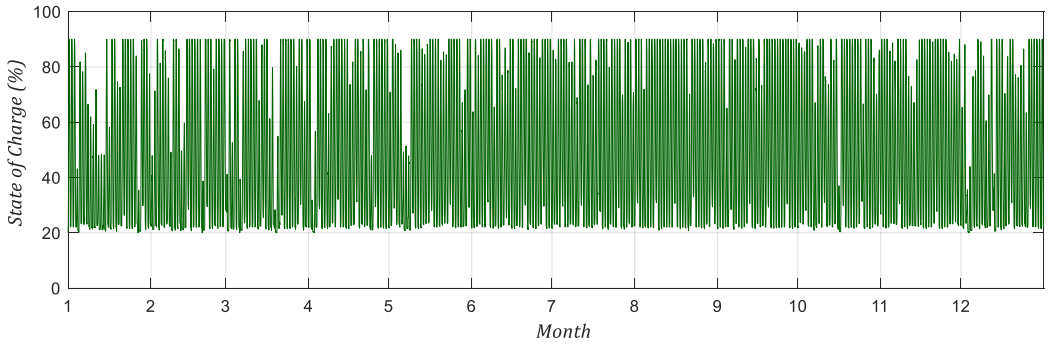

(a)

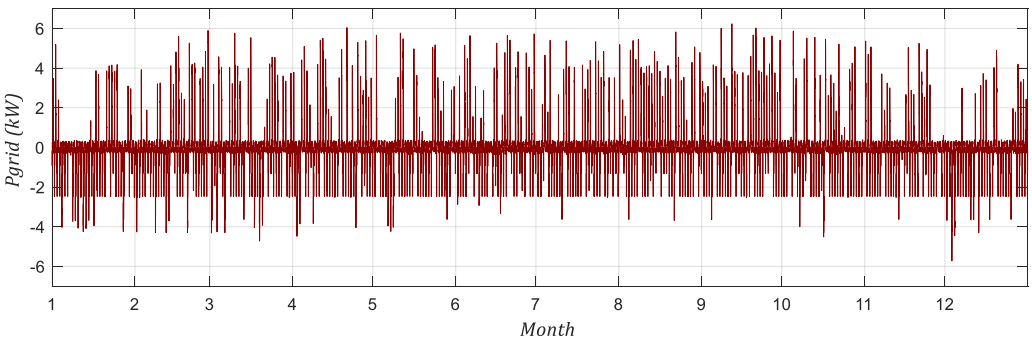

(b)

Figure 3.29 Optimization for maximizing the benefits: Simulated Annual Profiles. a) SOC and b) Power exchange with the grid.

Table 3.25 Computed evaluation Criteria – Optimization for maximizing the benefits

$P_{G,max}$ (kW)	$P_{G,min}$ (kW)	MPD (W/h)	APD (W/h)	EDG	PPV	$Annual\ Bill$ (€)
6,23	-5,72	23931,26	927,21	0,82	183,49	-61,78

3.3.2.2. Optimization with fixed Injection/Extraction power limits

Looking for a better performance of the energy exchange profile with the grid, a second optimization strategy is proposed, this seeks to use the battery to set the power limits injected and demanded to/from the grid. For this purpose, in addition to what has been done in the previous optimization process, a power limit is set to allow injection peaks up to this level and surpluses are used to charge the battery, in the same way, a limit is established for the extraction of power from the grid and when the demand exceeds this limit, the energy stored in the battery is used to supply the loads. Through the performance of different simulations, and also taking into account the objective of maximizing self-consumption, the best performance of the optimization was obtained with of the use of the battery for an injection limit of 0.5 kW and an extraction limit of 2 kW. Figure 3.30(a) presents the results of the optimization process, in this opportunity it is observed that for the first half of the optimization horizon, when there are surpluses of energy resulting from the generation of the PV array, after supplying the loads, the energy is injected into the grid up to a limited power of 0.5 kW and the rest is stored in the battery. Despite this, a peak of injection power still exists around the stage 34 because the battery reaches a SOC of 90%. On the other hand, the power demand from the grid is allowed up to the limit of 2kW, when this is reached, the energy stored in the battery is drained to feed the household's demand. Figure 3.30(b) presents the results of the simulation of the model.

Figure 3.31 shows the annual profiles for the SOC and the power exchange with the grid, while table 3.26 presents a summary of the parameters used to evaluate the power profile. As can be seen in Figure 3.31 (a) the SOC is maintained within the operation limits, however in Figure 3.31 (b) the presence of power peaks reaching 5.83 kW for injection and 5.72 kW for the extraction can be evidenced, again due to the occasional loss of control because the full charge of the battery. On the other hand, the MPD is reduced by 7.25% to a value of 20.3 kW/h, the APD is reduced by 50.42% to a value of 1.11 kW/h, while the PPV increased by 1.53% with respect to the scenario without battery. The value of the EDG is 0.76, that is, 76% of the energy demand is supplied by the PV generation and the battery, an increase of 54% and the annual debt for the electricity bill was reduced by 48.13% up to the value of € 73.21.

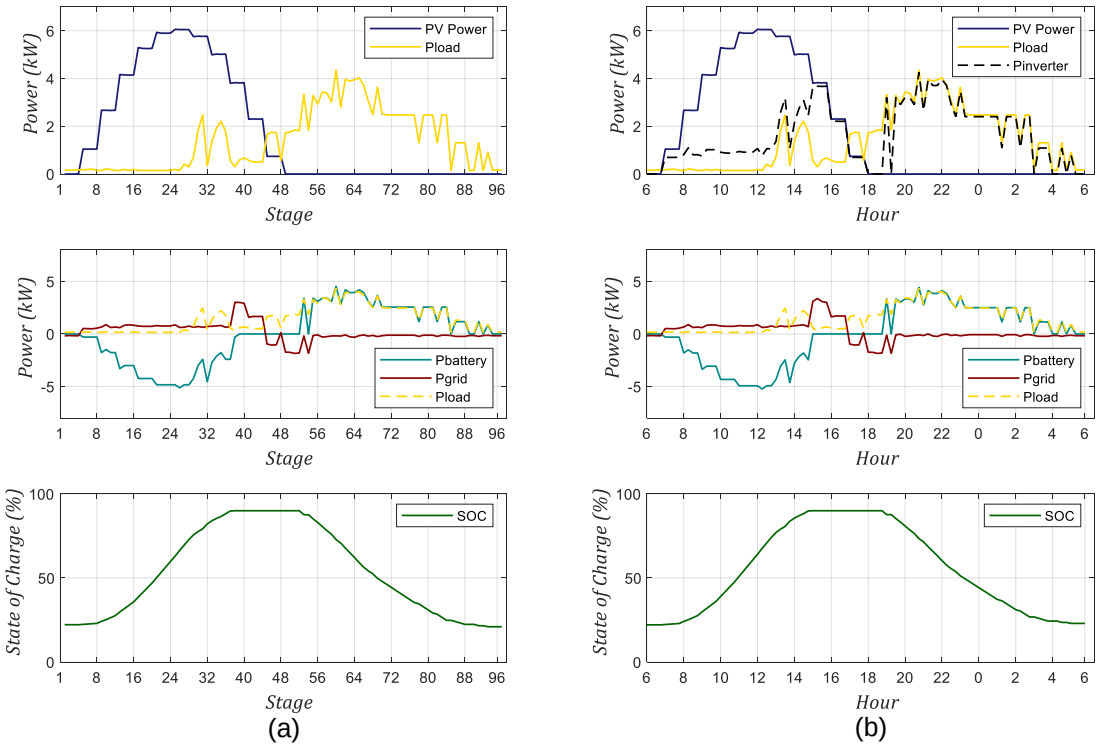

Figure 3.30 Optimization with fixed Pgrid Limits: Power and SOC profiles. a) Optimization process and b) Simulation results.

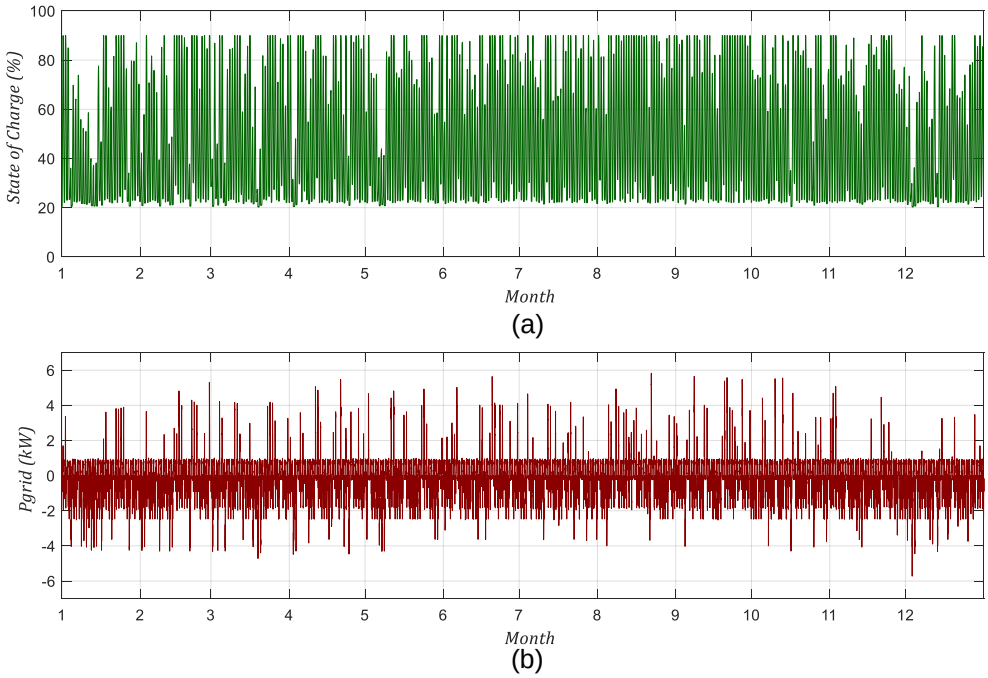

Figure 3.31 Optimization with fixed Pgrid Limits: Simulated Annual Profiles. a) SOC and b) Power exchange with the grid.

Table 3.26 Computed evaluation Criteria – Optimization with fixed Pgrid limits.

$P_{G,max}$ (kW)	$P_{G,min}$ (kW)	MPD (W/h)	APD (W/h)	EDG	PPV	$Annual\ Bill$ (€)
5,83	-5,72	20287,51	1110,98	0,76	-149,69	-73,21

3.3.2.3. Optimization with proposed Adaptive Injection/Extraction Limits

The problem of establishing fixed limits lies in the variability that the profiles of PV generation and demand by the loads can present, with days of high and low generation, as well as days with higher or lower demand for electrical energy. To solve this problem, the implementation of adaptive limits is proposed, that allow the control system to handle the aforementioned variations, while seeking to maximize self-consumption. For this, a philosophy similar to the previous process is followed, including in the dynamic programming the optimization of the limits of injection and extraction. The operation of this optimization is based on the fact that to maximize self-consumption, it is necessary to ensure the battery charge at the highest possible SOC with the generation of PV energy for the analyzed day, as well as the use of all that stored energy to supply the demand by the loads. The optimization of the use of the battery for maximum benefit represents the case with limits of injection and extraction to/from the grid with a value of zero, in this way, as explained above, all the excesses of energy are stored in the battery until it is reaches a maximum SOC, depending on the available energy, up to 90%, and then use this stored energy to meet the demand of the loads until the SOC drops to 20%. With this in mind, the search for the optimal value for these limits begins by assigning them a value of zero, the optimization of battery operation for the 24-hour horizon is performed and the maximum and minimum values of the SOC are analyzed for the process of charge and discharge of the battery respectively. In the case of the power injection to the grid limit, if the SOC does not reach a value of 90%, it is interpreted that the surplus energy can be completely stored in the battery, so no peaks exceeding the established limit are expected, on the contrary, if the SOC reaches 90%, power surpluses may be presented that will be injected into the grid causing peaks that exceed the limit; if this occurs, the limit is increased by a fixed value, the optimization of the battery operation and the evaluation of the SOC is done again. This process is repeated until finding the injection power limit that allows the battery to be charged up to the maximum level while avoiding power peaks. For the case of the power extraction limit from the grid, a similar procedure is followed, in this occasion the

optimization looks for the limit that allows to discharge the battery to the lowest level, while avoiding the presence of peaks in the power demand from the grid.

Figure 3.32(a) presents the results of this optimization process, for this particular day the power injection limit to the grid was established by the optimization process in 1.2 kW and the extraction limit was established in 0.3 kW, in the graph it is possible to observe that the profile Pgrid presents a flatter behavior without peaks, product of a better control of the SOC of the battery, which reaches its limits in a more moderate way compared to the optimization strategies presented before. Figure 3.32(b) shows the results of the simulation of the system model.

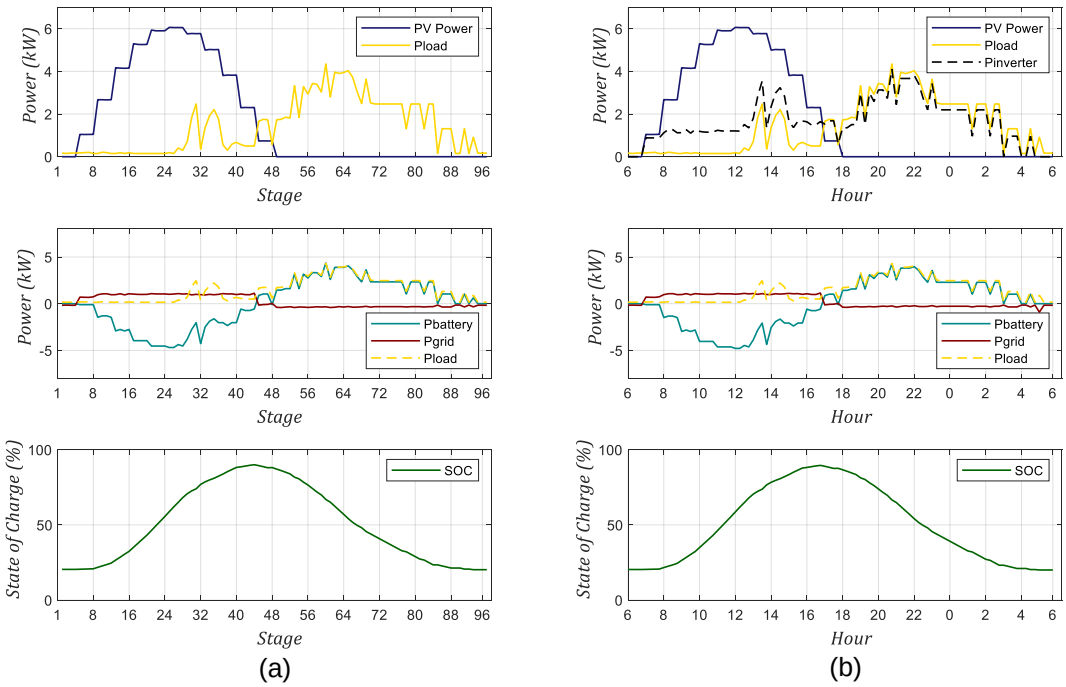

Figure 3.32 Optimization with adaptive Pgrid Limits: Power and SOC profiles. a) Optimization process and b) Simulation results.

Figure 3.33 shows the annual profiles for the SOC and the power exchange with the grid, while table 3.27 presents a summary of the parameters used to evaluate the power profile. As can be seen in Figure 3.33(a) the SOC is maintained within the operation limits, and, as a consequence of the adaptive limits optimization process, Figure 3.33(b) presents a more stable profile for power exchange with the grid, reaching peaks up to 2 kW for injection and 3.68 kW for the power extraction. MPD is reduced by 57.6% to a value of 9.28 kW/h, the APD is reduced by 82.3% to a value of 397.2 W/h and the PPV is reduced

by 75.6% with respect to the scenario without battery, to a minimum value of 36.03. The value of the EDG is 0.84, that is, 84% of the energy demand is supplied by the PV generation and the battery, an increase of 62%, and the annual debt for the electricity bill was reduced by 49.45% up to the value of € 71.35.

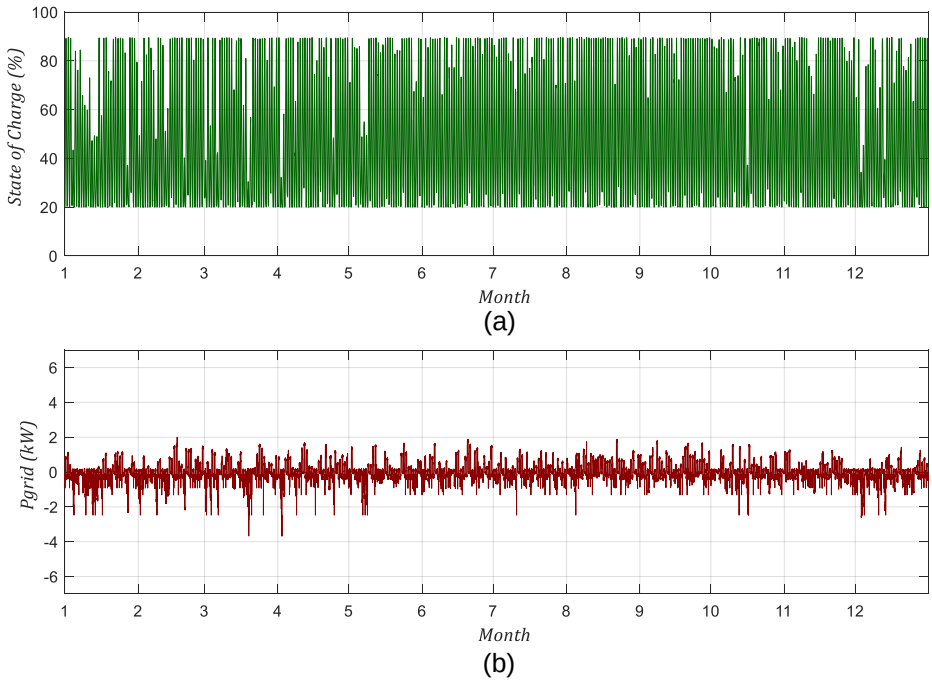

Figure 3.33 Optimization with adaptive Pgrid Limits: Simulated Annual Profiles. a) SOC and b) Power exchange with the grid.

Table 3.27 Computed evaluation Criteria – Optimization with adaptive Pgrid limits.

$P_{G,max}$ (kW)	$P_{G,min}$ (kW)	MPD (W/h)	APD (W/h)	EDG	PPV	$Annual\ Bill$ (€)
2,00	-3,68	9280,00	397,22	0,84	-36,03	-71,35

Table 3.28 presents a comparison of the performance of the different optimization strategies for the operation of the battery. There, strategy 1 corresponds to optimization for maximum benefit, strategy 2 corresponds to optimization with fixed injection/extraction limits, and strategy 3 corresponds to the optimization with adaptive injection/extraction power limits. For these strategies the evaluation parameters are represented as percentages of the parameters calculated for the case of the system without battery, in this way a negative percentage indicates a reduction in the value of the parameter, while a

positive percentage indicates an increase in its value. As shown in the table, strategy 3 presents the best results regarding the criteria for evaluating the power exchange profile with the grid, while obtaining a good impact on the annual value of the electricity bill; for this reason, this strategy was used to perform the optimization of the system operation for subsequent analyzes.

Table 3.28 Comparison of the different optimization strategies for the battery operation.

Parameter	Without Battery	Opt. Strategy 1	Opt. Strategy 2	Opt. Strategy 3
$P_{G,max}$ (kW)	6,36	6,23	5,83	**2**
$P_{G,min}$ (kW)	-6,97	-5,72	-5,72	**-3,68**
MPD (kW/h)	21,87	+9,4 %	-7,3 %	**-57,6 %**
APD (kW/h)	2,24	-58,6 %	-50,4 %	**-82,3 %**
EDG	0,22	+60,0 %	+54,0 %	**+62,0%**
PPV	147,42	+24,5 %	+1,5 %	**-75,6 %**
$Annual\ Bill$ (€)	-141,14	-56,3 %	-48,1 %	**-49,5 %**

3.3.2.4. Analysis of the sensitivity to the Forecast Error

Because the optimization process of the battery operation is based on the forecast of the generation profile and demand of electrical energy by the loads, the correct operation of this is affected by the error that may exist in that forecast. For the forecast of the load profile, as explained in section 3.2.4, it is possible to characterize the energy demand per hour and per day from the consumption trends of the inhabitants of the household, therefore it is possible to obtain a forecast of the demand quite close to the real behavior, then this factor does not exert great influence in the optimization process. On the other hand, forecasting the power generation by the PV system is a more complex process due to the large number of factors that can influence. For this reason, in this section an analysis of the sensitivity of the optimization process to the errors in the forecast of the PV power

generation is made. As an initial point is taken into account what is described in [51, 52], where it is mentioned that currently there are forecasting methods, which implementing Physical-deterministic methods based on the NOCT thermal model of the PV module and hybrid stochastic-deterministic models combining the Clear Sky Solar Radiation Model (CSRM) and Artificial Neural Networks (ANN), can reach Normalized Mean Absolute Errors (NMAE) between 6% to 9% in the PV power forecast. To evaluate the performance of the optimization process under these conditions, the irradiation and temperature profiles were modified to introduce NMAE of 6%, 8% and 9% in the PV power forecasts and new simulations were carried out including them; additionally, the persistent forecast method was evaluated, there the PV generation profile of the last day is used to forecast the next day PV generation profile. NMAE is computed from Equation (3.50), where S is the number of samples considered for the analysis, C is the net capacity of the plant (i.e. it is the maximum DC output power measured in the whole period), P_m is the measured power and P_f is the forecasted power [52].

$$NMAE_{\%} = \frac{1}{S \cdot C} \sum_{i=1}^{S} |P_m - P_f| \cdot 100 \tag{3.50}$$

To deal with the forecast errors an additional control block was added to the system model in SIMULINK, this is responsible for limiting the charge/discharge power of the battery P_{batt}, according to the available power (product of the PV generation) in real time. This is a simple control that operates as follows: if the currently available P_{PV} power is lower than forecasted one, P_{batt} is adjusted to the new level; on the other hand, if P_{PV} is greater than forecasted one, P_{batt} remains at the forecasted level. Tables 3.29 and 3.30 summarizes the performance of the optimization strategy for different the different NMAE values and the persistent forecast case, to compare the performance of the system without battery and the performance of the ideal optimization performed when evaluating the optimization strategy 3 are also included as reference points. As can be expected, as the NMAE increases, the performance of the optimization strategy worsens, however, these variations are still within acceptable operating margins providing considerable improvements to the energy exchange profile with the grid, while maintaining an acceptable economic benefit. The worst performance was obtained with the optimization with the persistent forecast, for this case the NMAE was computed as 13.7%. from these results it

can be concluded that the implementation of the optimization strategy is viable, obtaining better results as the forecast of the PV generation is improved.

Table 3.29 Comparison of the performance of the optimization strategy for different NMAE - Values.

Scenario	$P_{G,max}$ (kW)	$P_{G,min}$ (kW)	MPD (kW/h)	APD (kW/h)	EDG	PPV	$Annual\ Bill$ (€)
Without Battery	**6,36**	**-6,97**	**21,87**	**2,24**	**0,22**	**147,42**	**-141,14**
Ideal Opt. Strat. 3	2,00	-3,68	9,28	0,39	0,84	36,03	-71,35
NMAE = 6%	2,98	-4,00	9,55	0,68	0,81	42,72	-76,55
NMAE = 8%	3,82	-4,051	13,59	0,78	0,80	49,20	-78,36
NMAE = 9%	4,05	-4,071	14,40	0,85	0,79	52,57	-79,81
Persistent Forecast	5,12	-5,83	21,97	0,88	0,76	66,30	-84,31

Table 3.30 Comparison of the performance of the optimization strategy for different NMAE – Percentage of improvement related to the case Without Battery.

Scenario	$P_{G,max}$ (kW)	$P_{G,min}$ (kW)	MPD (kW/h)	APD (kW/h)	EDG	PPV	$Annual\ Bill$ (€)
Without Battery	**6,36**	**-6,97**	**21,87**	**2,24**	**0,22**	**147,42**	**-141,14**
Ideal Opt. Strat. 3	-68,6%	-47,2%	-57,6%	-82,6%	62,0%	-75,6%	-49,4%
NMAE = 6%	-53,1%	-42,6%	-56,3%	-69,6%	59,0%	-71,0%	-45,8%
NMAE = 8%	-39,9%	-41,9%	-37,9%	-65,2%	58,0%	-66,6%	-44,5%
NMAE = 9%	-36,3%	-41,6%	-34,2%	-62,1%	57,0%	-64,3%	-43,5%
Persistent Forecast	-19,5%	-16,4%	0,5%	-60,7%	54,0%	-55,0%	-40,3%

Chapter 4. Evaluation of the case studies: Results and Discussion.

The developed model of the system allows to carry out a sensitivity analysis to determine the optimal PV generator and battery size for each of the cases under study. This analysis is achieved by executing different simulations modifying the parameters of interest and using the results to calculate the criteria, on the one hand, technicians that allow to evaluate the profile of power exchange with the grid and on the other hand economic that allow to evaluate the viability of the investment, for a correct sizing of the micro-grid that allows to obtain the least impact when connected to the electric grid, for the benefit of the operator, while ensuring a maximum economic benefit, to obtain greater profitability for the end user.

4.1. Case Study 1

The analysis begins with the comparison of the performance of the system in relation to the power exchange profile with the grid, for different sizes of the battery. To this end, simulations of the system's annual performance were made for batteries with capacities between 5.12 kWh and 35.84 kWh, configurations available through the implementation of the lithium ion battery model RB100 manufactured by ReLion, while the installed power of the PV generator remains constant at 7.9 kWp and the forecast error is not included in the simulations to isolate the influence of these parameters in the analysis performed.. Table 4.1 presents the results of the calculations made for the different parameters of interest defined for the evaluation of the power profile, and Figure 4.1 shows these results in a graphical way for easy comparison. As can be seen in the figures 4.1 a), b), c) and d), as the battery size increases, the parameters APD, MPD, PPV, $P_{G,max}$ and $P_{G,min}$, are reduced, which indicates a better behavior of the power exchange profile with the grid. At the same time, as can be expected, increasing the size of the battery increases the EDG, which implies that a greater percentage of the annual energy demand is covered by the micro-grid, resulting in an annual reduction of up to 49.5% on the electricity bill, as can be observed in Figures 4.1 e) and f), there, negative values for the annual bill represent a debt with the grid operator for that value. From these results it is defined that the system

with a battery with a capacity of 35.84 kWh presents the best performance, in the same way, analyzes performed for larger sizes indicated an oversizing of the battery without greatly improving the performance of the system which leads to unnecessary expenses in the installation of the energy storage system.

Table 4.1 Case Study 1 - 7.9 kWp System: Comparison of system performance for different battery sizes.

Battery Capacity (kWh)	$P_{G,max}$ (kW)	$P_{G,min}$ (kW)	MPD (kW/h)	APD (kW/h)	EDG	PPV	$Annual\ Bill$ (€)
Without Battery	**6,36**	**-6,97**	**21,87**	**2,24**	**0,22**	**147,42**	**-141,14**
5,12	5,24	-4,54	17,50	1,57	0,30	193,93	-133,63
10,24	4,63	-3,08	15,24	1,22	0,39	235,12	-121,86
15,36	3,64	-3,67	14,75	0,94	0,51	481,73	-111,81
20,48	3,13	-3,68	14,06	0,77	0,60	212,41	-102,00
25,60	2,71	-2,68	11,89	0,57	0,69	130,35	-87,31
30,72	2,29	-3,67	10,05	0,49	0,77	54,69	-80,59
35,84	2,00	-3,68	9,28	0,40	0,84	36,03	-71,35

Once the storage capacity of the battery was defined, an analysis of the impact of the PV generator size on the performance of the system was carried out, for which simulations of systems with installed PV capacity of 5.3 to 9.9 kWp, limited by an installation area of about 60m^2, were carried out; this time the capacity of the battery remains constant and again the error in the forecast is excluded to avoid the influence of these parameters in the analyzed results. Table 4.2 presents the different configurations implemented to simulate different PV system sizes, the model developed in section 3.2 was adapted to include these changes.

Table 4.3 and Figure 4.2 present the results obtained for the analysis of the power exchange with the grid profile, for the system implemented with battery and without it for purposes of comparison and visualization of the influence of the battery on the operation of the micro-grid, this last one is represented by the letters NB, and is plotted with a dotted line in the figures. In Figures 4.2 (a) and (b), it can be seen that for the APD and MPD

parameters, the system with a 7.9 kWp size and a battery bank, presents the best performance when registering the lowest values, although the other systems present close results . On the other hand, in Figure 4.2 (c) it can be seen that for the PPV parameter, this system presents the worst performance when registering the highest value, probably because for this system the level of generation is closer to the consumption level, which leads to a greater variation in the exchange of power with the grid, in comparison with the larger systems where there is more PV energy to feed the loads in a more constant way, or in smaller systems where there is a deficit of Energy and electricity is imported from the grid more commonly. On the other hand, EDG, represented in Figure 4.2 (d), increases as the size of the PV do it as well, improving the percentage of the load demand that is covered by this system. Finally Figure 4.2 (e) presents the maximum power peaks of the exchange profile with the grid, as can be expected, as the generator size increases, the energy injection peaks do so in the same way, while the peaks of power extraction from the grid decrease with this, because there is more energy available to be stored in the battery and supply the subsequent demand by the loads.

Table 4.2 Case Study 1: Different configurations implemented for the simulation of the micro-grid**.**

Parameter	PV Generator				
	1	**2**	**3**	**4**	**5**
PV generator nominal Power (kWp)	5,3	6,6	7,9	9,2	9,9
Number of parallel branches	2	2	2	2	2
Number of modules in series	8	10	12	14	15
Model of the Inverter	Primo 6.0-1	Primo 7.6-1	Primo 7.6-1	Primo 10.0-1	Primo 10.0-1
Rated AC Power at 25°C (kVA)	6	7,6	7,6	10	10

To expand the information presented above, Table 4.4 and Figure 4.3 presents an analysis of the annual energy exchange with the grid, there the levels of Energy Generation and Consumption, Energy Exportation to the grid (H2G) and Importation from the gird (G2H), the Energy Importation Reduction, Energy Stored (Std) and Extracted (Exd) to/from the battery and Annual balance of the energy bill are reported, for the cases of the system implementation with and without battery (NB).

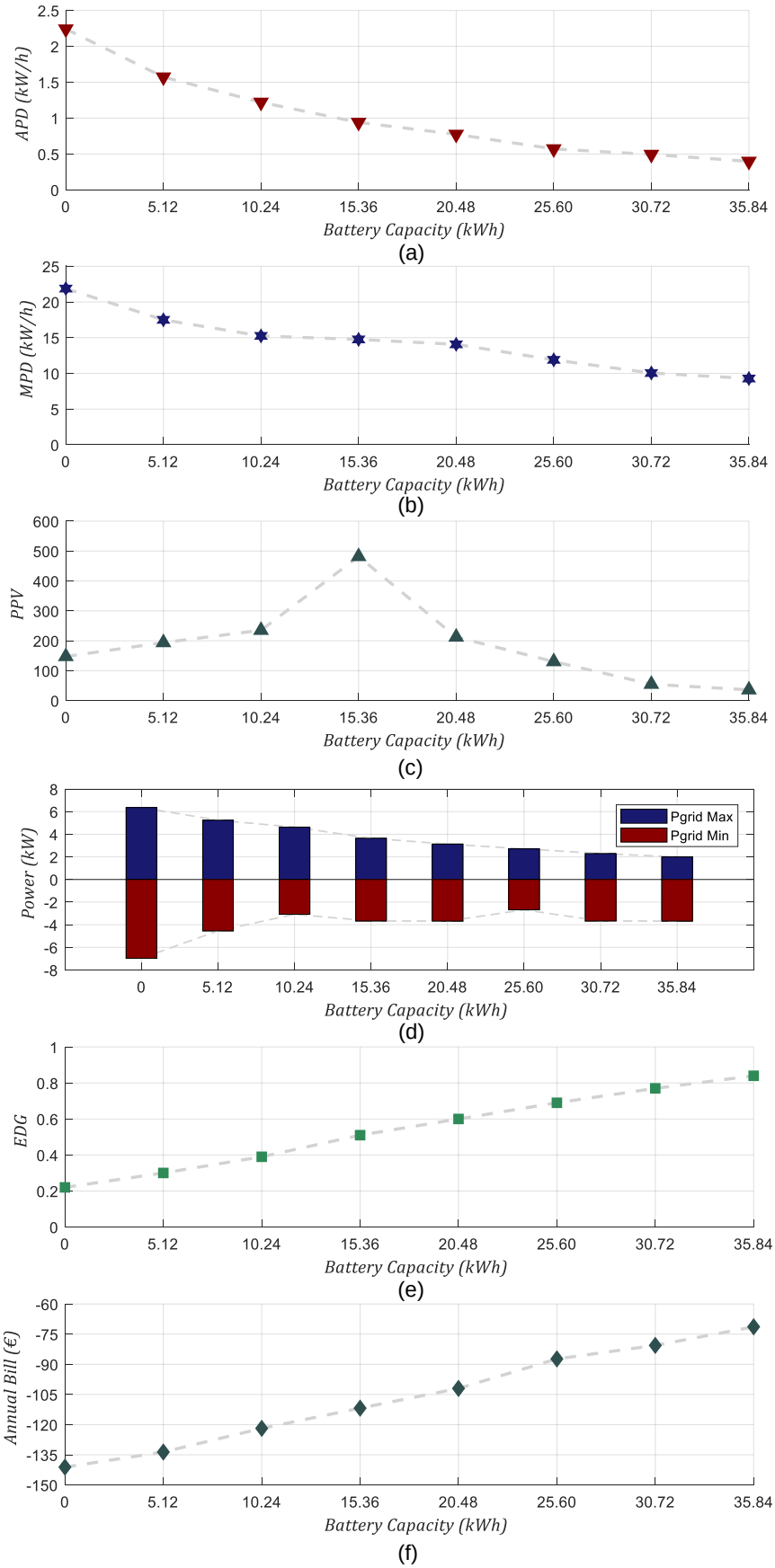

Figure 4.1 Case Study 1 - 7.9 kWp System**:** - Comparison of system performance for different battery sizes. a) APD, b) MPD, c) PPV, d) $P_{G,max}$ and $P_{G,min}$, e) EDG and f) $Annual\ Bill$.

Table 4.3 Case Study 1 – 35.84 kWh Battery: Comparison of system performance for different PV Generator Nominal Power.

PV Generator Nominal Power (kWp)		$P_{G,max}$ (kW)	$P_{G,min}$ (kW)	MPD (kW/h)	APD (kW/h)	EDG	PPV
5,3	**NB**	4,14	-6,97	18,46	2,09	0,21	6,33
	B	0,49	-3,68	11,65	0,57	0,61	1,46
6,6	**NB**	5,25	-6,97	19,7	2,16	0,22	15,01
	B	1,24	-3,67	10,59	0,44	0,74	2,25
7.9	**NB**	6,36	-6,97	21,87	2,24	0,22	147,42
	B	2	-3,07	9,51	0,4	0,83	35,97
9.2	**NB**	7,42	-6,97	23,96	2,32	0,23	16,41
	B	2,76	-2,86	11,32	0,41	0,85	3,91
9.9	**NB**	7,96	-6,97	25,42	2,36	0,23	11,67
	B	3,11	-2,67	12,59	0,43	0,87	2,77

Table 4.4 Case Study 1 – 35.84 kWh Battery: Analysis of the annual energy exchange with the grid

PV Generator Nominal Power (kWp)		Gen. (MWh)	Con. (MWh)	H2G (MWh)	G2H (MWh)	Battery Energy (MWh)		Annual Bill (€)
						Std	Exd	
5,3	**NB**	8,90	12,62	5,79	9,97	4,96	4,75	-643,75
	B			1,04	5,49			-615,96
	Red. (%)			82,07	44,94			
6,6	**NB**	11,13	12,62	7,88	9,88	6,77	6,47	-377,13
	B			1,37	3,73			-337,26
	Red. (%)			82,58	62,25			
7.9	**NB**	13,35	12,62	10,05	9,82	7,76	7,42	-136,83
	B			2,54	2,70			-74,06
	Red. (%)			74,71	72,53			
9.2	**NB**	15,58	12,62	12,06	9,78	8,17	7,80	-8,86
	B			4,19	2,35			67,33
	Red. (%)			65,28	75,93			
9.9	**NB**	16,69	12,62	13,13	9,76	8,31	7,93	50,51
	B			5,12	2,19			128,59
	Red. (%)			61	77,51			

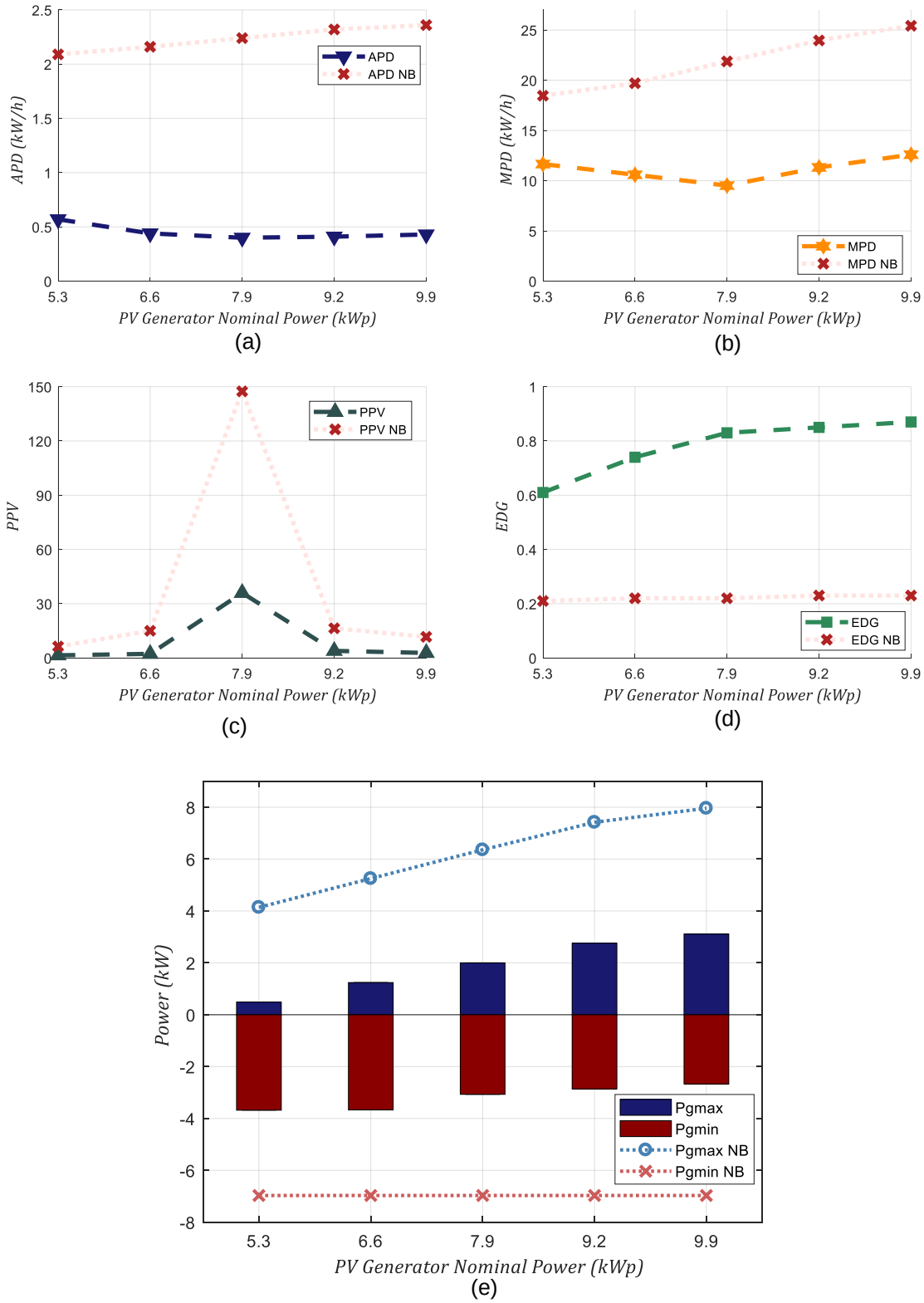

Figure 4.2 Case Study 1 – 35.84 kWh Battery System: Comparison of system performance for different PV generator sizes. a) $\boldsymbol{APD}$, b) $\boldsymbol{MPD}$, c) $\boldsymbol{PPV}$, d) $\boldsymbol{EDG}$ and e) $\boldsymbol{P_{G,max}}$ and $\boldsymbol{P_{G,min}}$.

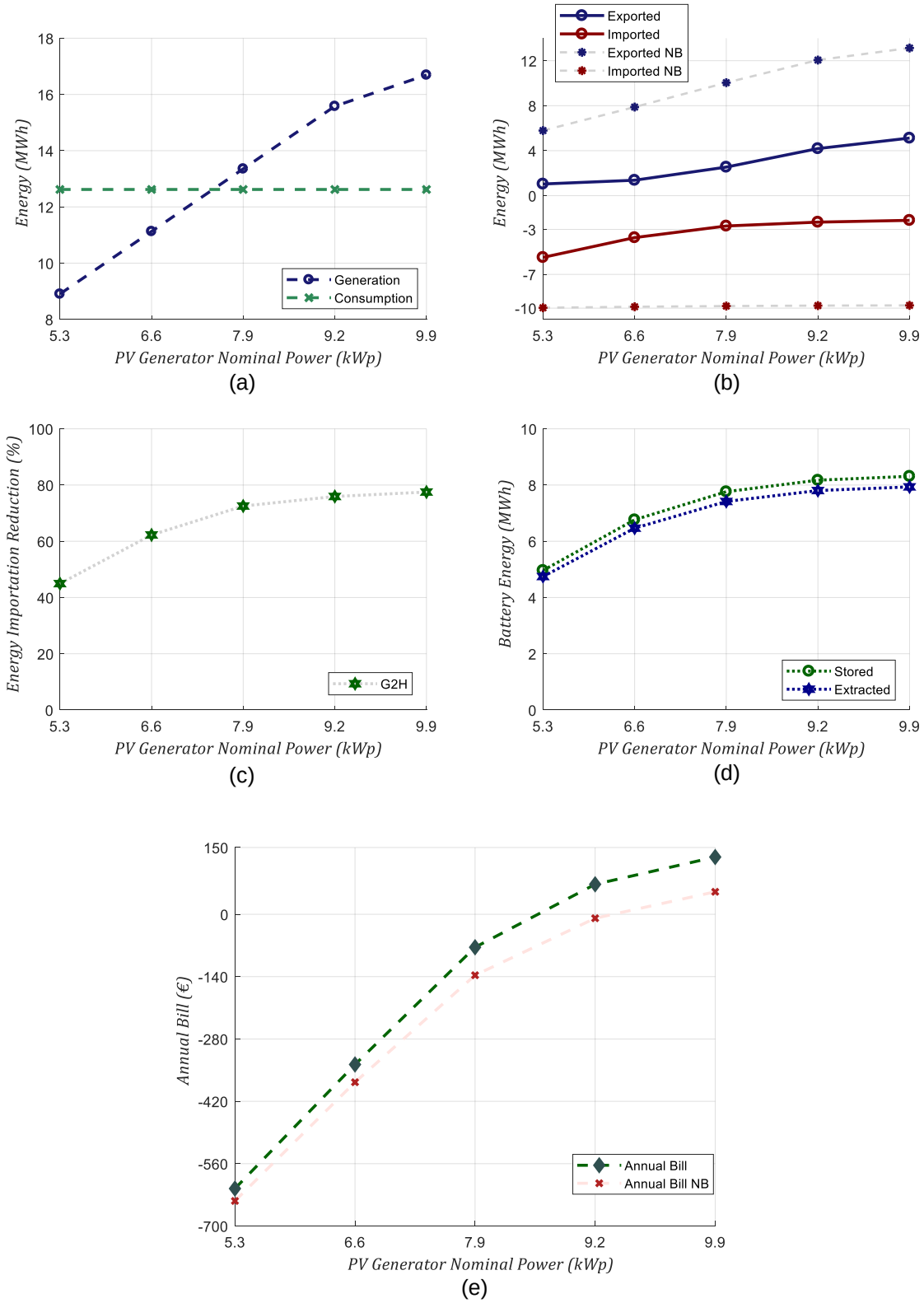

Figure 4.3 Case Study 1 – 35.84 kWh Battery: Analysis of the annual energy exchange with the grid. a) Energy Generation and Consumption, b) Energy Exported to the grid H2G and Imported from the gird G2H, c) Energy Importation Reduction, d) Energy exchange with the battery, e) Annual balance of the energy bill.

In Figure 4.3 (a) it can be seen that the power generation levels exceed the consumption level from a PV generator size equal or bigger than 7.9 kWp. Figure 4.3 (b) shows how the level of exportation grows as the size of the generator increases, while the import of energy from the grid decreases, here are presented as reference the values of export and import of energy for the system without battery, and Figure 4.3 (c) shows the percentage of reduction in the import, plotting the above described. Figure 4.3 (d) presents the values for the energy stored and extracted from the battery, and finally Figure 4.3 (e) shows the variations in the annual electricity bill with respect to changes in the size of the system. As can be seen, the most favorable values for the final consumer are obtained for the larger systems, reaching a profit of up to € 128.59 for the system with an installed generation capacity of 9.9 kWp under the actual electricity tariffs.

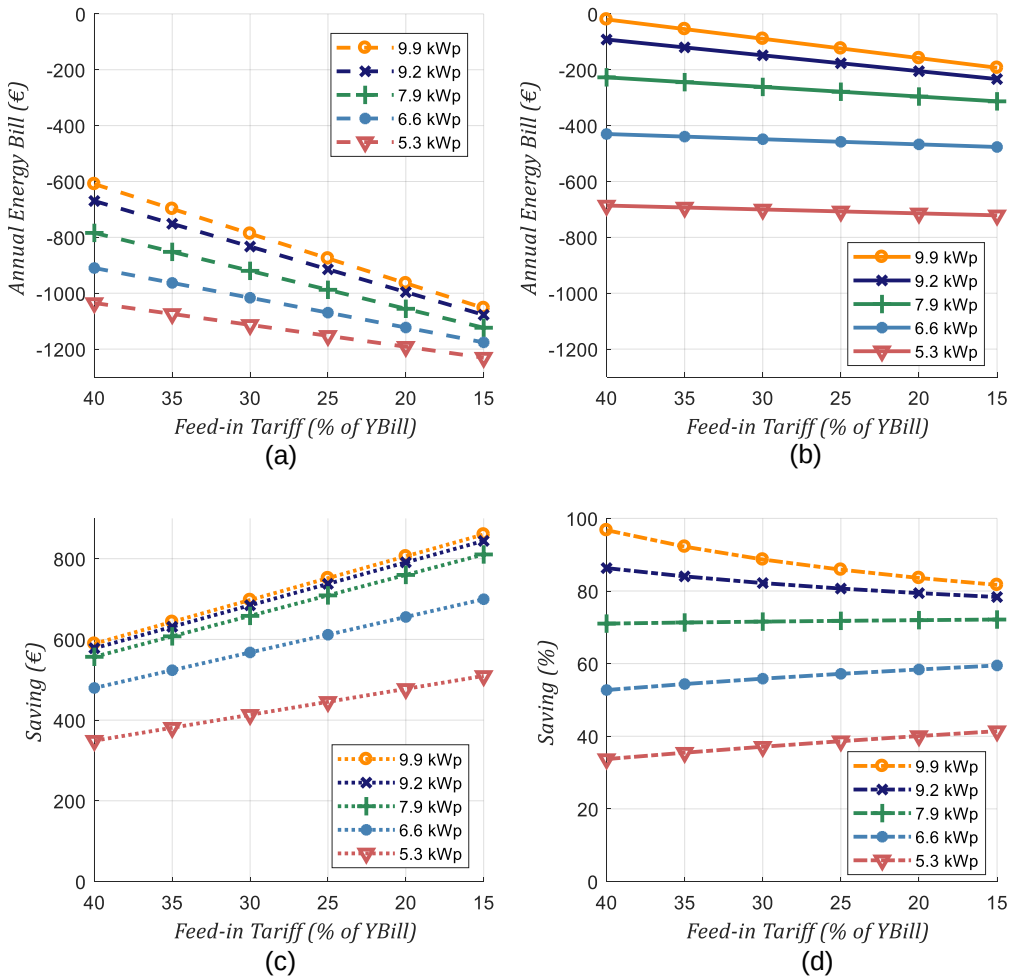

Figure 4.4 Case Study 1 – 35.84 kWh Battery: Annual Bill (€) for different PV generator sizes (kWp) and Feed-in Tariffs (% of the market electricity price). a) Annual Bill for the system without batteries, b) Annual Bill for the system with batteries, c) Savings in the annual bill expressed in € due to the battery implementation, d) Savings in the annual bill expressed in %.

Now, to make an evaluation of the economic performance of the system throughout its useful life, which can be considered over a period of 20 years, it is necessary to take into account changes in the Feed-in Tarff $Y_{Feed-in}$ from the current values that reach 90% of the price of electric power established by the grid operator Y_{Bill} due to the benefits implemented by the current regulations, to values that could be taken in the near future due to the restructuring of these benefits that will be realized when the amount of annual energy exported by this type of systems nationwide, exceeds 4% of the national commercial demand of the previous year [13]. For this reason, and taking as a reference the current tariffs registered in Australia [70, 71] and Portugal [61], where$Y_{Feed-in}$ rates of up to 25% and 15% of the value of Y_{Bill} are presented respectively, the economic performance of the system is analyzed for scenarios with $Y_{Feed-in}$ values between 40% and 15% of Y_{Bill}.

Table 4.5 Case Study 1 – 35.84 kWh Battery: Annual Bill (€) for different PV generator sizes (kWp) and Feed-in Tariffs (% of the market electricity price).

PV Generator Nominal Power (kWp)		Annual Bill (€)					
		40%	**35%**	**30%**	**25%**	**20%**	**15%**
5,3	**NB**	-1035,06	-1074,19	-1113,32	-1152,45	-1191,58	-1230,71
	B	-686,12	-693,14	-700,15	-707,17	-714,19	-721,20
	Sav. (%)	33,71	35,47	37,11	38,64	40,06	41,40
6,6	**NB**	-909,75	-963,01	-1016,27	-1069,53	-1122,80	-1176,06
	B	-430,07	-439,35	-448,63	-457,91	-467,19	-476,47
	Sav. (%)	52,73	54,38	55,86	57,19	58,39	59,49
7.9	**NB**	-784,04	-851,96	-919,88	-987,80	-1055,72	-1123,64
	B	-227,18	-244,36	-261,54	-278,72	-295,89	-313,07
	Sav. (%)	71,02	71,32	71,57	71,78	71,97	72,14
9.2	**NB**	-669,87	-751,39	-832,91	-914,43	-995,95	-1077,47
	B	-91,79	-120,10	-148,41	-176,71	-205,02	-233,33
	Sav. (%)	86,30	84,02	82,18	80,68	79,41	78,34
9.9	**NB**	-609,15	-697,92	-786,69	-875,46	-964,23	-1053,00
	B	-19,77	-54,39	-89,01	-123,63	-158,26	-192,88
	Sav. (%)	96,75	92,21	88,69	85,88	83,59	81,68

Table 4.5 and Figure 4.4 present the results of the $Y_{Feed-in}$ influence on the annual energy bill, with reference to the different sizes of the PV generation system and the implementation of the micro-grid with and without batteries. When comparing figures 4.4 (a) and (b), apart from the effect of the implementation of the battery in the reduction of the annual energy bill, it can be evidenced a lower sensitivity of the economic performance of system implemented with batteries (Figure 4.4(b)) to the changes in $Y_{Feed-in}$, represented in a lower slope of the curves plotted in relation to the system without battery (Figure 4.4(a)), due to the increase in the self-consumption of the generated energy, in the same way, in graph 4.4 (b) it is evident that the systems with greater PV installed capacity present a greater sensitivity to changes in $Y_{Feed-in}$ due to the increase in the amount of energy injected into the grid. Finally, figures 4.4(c) and (d) show the savings obtained with each system, finding that this increases with the size of the PV generator.

In the next stage of the analysis the calculation of some parameters that allow to know the viability and the profitability of the installation of the micro-grid was carried out, for this purpose, the table 4.6 presents a brief summary of these parameters and the equations used for its calculation. In this section, for the calculation of the LCOE, taking into account that the battery has a useful life of 7000 cycles, a total time of the project T of 20 years is established, additionally contemplating a useful life of 15 years for the inverter, having to be replaced once within this period. The value of the initial investment (I_0) was calculated based on the size of the different components of the micro-grid and its average cost according to the market analysis carried out in section 3.1.3, the installation costs ($Install_0$) and maintenance and operation (MO_t) are assumed as 10% and 2% of the value of the PV generator [72, 73], respectively , the annual energy output during the first-year operation (kWh) (S_t) is calculated from the simulations carried out, the degradation rate (d) is taken as 0.8%/year, as indicated by the solar panel manufacturer [43], finally the nominal discount rate (r_n) and the inflation (e) are assumed as 4.6% and 3.1% for the Colombian case according to what is reported in [72, 73].

In order to evaluate the LCOE, table 4.7 presents the results of the analysis carried out regarding the different sizes of the system and different values for the price of the energy storage system (€/kWh), In order to make a prediction of the behavior of this parameter against the possible evolution that can take the market of lithium-ion batteries. Figure 4.5(a) presents these results graphically, plotting additionally the actual market price (AP) of electric power in the city under study (dotted red line); there it can be observed that

this value decreases with the increase in the size of the PV generator, presenting the lowest values for the system with a PV capacity of 9.9 kWp, falling below the AP threshold for a battery price below 540 € / kWh. In the same way, the influence of the battery price can be observed, since when the latter decreases, the LCOE decreases in a general way, at the same time that the difference between the systems with different sizes is reduced.

Table 4.6 Parameters used to evaluate the financial aspects of the installation of the micro-grid [76, 77].

Criteria	Description
Levelized Cost of Energy (LCOE)	LCOE is equal to the ratio of the sum of total cost incurring during the lifetime of the project to the units of electricity generated by the installation over its life service. In this way LCOE considers overall costs occurring during the project lifespan and the associated energy production. It can be computed from Equation (4.1)

$$LCOE = \frac{\sum_{t=0}^{T}(I_0 + Install_0 + MO_t)/(1+r)^t}{\sum_{t=0}^{T} S_t(1-d)^t/(1+r)^t} \quad (4.1)$$

Where, T is the total time of the Project, I_0 is the Initial Investment (€), $Install_0$ Installation Cost (€), MO_t is the Maintenance and Operation Cost (€), S_t denotes the annual energy output during the first-year operation (kWh), d is the degradation rate (%) of the PV system over the specified period, finally, r is the real discount rate which can be computed from Equation (4.2), where r_n is the nominal discount rate and e is the inflation.

$$r = \frac{(1+r_n)}{(1+e)} - 1 \quad (4.2)$$

Net Present Value (NPV)	NPV is commonly used to evaluate the profitability of an investment by calculating the difference between the discounted values of cash flows over the lifetime of projects. The NPV compares the present value of all cash inflows with the present value of all cash outflows associated with an investment project according to Equation (4.3).

$$NPV = \sum_{t=0}^{T} \frac{C_t}{(1+r)^t} \quad (4.3)$$

C_t represents the net cash flow. NPV takes the present value of the money into consideration. It is the most accepted standard method used in financial assessments for long-term project.

Profitability Index (PI) PI indicates how much profit or loss the project makes in a certain amount of time. It is calculated by dividing the NPV value by the initial investment and adding 1, as shown in Equation (4.4).

$$PI = \frac{NPV}{I_0} + 1 \tag{4.4}$$

Payback Period (PBP) The payback period is the length of time required to recover the cost of an investment, it can be computed from Equation (4.5).

$$PBP = \frac{I_0}{Income\ or\ savings} \tag{4.5}$$

Table 4.7 Case Study 1 - LCOE (€) for different PV generator sizes (kWp) and battery prices (€/kWh)

PV Generator Nominal Power (kWp)	LCOE (€)					
	600	**500**	**400**	**300**	**200**	**100**
5,3	0,23	0,21	0,18	0,16	0,13	0,10
6,6	0,20	0,18	0,16	0,14	0,12	0,09
7,9	**0,17**	**0,15**	**0,13**	**0,12**	**0,10**	**0,08**
9,2	0,16	0,14	0,13	0,11	0,10	0,08
9,9	0,15	0,13	0,12	0,11	0,09	0,08

In a similar way table 4.8 presents the results of the calculation of the parameter PI for a Feed-in Tarif of 90% of Y_{Bill} and the same variations indicated above, and graph 4.5(b) shows them graphically, indicating in addition the limit of profitability, which for this variable has a value of 1, represented by a dotted red line. This variable allows to establish the point at which the investment made for the installation of the micro-grid becomes profitable; for values lower than 1, the projection of the benefits during the useful life of the system is negative, that is, the investment generates losses. A value equal to 1 indicates that the initial investment is recovered, while higher values indicate the investment is recovered and in addition profits are generated. In this way it is possible to analyze in the figure that

the systems of 7.9, 9.2 and 9.9 kWp present the best performance, with a very similar profitability, exceeding the threshold to obtain benefits when the price of the battery falls below 575 €/kWh approximately; as this price falls, these systems become more profitable, marking a reference for prices below 400 €/kWh, from which the 7.9 kWp system becomes more profitable than the others.

Table 4.8 Case Study 1 - PI for different PV generator sizes (kWp) and battery prices (€/kWh). at a Feed-in Tariff of 90% of the market electricity price.

PV Generator Nominal Power (kWp)	PI					
	600	**500**	**400**	**300**	**200**	**100**
5,3	0,73	0,84	0,98	1,17	1,46	1,94
6,6	0,84	0,96	1,11	1,32	1,62	2,10
7,9	**0,98**	**1,11**	**1,28**	**1,51**	**1,84**	**2,36**
9,2	0,97	1,10	1,25	1,47	1,76	2,21
9,9	0,99	1,12	1,28	1,49	1,79	2,23

As can be seen in the previous section, the highest profitability is obtained for the lowest battery price analyzed: € 100/kWh, to expand this analysis table 4.9 presents a summary of the calculations made for the NPV considering the different sizes of the simulated systems and different Feed-in tariffs, in order to analyze their performance against variations in the currently established benefits. Additionally, table 4.10 presents a summary of the calculation of the IP under these conditions that helps complement the information. Figures 4.5 (c) and (d) show this data graphically. NPV allows to evaluate the profitability of an investment made in the long term, the higher this value the more profitable the project evaluated. In Figure 4.5(c) it can be seen that the 9.9 kWp system has a higher NVP for Feed-in Tariffs higher than 33% of Y_{Bill} approximately, but for tariffs below this threshold the 7.9 kWp system presents the better performance, additionally taking into account that the initial investment is lower when installing a smaller number of panels and implementing a lower rated power inverter. This is due to the greater sensitivity of systems with higher installed power to variations in $Y_{Feed-in}$, since they inject more excess energy into the grid. This same effect is observed in Figure 4.5 (d), where the 7.9 kWp system has a higher PI, with a lower sensitivity to variations in the Feed-in Tarif.

Table 4.9 Case Study 1 - NPV (k€) for different PV generator sizes (kWp) and Feed-in Tariffs (% of the market electricity price). Battery price of 100 €/kWh.

PV Generator Nominal Power (kWp)	NPV (k€)						
	90%	40%	35%	30%	25%	20%	15%
5,3	10,23	8,91	8,78	8,65	8,52	8,38	8,25
6,6	13,26	11,52	11,34	11,17	10,99	10,82	10,64
7,9	**17,21**	**14,33**	**14,01**	**13,69**	**13,36**	**13,04**	**12,72**
9,2	17,06	14,06	13,53	13,00	12,47	11,93	11,40
9,9	17,71	14,92	14,27	13,61	12,96	12,31	11,66

Table 4.10 Case Study 1 - PI for different PV generator sizes (kWp) and Feed-in Tariffs (% of the market electricity price). Battery price of 100 €/kWh.

PV Generator Nominal Power (kWp)	PI						
	90%	40%	35%	30%	25%	20%	15%
5,3	1,94	1,82	1,81	1,79	1,78	1,77	1,76
6,6	2,10	1,96	1,94	1,93	1,91	1,90	1,88
7,9	**2,36**	**2,13**	**2,10**	**2,08**	**2,05**	**2,03**	**2,00**
9,2	2,21	2,00	1,96	1,92	1,89	1,85	1,81
9,9	2,23	2,04	1,99	1,95	1,90	1,85	1,81

Table 4.11 Case Study 1 - PBP for different PV generator sizes (kWp) and Feed-in Tariffs (% of the market electricity price). Battery price of 100 €/kWh.

PV Generator Nominal Power (kWp)		PBP						
		90%	40%	35%	30%	25%	20%	15%
7.9	**NB**	3,96	6,87	7,45	8,13	8,95	9,95	11,20
	B	7,74	8,56	8,67	8,77	8,88	8,99	9,11
9.2	**NB**	4,54	7,64	8,34	9,18	10,22	11,52	13,20
	B	8,00	8,83	8,99	9,16	9,34	9,52	9,72
9.9	**NB**	4,58	7,54	8,26	9,13	10,20	11,56	13,34
	B	7,94	8,67	8,86	9,06	9,26	9,48	9,71

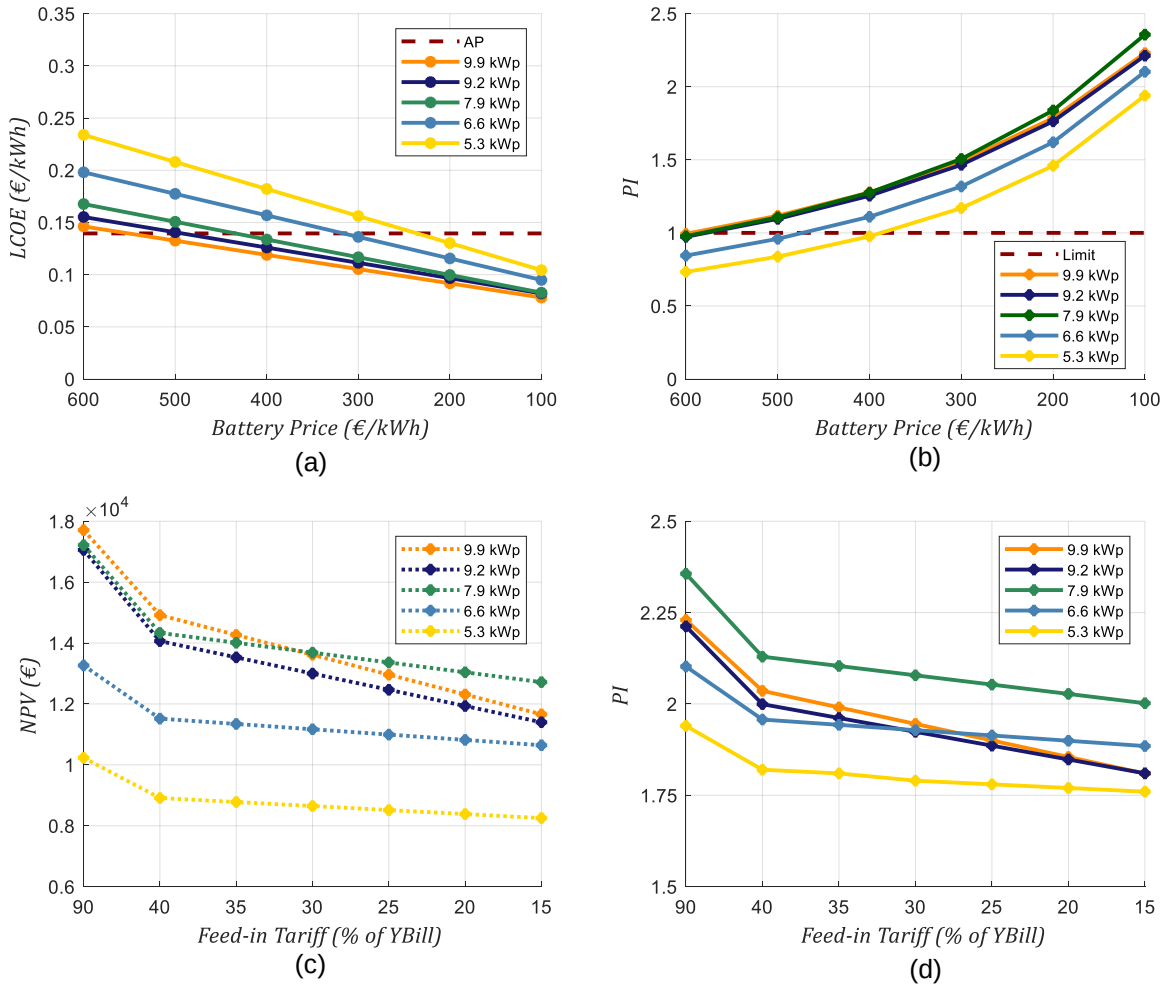

Figure 4.5 Case Study 1 - Parameters used to evaluate the financial aspects of the installation of the micro-grid. a) LCOE vs different Battery prices, b) PI vs different Battery prices, c) NVP vs different Feed-in Tariffs and d) PI vs different Feed-in Tariffs

Finally, Table 4.11 and Figure 4.6 show the behavior of the PBP for the systems of 7.9, 9.2 and 9.9 kWp, in the front of variations in the Feed-in tariff, compared with the performance of the micro-grid without battery (curves labeled as NB); as it can be observed, the sensitivity of the micro-grid without batteries to these changes means that for the systems with installed capacity of 9.2 and 9.9 kWp, the PBP of these systems exceeds the PBP of the micro-grid with battery for a $Y_{Feed-in}$ of about 30% of Y_{Bill} , increasing the difference between the two as $Y_{Feed-in}$ decreases. Something similar happens for the 7.9 kWp system, with the inflection point being $Y_{Feed-in}$ below 25% of Y_{Bill}. Thanks to this analysis, it can be seen that the evolution in the Colombian market conditions will set the conditions for the implementation of micro-grids with energy storage systems, where in

spite of making a greater initial investment due to the additional components of the system, its optimal operation makes them more profitable in the long term.

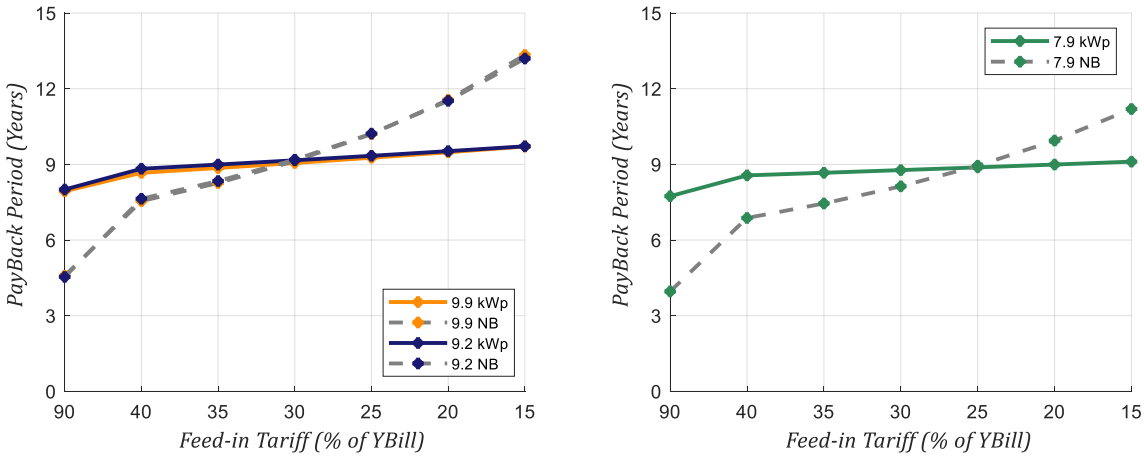

Figure 4.6 PBP vs different Feed-in Tariffs.

4.2. Case Study 2

In a similar way to the previous section, the comparison of the performance of the system in relation to the power exchange profile with the grid, for different sizes of the battery was made. To this end, simulations of the system's annual performance were made for batteries with capacities between 1.92 kWh and 7.68 kWh, configurations available through the implementation of the lithium ion battery model RB40 manufactured by ReLion, while the installed power of the PV generator remains constant at 1.65 kWp and the forecast error is not included in the simulations to isolate the influence of these parameters in the analysis performed. Table 4.12 presents the results of the calculations made for the different parameters of interest defined for the evaluation of the power profile, and Figure 4.7 shows these results in a graphical way for easy comparison. As can be seen in the figures 4.1 a), b), c) and d), as the battery size increases, the parameters APD, MPD, PPV, $P_{G,max}$ and $P_{G,min}$, are reduced, which indicates a better behavior of the power exchange profile with the grid. At the same time, as can be expected, increasing the size of the battery increases the EDG, which implies that a greater percentage of the annual energy demand is covered by the micro-grid, resulting in an annual reduction of up to 84.5% on the electricity bill, as can be observed in Figures 4.1 e) and f), there, negative values for the annual bill represent a debt with the grid operator for that value. From these results it is defined that the system with a battery with a capacity of 7.68 kWh presents the best

performance, however, the convenience of a storage system with this capability will be discussed later.

Table 4.12 Case Study 2 – 1.65 kWp System: Comparison of system performance for different battery sizes.

Battery Capacity (kWh)	$P_{G,max}$ (kW)	$P_{G,min}$ (kW)	MPD (kW/h)	APD (kW/h)	EDG	PPV	$Annual\ Bill$ (€)
Without Battery	**1,19**	**-1,75**	**5,54**	**0,27**	**0,31**	**60,24**	**-18,78**
1,92	0,92	-1,56	4,94	0,19	0,47	86,25	-15,48
3,84	0,93	-1,53	4,80	0,12	0,67	75,51	-10,07
5,76	0,93	-1,06	3,80	0,11	0,81	71,34	-5,56
7,68	0,93	-1,53	4,80	0,10	0,88	45,83	-2,90

As before, an analysis of the impact of the PV generator size on the performance of the system was carried out, for which simulations of systems with installed PV capacity of 1.65 to 2.97 kWp were carried out; this time the batteries with capacities of 5,76 and 7,68 kWh are taken into account, and again the error in the forecast is excluded to avoid the influence of these parameters in the analyzed results. Table 4.13 presents the different configurations implemented to simulate different PV system sizes, the model developed in section 3.2 was adapted to include these changes.

Table 4.13 Case Study 2: Different configurations implemented for the simulation of the micro-grid**.**

Parameter	PV Generator				
	1	**2**	**3**	**4**	**5**
PV generator nominal Power (kWp)	1,65	1.98	2,31	2,64	2,97
Number of parallel branches	1	1	1	1	1
Number of modules in series	5	6	7	8	9
Model of the Inverter	Galvo 1.5-1	Primo 2.0-1	Primo 2.5-1	Primo 3.1-1	Primo 3.1-1
Rated AC Power at 25°C (kVA)	1.5	2	2.5	3.1	3.1

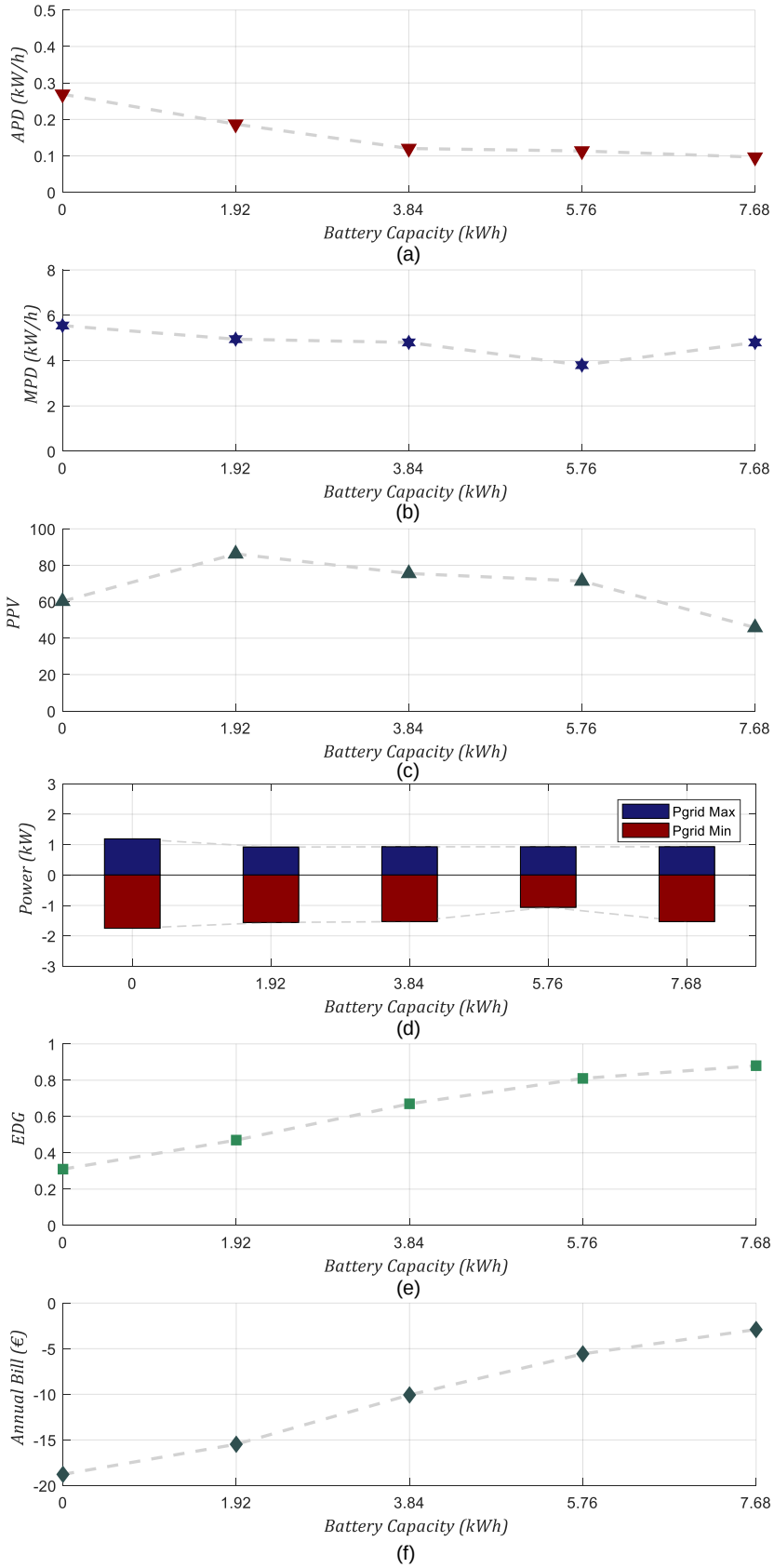

Figure 4.7 Case Study 2 – 1.5 kWp System: - Comparison of system performance for different battery sizes. a) APD, b) MPD, c) PPV, d) $P_{G,max}$ and $P_{G,min}$, e) EDG and f) $Annual\ Bill$.

An analysis similar to that explained in the previous section was carried out, the following tables and figures show the results obtained, there the label NB stands for a system without battery, label B1 for a system with a battery of 5.76 kWh and label B2 for a system with a battery of 7.8 kWh; at the end the main remarks are summarized.

Table 4.14 Case Study 2 : Comparison of system performance for different PV Generator Sizes.

PV Generator Nominal Power (kWp)		$P_{G,max}$ (kW)	$P_{G,min}$ (kW)	MPD (kW/h)	APD (kW/h)	EDG	PPV
1,65	**NB**	1,19	-1,75	5,54	0,27	0,31	60,24
	B1	0,93	-1,06	3,80	0,11	0,81	71,34
	B2	0,93	-1,53	4,80	0,10	0,88	45,83
1,98	**NB**	1,45	-1,75	5,54	0,29	0,32	11,10
	B1	1,15	-0,71	4,34	0,13	0,84	4,62
	B2	1,15	-1,53	4,80	0,11	0,93	3,49
2,31	**NB**	1,71	-1,75	6,13	0,31	0,32	6,94
	B1	1,36	-0,48	5,75	0,14	0,85	3,26
	B2	1,37	-0,36	5,75	0,12	0,94	2,65
2,64	**NB**	1,97	-1,75	6,86	0,33	0,33	5,34
	B1	1,58	-0,38	6,55	0,16	0,86	2,79
	B2	1,60	-0,34	6,55	0,13	0,94	2,37
2,97	**NB**	2,24	-1,75	7,67	0,36	0,33	4,50
	B1	1,81	-0,38	7,34	0,17	0,87	2,55
	B2	1,81	-0,24	7,34	0,15	0,95	2,23

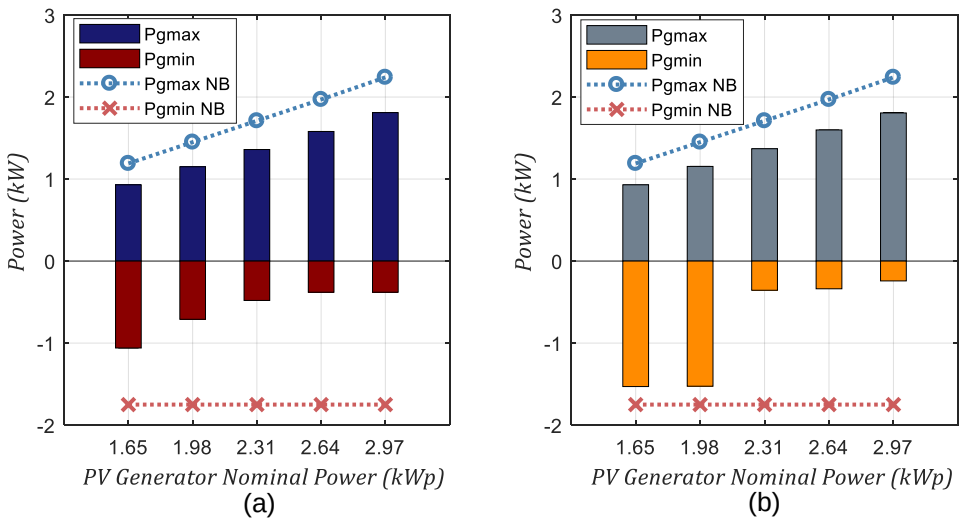

Figure 4.8 Case Study 2 – Comparison of system performance for different PV generator sizes: $P_{G,max}$ and $P_{G,min}$. a) microgrid with a 5.76 kWh Battery, b) microgrid with a 7.68 kWh Battery

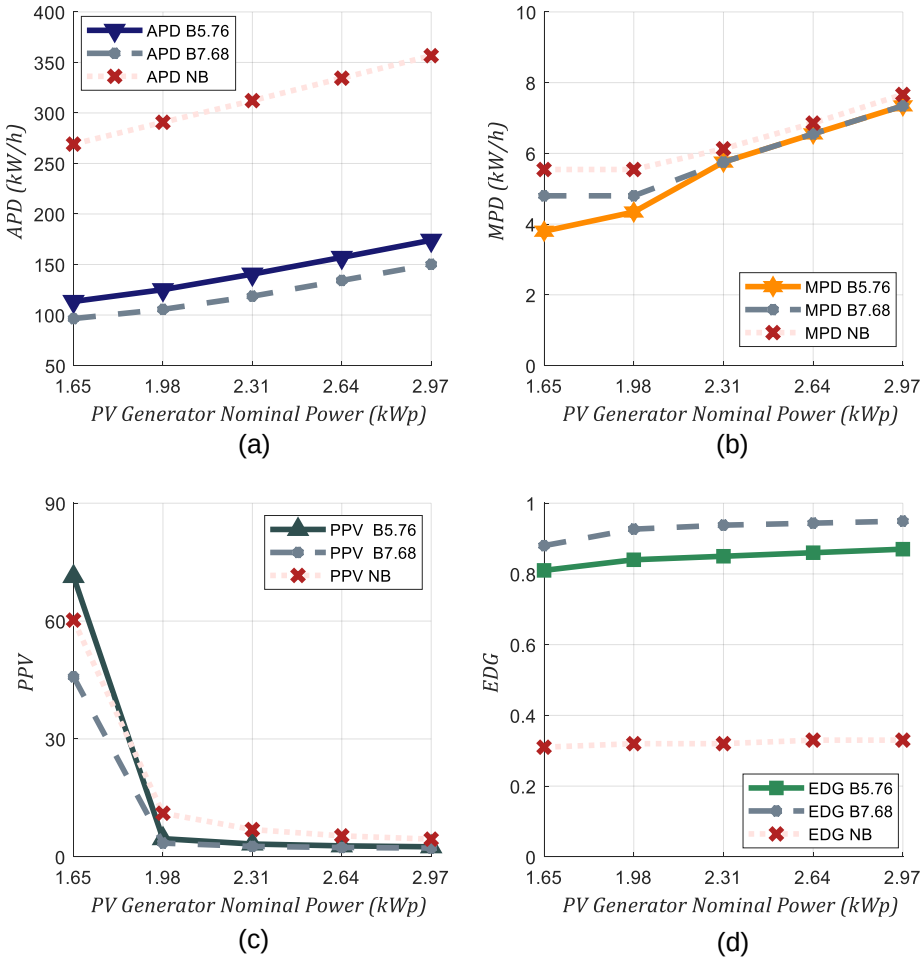

Figure 4.9 Case Study 2 Comparison of system performance for different PV generator sizes. a) $\boldsymbol{APD}$, b) $\boldsymbol{MPD}$, c) $\boldsymbol{PPV}$ and d) $\boldsymbol{EDG}$

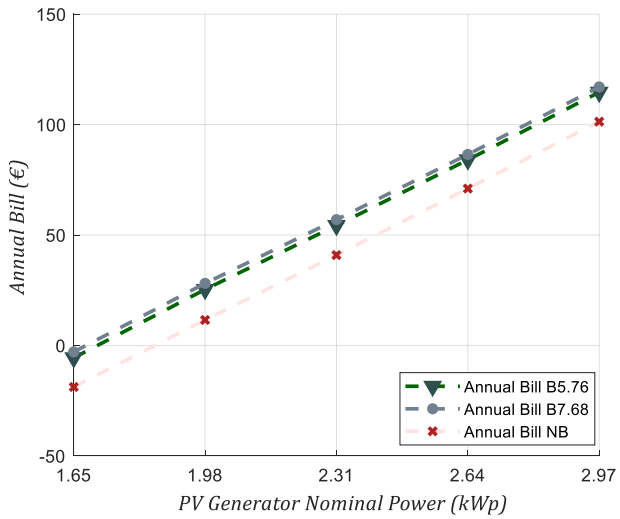

Figure 4.10 Case Study 2: Analysis of the annual energy exchange with the grid. Annual balance of the energy bill.

Table 4.15 Case Study 2 – 5.76 kWh Battery: Analysis of the annual energy exchange with the grid

PV Generator Nominal Power (kWp)		Gen. (MWh)	Con. (MWh)	H2G (MWh)	G2H (MWh)	Battery Energy Std	Battery Energy Exd	Annual Bill (€)
1,65	**NB**	2,78	2,54	1,85	1,74			-18,78
	B1			0,51	0,49	1,40	1,33	-5,56
	Red. (%)			72,22	72,04			
1,98	**NB**	3,34	2,54	2,37	1,73			11,56
	B1			0,96	0,40	1,47	1,41	25,38
	Red. (%)			59,49	76,68			
2,31	**NB**	3,90	2,54	2,88	1,71			40,94
	B1			1,44	0,37	1,50	1,44	54,34
	Red. (%)			49,94	78,24			
2,64	**NB**	4,45	2,54	3,40	1,71			71,05
	B1			1,95	0,36	1,51	1,45	84,06
	Red. (%)			42,63	79,04			
2,97	**NB**	5,01	2,54	3,94	1,70			101,36
	B1			2,48	0,34	1,52	1,46	114,66
	Red. (%)			36,98	79,88			

Table 4.16 Case Study 2 – 7.68 kWh Battery: Analysis of the annual energy exchange with the grid

PV Generator Nominal Power (kWp)		Gen. (MWh)	Con. (MWh)	H2G (MWh)	G2H (MWh)	Battery Energy Std	Battery Energy Exd	Annual Bill (€)
1,65	**NB**	2,78	2,54	1,85	1,74			-18,78
	B2			0,33	0,31	1,59	1,52	-2,90
	Red. (%)			81,95	82,46			
1,98	**NB**	3,34	2,54	2,37	1,73			11,56
	B2			0,74	0,19	1,70	1,64	25,38
	Red. (%)			68,85	89,21			
2,31	**NB**	3,90	2,54	2,88	1,71			40,94
	B2			1,22	0,16	1,73	1,67	56,99
	Red. (%)			57,65	90,80			
2,64	**NB**	4,45	2,54	3,40	1,71			71,05
	B2			1,73	0,14	1,75	1,68	86,50
	Red. (%)			49,21	91,59			
2,97	**NB**	5,01	2,54	3,94	1,70			101,36
	B2			2,26	0,13	1,75	1,68	117,07
	Red. (%)			42,65	92,42			

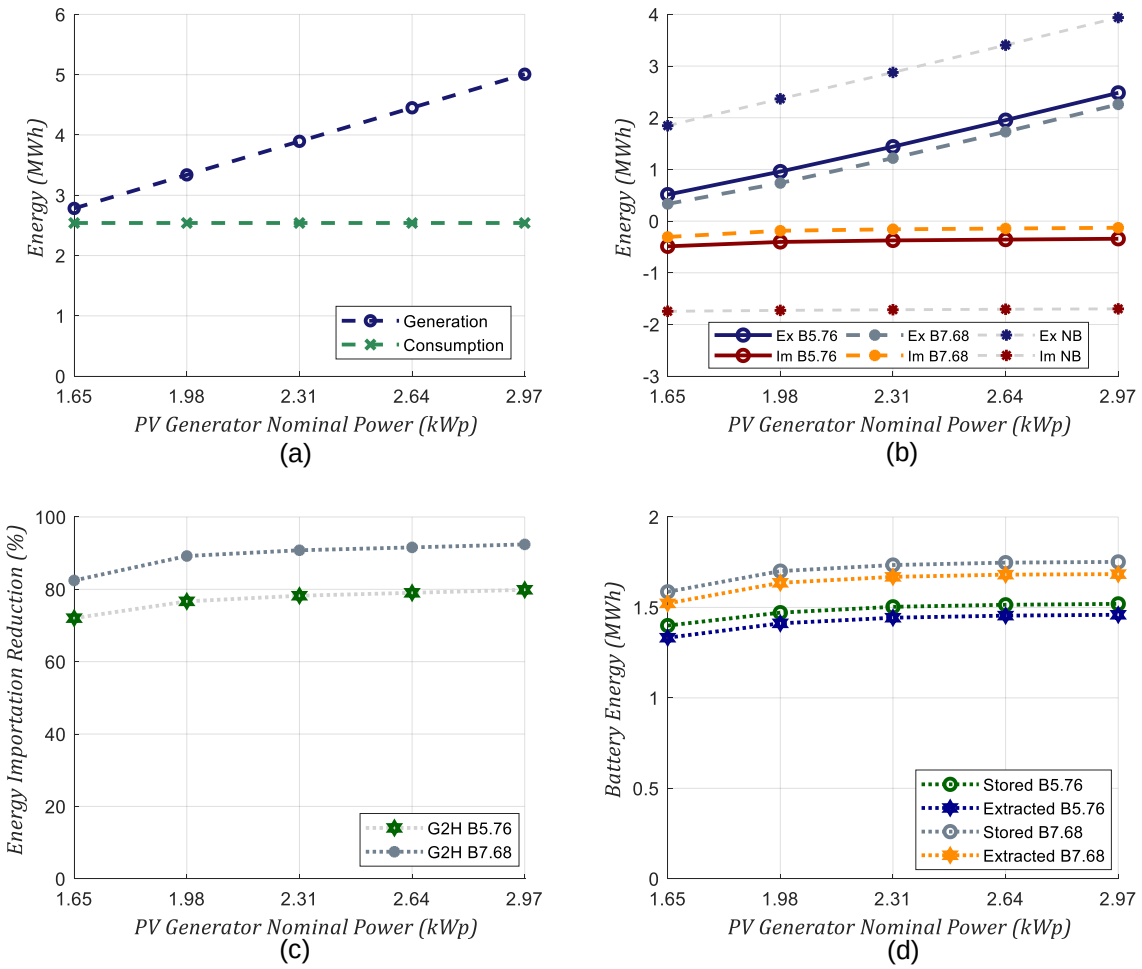

Figure 4.11 Case Study 2: Analysis of the annual energy exchange with the grid. a) Energy Generation and Consumption, b) Energy Exported to the grid H2G and Imported from the gird G2H, c) Energy Importation Reduction, d) Energy exchange with the battery.

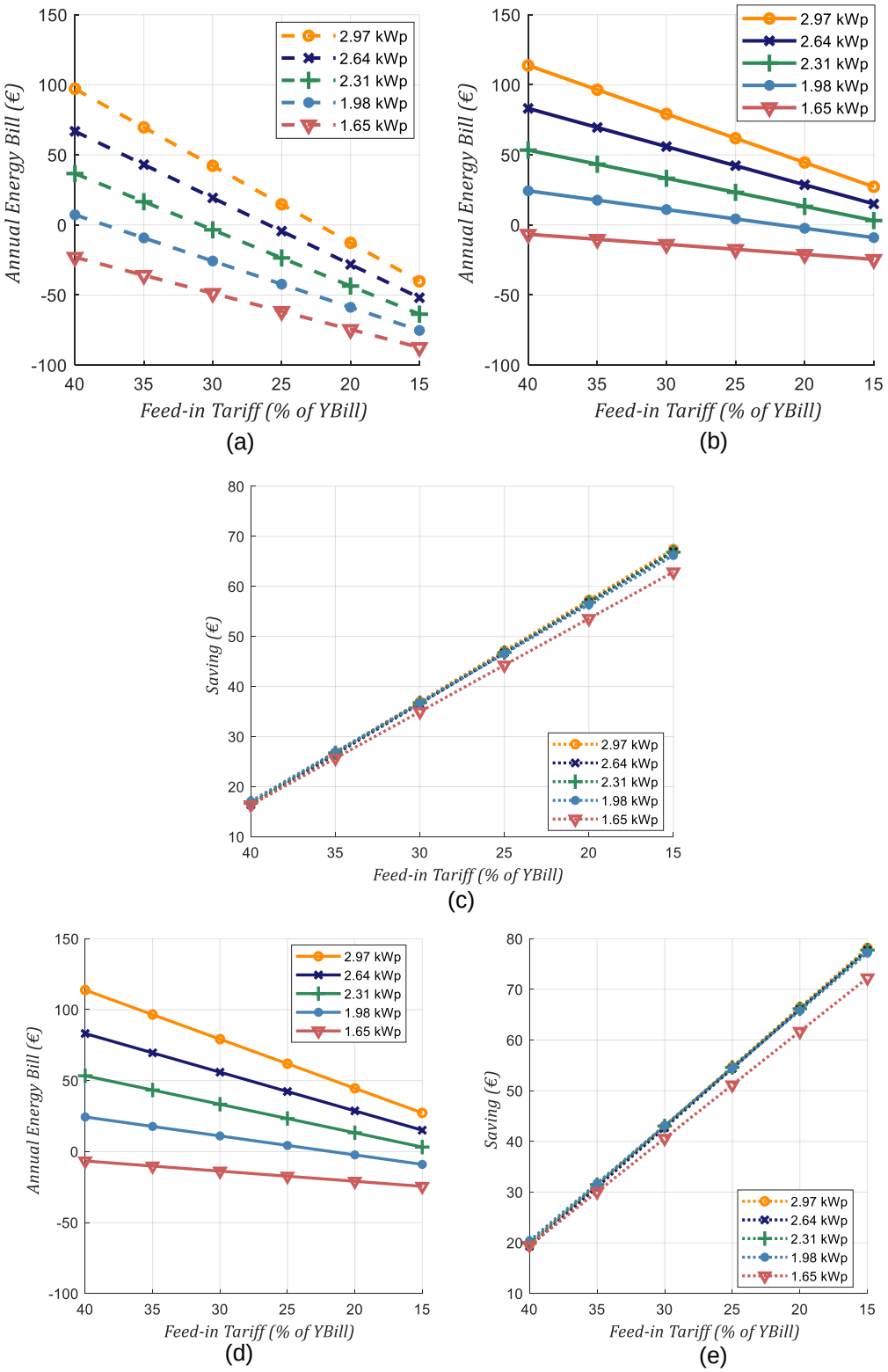

Figure 4.12 Case Study 2 – Annual Bill (€) for different PV generator sizes (kWp) and Feed-in Tariffs (% of the market electricity price). a) Annual Bill for the system without batteries, b) Annual Bill for the system with a 5.76 kWh battery, c) Savings in the annual bill due to the battery implementation, d) Annual Bill for the system with a 7.68 kWh battery, e) Savings in the annual bill

Table 4.17 Case Study 2 – 5.76 kWh Battery: Annual Bill (€) for different PV generator sizes (kWp) and Feed-in Tariffs (% of the market electricity price).

PV Generator Nominal Power (kWp)		Annual Bill (€)					
		40%	35%	30%	25%	20%	15%
1,65	NB	-23,01	-35,89	-48,76	-61,64	-74,51	-87,39
	B	-6,63	-10,20	-13,78	-17,36	-20,93	-24,51
	Sav. (€)	16,38	25,68	34,98	44,28	53,58	62,88
1,98	NB	7,28	-9,22	-25,73	-42,23	-58,73	-75,23
	B	24,38	17,70	11,01	4,33	-2,35	-9,04
	Sav. (€)	17,10	26,92	36,74	46,56	56,38	66,19
2,31	NB	36,69	16,62	-3,45	-23,51	-43,58	-63,65
	B	53,41	43,37	33,32	23,28	13,23	3,18
	Sav. (€)	16,73	26,75	36,77	46,79	56,81	66,83
2,64	NB	66,82	43,07	19,32	-4,42	-28,17	-51,92
	B	83,18	69,55	55,93	42,31	28,68	15,06
	Sav. (€)	16,36	26,48	36,60	46,73	56,85	66,97
2,97	NB	97,15	69,68	42,21	14,74	-12,73	-40,20
	B	113,82	96,51	79,19	61,88	44,57	27,26
	Sav. (€)	16,66	26,82	36,98	47,14	57,30	67,46

Table 4.18 Case Study 2 – 7.68 kWh Battery: Annual Bill (€) for different PV generator sizes (kWp) and Feed-in Tariffs (% of the market electricity price).

PV Generator Nominal Power (kWp)		Annual Bill (€)					
		40%	35%	30%	25%	20%	15%
1,65	NB	-23,01	-35,89	-48,76	-61,64	-74,51	-87,39
	B	-3,51	-5,84	-8,16	-10,49	-12,81	-15,14
	Sav. (€)	19,50	30,05	40,60	51,15	61,70	72,25
1,98	NB	7,28	-9,22	-25,73	-42,23	-58,73	-75,23
	B	27,67	22,53	17,39	12,25	7,11	1,97
	Sav. (€)	20,39	31,75	43,12	54,48	65,84	77,20
2,31	NB	36,69	16,62	-3,45	-23,51	-43,58	-63,65
	B	56,60	48,10	39,60	31,10	22,60	14,10
	Sav. (€)	19,91	31,48	43,05	54,61	66,18	77,75
2,64	NB	66,82	43,07	19,32	-4,42	-28,17	-51,92
	B	86,14	74,08	62,02	49,95	37,89	25,83
	Sav. (€)	19,32	31,01	42,69	54,38	66,06	77,75
2,97	NB	97,15	69,68	42,21	14,74	-12,73	-40,20
	B	116,75	100,99	85,24	69,48	53,73	37,97
	Sav. (€)	19,59	31,31	43,03	54,74	66,46	78,17

As can be seen in Figure 4.7, as in the previous section, the increase in the size of the battery contributes to the improvement of the power exchange profile with the grid. On the other hand, in Figures 4.8 and 4.9 the impact of the size of the PV generator system on the evaluated parameters can be observed, this time taking into account two sizes of the battery; as evidenced, the behavior is very similar to that presented in the case of study 1, with the observation that the larger battery slightly improves the results obtained. On the other hand, the results presented in figure 4.10 allow us to foresee that the impact of the larger battery on the economic benefits obtained with the operation of the system are not very significant.

Figure 4.11(a) shows that the annual energy generation of the different simulated systems is greater than the annual consumption of the household under study, while figures 4.11(b), (c) and (d) show that, as can be expected, the larger battery stores a greater amount of energy, increasing self-consumption. On the other hand, figure 4.12 shows that both the size of the generation system and the size of the battery do not generate a great impact on the savings in the annual energy bill, presenting very similar results for the cases evaluated.

On the other hand, Figures 4.13 to 4.17 summarize the results of the analysis of the financial parameters, performed in a similar way to that explained in the previous section. Figure 4.13 allows comparing the trajectory of the LCOE against changes in the size of the PV system and variations in the price of the battery, for two different battery sizes. As a result, the system with an installed capacity of 2.97 kWp and a battery of 5.76 kWh has the lowest values for this parameter. On the other hand, in Figure 4.14 it can be seen that the system with a better PI is the one formed by a PV generation system of 1.65 kWp and the battery of 5.76 kWh, reaching the level of profitability for a battery prices lower than € 400 / kWh. in Figures 4.15 and 4.16 we can observe the sensitivity of the systems to the changes in Feed-in tariff, showing that in this scenario the low performance is obtained again by the microgrid with a PV generation system of 1.65 kWp and the battery of 5.76 kWh. Finally, Figure 4.17 presents a comparison of the PBP between this system implemented with and without batteries, under a battery price scenario of € 100/kWh, there is evident that for Feed-in tariffs lower than 40% of Y_{Bill}, a better return on investment is obtained with the micro-grid that uses an energy storage system, as a result of optimizing the generation of electricity for self-consumption.

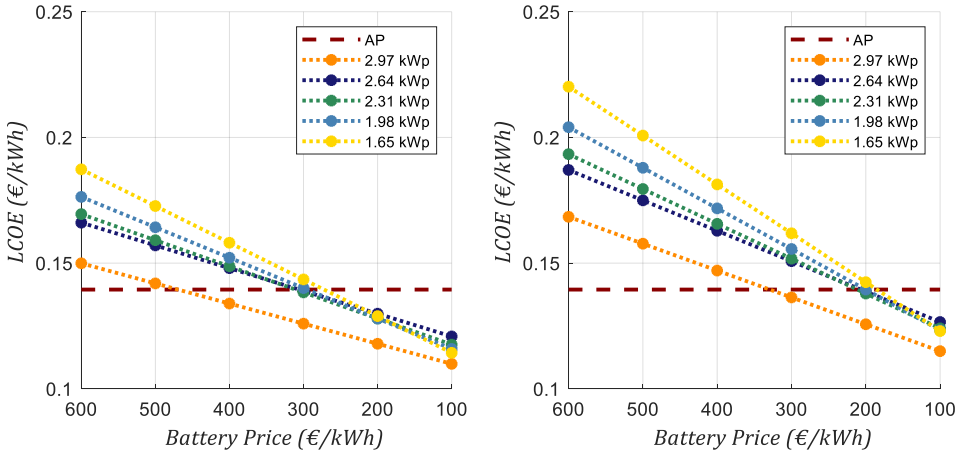

Figure 4.13 Case Study 2 – LCOE vs Battery Price. a) system with a 5.76 kWh battery and b) system with a 7.68 kWh battery

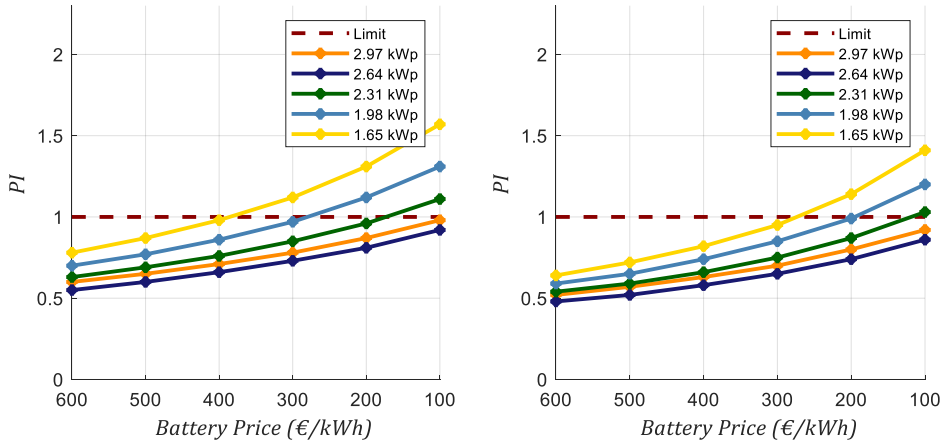

Figure 4.14 Case Study 2 – PI vs Battery Price. a) system with a 5.76 kWh battery and b) system with a 7.68 kWh battery

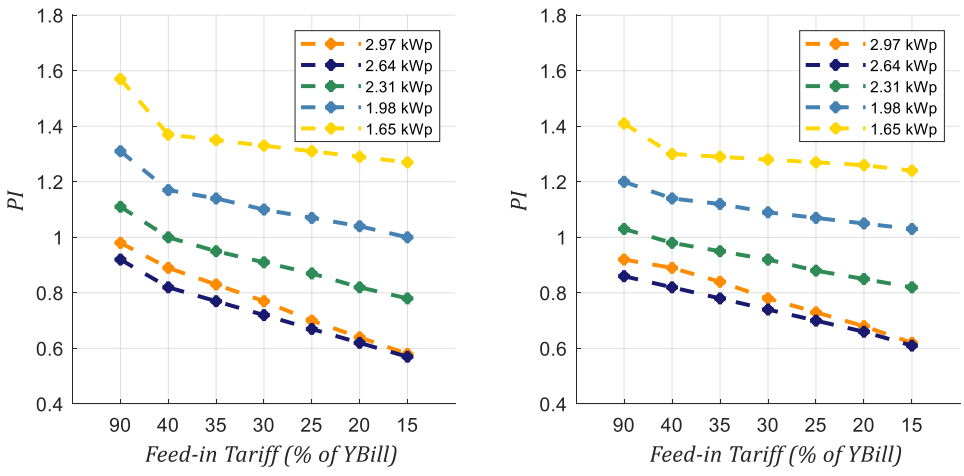

Figure 4.15 Case Study 2 – PI vs Feed-in Tariff. a) system with a 5.76 kWh battery and b) system with a 7.68 kWh battery

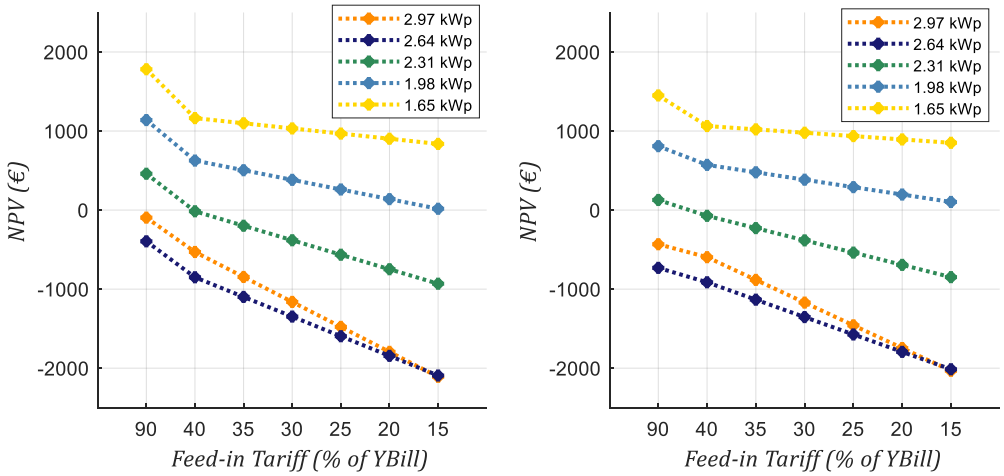

Figure 4.16 Case Study 2 – NPV vs Feed-in Tariff a) system with a 5.76 kWh battery and b) system with a 7.68 kWh battery

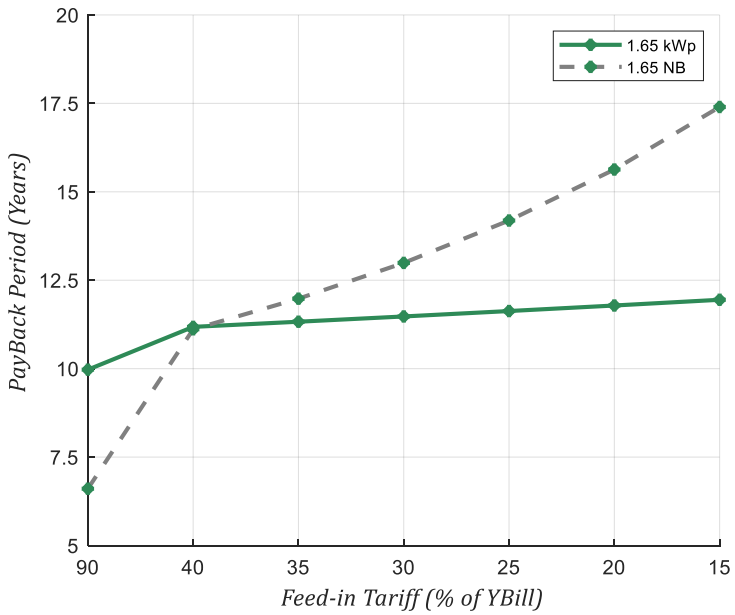

Figure 4.17 Case Study 2 – PBP vs Feed-in Tariff. System with a PV generator of 1.65 kWp and a 5.76 kWh battery.

Chapter 5. Conclusions and recommendations

Currently, the Colombian electricity sector presents great opportunities for the implementation of electric power generation systems from unconventional energy sources such as photovoltaic solar energy, these opportunities arise from the need to strengthen the national energy matrix with the objective of to be able to supply the increasing demand for electrical energy of the country, at the same time as the generation system, mainly dominated by generation of hydroelectric energy, is strengthened in face of environmental crises such as those experienced in the past. This policy is reflected in the government resolutions signed relatively recently, through which it seeks to promote the distributed implementation of this type of systems, offering attractive pricing conditions that encourage the penetration of these technologies in the Colombian electricity market.

Under this scenario, the model developed through the methodology implemented in this work represents a useful tool to analyze the behaviour of a micro-grid with photovoltaic solar energy and an energy storage system, within the Colombian energy context, thus allowing to evaluate the performance of the system when it is connected to the main electrical grid, an important factor to consider in order to ensure the stability and correct operation of the grid in front of the large-scale implementation of this technology, while allowing a financial analysis to assess the profitability of the investment and, in this way, to realize the correct sizing of the different subsystems which make up the micro-grid.

Based on the analysis performed on the electricity billing model implemented in the City of Cúcuta, it is possible to conclude that the best way to take advantage of the implementation of the energy storage system in the micro-grid is to optimize its operation to maximize self-consumption of the energy generated by the PV system. This is because, on the one hand, electricity is currently invoiced based on the Inclining block rate (IBR) model, which has a constant rate for the whole month, and additional discounts, which are only available for socioeconomic strata 1, 2 and 3, can be only accessed by not exceeding a consumption threshold established by the grid operator; and on the other hand, the Feed-in tariff is lower than the cost of the electric power consumed, therefore, the greatest economic benefit is obtained by using for self-consumption the energy generated by the PV system and stored in the battery system.

As demonstrated in section 3.3, dynamic programming is a powerful tool to develop the strategy for optimizing the operation of the micro-grid, allowing through the developed algorithm, to optimize both the main objective, which is to maximize the benefits generated by the operation of the system, and at the same time the power exchange profile with the grid is improved.

From an economic point of view, based on the analysis of the case studies evaluated, it is possible to determine that under the current conditions of the electricity market and the current price of batteries, the economic investment for the energy storage system is quite high compared to the total cost of the system, and the economic benefits obtained by its implementation do not justify the additional expense. However, taking into account that the current tariffs for the injection of energy into the grid can be reduced in the next few years, and that the cost of the technology for the manufacture of the batteries is expected to decrease, the implementation of these systems and the optimization of their operation will be essential to ensure the profitability of the installation as evidenced by the results obtained in chapter 4. In this sense, the projects to carry out the installation of micro-grids could be considered in two stages, a first investment for the installation of the PV generator and its start-up connected to the grid to take advantage of the current tariff conditions, and a second stage that contemplates the acquisition of the energy storage system and the components that ensure its correct operation, when the market conditions favor its implementation.

Finally, to carry out future research derived from this work, it is recommended to implement additional Demand Side Management strategies that allow the optimization of the electric power consumption by the household, helping to maximize the benefits obtained by the end user. In this sense and due to the lack of formally structured databases that provide access to this information, to improve simulations and bring them closer to more real scenarios, it is necessary to read and record power generation profiles by real photovoltaic systems installed in the city of Cúcuta, as well as real load profiles that allow to evaluate the performance of the models developed in section 3.2. Additionally, as mentioned when analyzing the technology currently available in the market, it is necessary to develop charge controllers that allow a more extensive control of the power exchange with the battery, in order to guarantee the correct control of the operation of the micro-grid.

References

[1] A. M. Macías Parra, “Generación eléctrica bajo escenarios de cambio climático,” 2013. [Online]. Available: http://www1.upme.gov.co/sites/default/files/generacion_electrica_bajo_escenarios_cambio_climatico.pdf. [Accessed 18 Mayo 2018].

[2] International Energy Agency, “TRENDS 2018 IN PHOTOVOLTAIC APPLICATIONS - EXECUTIVE SUMMARY,” 2018.

[3] Energy Mining Planning Unit UPME, “Monthly report of generation variables and Colombian Electricity Market (in Spanish),” January 2014. [Online].

[4] J. Hernández, C. L. Trujillo and F. Santamaría, *Photovoltaic Projects Developed in Non-Interconnected Zones in Colombia,* 2015.

[5] XM S.A. E.S.P., “Supply and Generation Report (in Spanish),” April 2015. [Online]. Available: http://www.xm.com.co/Informes%20Mensuales%20de%20Anlisis%20del%20Mercado/02_Informe_Oferta_y_Generacion_TXR_04_2015.pdf. [Accessed 12 February 2019].

[6] XM S.A. E.S.P, “Supply and Generation Report (in Spanish),” December 2015. [Online]. Available: http://www.xm.com.co/Informes%20Mensuales%20de%20Anlisis%20del%20Mercado/02_Informe_Oferta_y_Generacion_12_2015.pdf. [Accessed 12 February 2019].

[7] XM S.A. E.S.P., “Supply and Generation Report (in Spanish),” March 2016. [Online]. Available: http://www.xm.com.co/Informes%20Mensuales%20de%20Anlisis%20del%20Mercado/02_Informe_Oferta_y_Generacion_TXF_03_2016.pdf. [Accessed 12 February 2019].

[8] Unidad de Planeación Minero Energética UPME, “Proyección Regional de demanda de Energía Eléctrica y Potencia Máxima en Colombia,” Bogotá, Colombia, 2017.

[9] The Solar Guide, “Top 5 Successful solar projects in Colombia,” [Online]. Available: http://www.laguiasolar.com/top-5-proyectos-exitosos-de-energia-solar-en-colombia/. [Accessed 12 February 2019].

[10] Institute of Hydrology, Meteorology and Environmental Studies (IDEAM), “Irradiadición Global Horizontal Media Diaria,” 2014. [Online]. Available: http://atlas.ideam.gov.co/visorAtlasRadiacion.html. [Accessed 12 February 2019].

[11] Solargis, “Solar resource map of Germany,” 2018. [Online]. Available: https://solargis.com/maps-and-gis-data/download/germany/. [Accessed 12 February 2019].

[12] Colombian Congress, “Law 1715 - 2014,” 2014.

[13] Colombian Energy and Gas Regulation Commission, CREG, *Resolución No. 030 de 2018. Por la cual se regulan las actividades de autogeneración a pequeña escala y de generación distribuida en el Sistema Interconectado Nacional,* Bogotá, 2018.

[14] D. E. Olivares, A. Mehrizi-Sani, A. H. Etemadi, C. A. Cañizares, R. Iravani, M. Kazerani, A. H. Hajimiragha, O. Gomis-Bellmunt, M. Saeedifard, R. Palma-Behnke, G. A. Jiménez-Estévez and N. D. Hatziargyriou, “Trends in Microgrid Control,” *IEEE TRANSACTIONS ON SMART GRID,* vol. 5, no. 4, pp. 1905-1919, 2014.

[15] A. Hirsch, Y. Parag and J. Guerrero, “Microgrids: A review of technologies, key drivers, and outstanding issues,” *Renewable and Sustainable Energy Reviews,* vol. 90, pp. 402-411, 2018.

[16] F. Martín Martínez, A. Sánchez Miralles and M. Rivier, “A literature review of Microgrids: A functional layer based classification,” *Renewable and Sustainable Energy Reviews,* vol. 62, pp. 1133-1153, 2016.

[17] M. H. Rashid , Power Electronics Handbook Devices, Circuits, and Applications, Third ed., Elsevier and Butterworth-Heinemann, 2011.

[18] B. Pillot, M. Muselli, P. Poggi and J. Batista Dias, “Historical trends in global energy policy and renewable power system issues in Sub-Saharan Africa: The case of solar PV,” *Energy Policy,* vol. 127, pp. 113-124, 2019.

[19] X. Li, M. Paster and J. Stubbins, “The dynamics of electricity grid operation with increasing renewables and the path toward maximum renewable deployment,” *Renewable and Sustainable Energy Reviews,* vol. 47, pp. 1007-1015, 2015.

[20] P. Warren, “A review of demand-side management policy in the UK,” *Renewable and Sustainable Energy Reviews,* vol. 29, pp. 941-951, January 2014.

[21] K. Karunanithi, S. Saravanan, B. R. Prabakar, S. Kannan and C. Thangaraj, “Integration of Demand and Supply Side Management strategies in Generation Expansion Planning,” *Renewable and Sustainable Energy Reviews,* vol. 73, pp. 966-982, June 2017.

[22] “Demand Side Management – Module 14. Sustainable energy regulation and policy,” 17 December 2010. [Online]. Available: http://africa-toolkit.reeep.org/modules/Module14.pdf. [Accessed 3 February 2019].

[23] K. Zhou and S. Yang, “Demand side management in China: The context of China’s power industry reform,” *Renewable and Sustainable Energy Reviews,* vol. 47, pp. 954-965, July 2015.

[24] C. W. Gellings, “The Concept of Demand-Side Management for Electric Utilities,” *PROCEEDINGS OF THE IEE,* vol. 73, no. 10, pp. 1468-1470, October 1985.

[25] U.S. Department of Energy, “Benefits of demand response in electricity markets and recommendations for achieving them,” Washington, DC, USA, 2006.

[26] M. Hussain and Y. Gao, “A review of demand response in an efficient smart grid environment,” *The Electricity Journal,* vol. 31, pp. 55-63, 2018.

[27] A. Rezaee Jordehi, “Optimisation of demand response in electric power systems, a review,” *Renewable and Sustainable Energy Reviews,* vol. 103, pp. 308-319, 2019.

[28] J. Torriti, “Price-based demand side management: Assessing the impacts of time-of-use tariffs on residential electricity demand and peak shifting in Northern Italy,” *Energy,* vol. 44, pp. 576-583, 2012.

[29] T. Kato, A. Tokuhara, Y. Ushifusa, A. Sakurai, K. Aramaki and F. Maruyama, “Consumer responses to critical peak pricing: Impacts of maximum electricity-saving behavior,” *The Electricity Journal,* vol. 29, pp. 12-19, 2016.

[30] D. Jang, J. Eom, M. J. Park and J. J. Rho, "Variability of electricity load patterns and its effect on demand response: A critical peak pricing experiment on Korean commercial and industrial customers," *Energy Policy,* vol. 88, pp. 11-26, 2016.

[31] R. Deng, Z. Yang, M.-Y. Chow and J. Chen, “A Survey on Demand Response in Smart Grids: Mathematical Models and Approaches,” *IEEE Transactions on Industrial Informatics,* vol. 11, pp. 570-582, 2015.

[32] A.-H. Mohsenian-Rad, V. W. Wong, J. Jatskevich and R. Schober, “Optimal and autonomous incentive-based energy consumption scheduling algorithm for smart grid,” in *2010 Innovative Smart Grid Technologies (ISGT)*, Gothenburg, Sweden, 2010.

[33] M. Shad, A. Momeni, R. Errouissi, C. P. Diduch, M. E. Kaye and L. Chang, “Identification and Estimation for Electric Water Heaters in Direct Load Control Programs,” *IEEE Transactions on Smart Grid,* vol. 8, pp. 947-955, March 2017.

[34] S. P. Bradley, A. C. Hax and T. L. Magnanti, Applied Mathematical Programming, Addison-Wesley, 1997.

[35] A. Lew and H. Mauch, Dynamic Programming A Computational Tool, Springer, 2007.

[36] R. E. Bellman, Dynamic Programming, Princeton, New Jersey: Princeton University Press, 1957.

[37] Banco de la República, Colombia. , “Tasas de cambio - Monedas de Reserva,” 2019. [Online]. Available: http://www.banrep.gov.co/es/monedas-reserva. [Accessed 4 February 2019].

[38] Centrales Eléctricas del Norte de Santander S.A E.S.P, “Tarifas de energía,” February 2019. [Online]. Available: https://www.cens.com.co/Portals/1/documentos/tarifas/Tarifa_CENS_201901.pdf. [Accessed 5 February 2019].

[39] UNIVERSIDAD NACIONAL DE COLOMBIA, “Determinación del consumo final de energía en los sectores residencial, urbano y comercial, y determinación de consumo para equipos domésticos de energía eléctrica y gas,” Bogotá, 2006.

[40] Consorcio CORPOEMA, “Determinación del consumo básico de subsistencia en los sectores residencial, comercial y hotelero en el departamento Archipiélago de San Andrés, Providencia y Santan Catalina,” Bogotá, 2010.

[41] Departamento Administrativo Nacional de Estadística (DANE), “Mapas de Características Sociodemográficas,” 2018. [Online]. Available: https://www.dane.gov.co/index.php/estadisticas-por-tema/demografia-y-poblacion/censo-nacional-de-poblacion-y-vivenda-2018/donde-estamos/mapas-tematicos. [Accessed 5 February 2019].

[42] International Finance Corporation, “Utility-Scale Solar Photovoltaic Power Plants - A Project Developer’s Guide,” Washington, D.C., 2015.

[43] Canadian Solar Inc., *Canadian Solar MAXPOWER CS6U- 325| 330| 335P Datasheet,* 2018.

[44] JA Solar Holdings Co. Ltd., *JAP72S01 310-330 1000V Cypress Series Multicristalline Silicon Solar Module - Data Sheet,* 2017.

[45] S. Ramirez Castaño, Redes de Distribución de Energía, Third ed., Manizales: Universidad Nacional de Colombia, 2004.

[46] Fronius USA LLC, *FRONIUS GALVO: TECHNICAL DATA,* 2017.

[47] Fronius USA LLC, *Fronius Primo - Technical Data,* 2018.

[48] Fronius USA LLC Solar Electronics Division, “Fronius Galvo 208-240 - Installation Instruction,” 2018. [Online]. Available: https://www.fronius.com/en-us/usa/photovoltaics/products/all-products/inverters/fronius-galvo/fronius-galvo-1-5-1-208-240. [Accessed 24 January 2019].

[49] A. Rezaee Jordehi, “Parameter estimation of solar photovoltaic (PV) cells: A review,” *Renewable and Sustainable Energy Reviews,* vol. 61, pp. 354-371, 2016.

[50] J. Bai, S. Liu, Y. Hao, Z. Zhang, M. Jiang and Y. Zhang, "Development of a new compound method to extract the five parameters of PV modules," *Energy Conversion and Management,* vol. 79, pp. 294-303, 2014.

[51] N. Karami, N. Moubayed and R. Outbib, "General review and classification of different MPPT Techniques," *Renewable and Sustainable Energy Reviews,* vol. 68, pp. 1-18, 2017.

[52] S. M. Mousavi and M. Nikdel, "Various battery models for various simulation studies and applications," *Renewable and Sustainable Energy Reviews,* vol. 32, pp. 477-485, 2014.

[53] The MathWorks, Inc., "Battery - Implement generic battery model," [Online]. Available: https://es.mathworks.com/help/physmod/sps/powersys/ref/battery.html. [Accessed 24 January 2019].

[54] RELiON Batteries LLC, *RB100 LITHIUM IRON PHOSPHATE BATTERY SPECIFICATIONS,* 2018.

[55] L. G. Swan and V. Ismet Ugursal, "Modeling of end-use energy consumption in the residential sector: A review of modeling techniques," *Renewable and Sustainable Energy Reviews,* vol. 13, pp. 1819-1835, 2009.

[56] M. A. López Rodríguez, I. Santiago, D. Trillo Montero, J. Torriti and A. Moreno Munoz, "Analysis and modeling of active occupancy of the residential sector in Spain: An indicator of residential electricity consumption," *Energy Policy,* vol. 62, pp. 742-751, 2013.

[57] J. Torriti, "Demand Side Management for the European Supergrid: Occupancy variances of European single-person households," *Energy Policy,* vol. 44, pp. 199-206, 2012.

[58] V. H. Queja, J. Almoroxa, J. A. Arnaldob and L. Saitoc, "ANFIS, SVM and ANN soft-computing techniques to estimate daily global solar radiation in a warm sub-humid environment," *Journal of Atmospheric and Solar–Terrestrial Physics,* vol. 155, no. 1, pp. 62-70, 2017.

[59] J. Antonanzas, N. Osorio, R. Escobar, R. Urraca, F. Martinez-de-Pison and F. Antonanzas-Torres, "Review of photovoltaic power forecasting," *Solar Energy,* vol. 136, pp. 78-111, 2016.

[60] J. M. Santos, P. S. Moura and A. T. de Almeida, "Technical and economic impact of residential electricity storage at local and grid level for Portugal," *Applied Energy,* vol. 128, pp. 254-264, September 2014.

[61] F. M. Vieira, P. S. Moura and A. T. de Almeida, "Energy storage system for self-consumption of photovoltaic energy in residential zero energy buildings," *Renewable Energy,* vol. 103, pp. 308-320, April 2017.

[62] I. Ranaweera and O.-M. Midtgård, "Optimization of operational cost for a grid-supporting PV system with battery storage," *Renewable Energy,* vol. 88, pp. 262-272, April 2016.

[63] D. Arcos-Aviles, J. Pascual, F. Guinjoan, L. Marroyo, P. Sanchis and M. P. Marietta, "Low complexity energy management strategy for grid profile smoothing of a residential grid-connected microgrid using generation and demand forecasting," *Applied Energy,* vol. 205, pp. 69-84, November 2017.

[64] D. Arcos-Aviles, J. Pascual, L. Marroyo, P. Sanchis and F. Guinjoan, "Fuzzy Logic-Based Energy Management System Design for Residential Grid-Connected Microgrids," *IEEE TRANSACTIONS ON SMART GRID,* vol. 9, no. 2, pp. 530-543, March 2018.

[65] J. Pascual, J. Barricarte, P. Sanchis and L. Marroyo, "Energy management strategy for a renewable-based residential microgrid with generation and demand forecasting," *Applied Energy,* vol. 158, pp. 12-25, November 2015.

[66] D. Arcos-Aviles, . N. Espinosa, . F. Guinjoan, L. Marroyo and P. Sanchis, “Improved fuzzy controller design for battery energy management in a grid connected microgrid,” in *IECON 2014 - 40th Annual Conference of the IEEE Industrial Electronics Society*, Dallas, TX, USA, 2014.

[67] J. Li and M. A. Danzer, “Optimal charge control strategies for stationary photovoltaic battery systems,” *Journal of Power Sources,* vol. 258, pp. 365-373, July 2014.

[68] S. Sobri, S. Koohi-Kamali and N. Rahim, “Solar photovoltaic generation forecasting methods: A review,” *Energy Conversion and Management,* vol. 156, pp. 459-497, January 2018.

[69] E. Ogliari, A. Dolara, G. Manzolini and S. Leva, “Physical and hybrid methods comparison for the day ahead PV output power forecast,” *Renewable Energy,* vol. 113, pp. 11-21, December 2017.

[70] L. Poruschi, C. Ambrey and J. Smart, “Revisiting feed-in tariffs in Australia: A review,” *Renewable and Sustainable Energy Reviews,* vol. 82, pp. 260-270, February 2018.

[71] Mark Intell, “International comparison of Australia’s household electricity prices,” 2016.

[72] J. Al-Saqlawi, K. Madani and N. Mac Dowell, “Techno-economic feasibility of grid-independent residential roof-top solar PV systems in Muscat, Oman,” *Energy Conversion and Management,* vol. 178, pp. 322-334, December 2018.

[73] A. Ghafoor and A. Munir, “Design and economics analysis of an off-grid PV system for household electrification,” *Renewable and Sustainable Energy Reviews,* vol. 42, pp. 496-502, February 2015.

[74] Banco de la República, Colombia, “Indicador Bancario de Referencia (IBR),” December 2018. [Online]. Available: http://www.banrep.gov.co/es/indicador-bancario-referencia-ibr. [Accessed 12 February 2019].

[75] Banco de la República, Colombia, “Indicadores de inflación básica y su variación anual,” December 2018. [Online]. Available: http://www.banrep.gov.co/es/indicadores-inflacion-basica-y-su-variacion-anual. [Accessed 12 February 2019].

[76] K. Branker, M. Pathak and J. Pearce, “A review of solar photovoltaic levelized cost of electricity,” *Renewable and Sustainable Energy Reviews,* vol. 15, pp. 4470-4482, December 2011.

[77] S. Rodrigues, R. Torabikalaki, F. Faria, N. Cafofo, X. Chen, A. Ramezani, H. Mata-Lima and F. Morgado-Dias, “Economic feasibility analysis of small scale PV systems in different countries,” *Solar Energy,* vol. 131, pp. 81-95, June 2016.

[78] *Resolution 070198, Regulatory Commission for Energy and Gas (in Spanish), CREG,* 1998.